

CONCRETE STRUCTURES

ANNUAL TECHNICAL JOURNAL



Gábor Madaras – Attila Várdai

BONDS BETWEEN DENMARK AND HUNGARY

2

György Farkas – István Völgyi – Péter Hegyi

INNOVATIVE STRUCTURES OF ELI-ALPS RESEARCH CENTRE IN HUNGARY

10

Olivér Czoboly – György L. Balázs

POSSIBLE MECHANICAL DETERIORATION OF FIBRES INFLUENCED BY MIXING IN CONCRETE

18

Rita Vajk – István Sajtos

THE EFFECT OF AGGREGATE SIZE ON THE BEHAVIOUR OF BEAMS WITHOUT SHEAR REINFORCEMENT

24

Viktor Hlavička – Éva Lublói

EXPERIMENTAL AND NUMERICAL MODELING OF FASTENING ELEMENTS

31

Sándor Sólyom – György L. Balázs –

Adorján Borosnyói

MATERIAL CHARACTERISTICS AND BOND TESTS FOR FRP REBARS

38

Réka Anna Nagy

REINFORCEMENT CORROSION IN ASPECT OF CRACK WIDTH OF CONCRETE

45

Zoltán Gyurkó – Adorján Borosnyói

STATIC HARDNESS TESTING AND DEMOELLING OF HARDENED CONCRETE

52

Emese Gál – Adorján Borosnyói

FREEZE-THAW SALT SCALING RESISTANCE OF HPC WITH COMBINED METAKAOLIN AND SILICA FUME SLURRY USAGE

57

Sándor Sólyom – György L. Balázs

BOND STRENGTH OF FRP REBARS

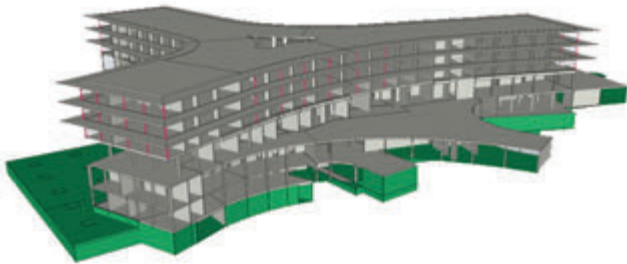
62

2015

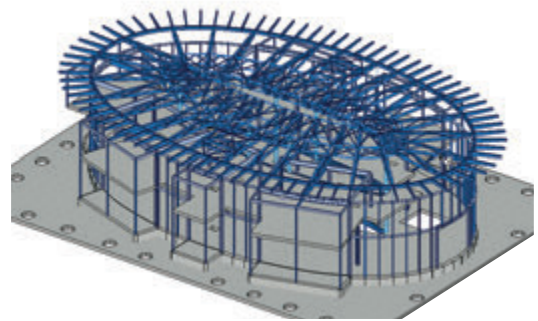
Vol. 16

Kombiniert beliebig

Kurhaus Oberwaid, St. Gallen
Grünenfelder + Lorenz AG Bauingenieure, St. Gallen

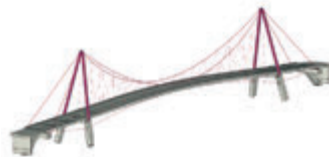


Clinique des Grangettes, Chêne-Bougeries
INGENI SA Genève
Architecte: Brodbeck & Roulet SA

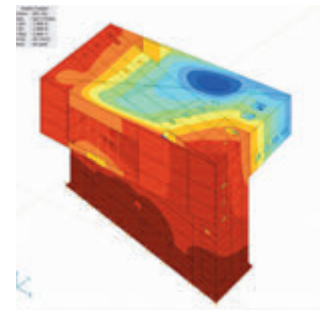


Vielseitig einsetzbar

Solothurn Entlastung West, Aaresteg
Fürst Laffranchi Bauingenieure GmbH, Aarwangen

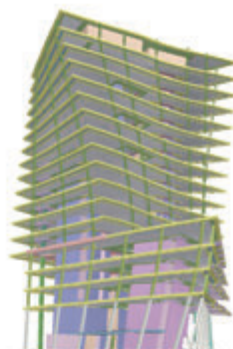
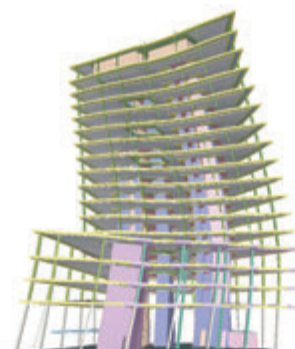
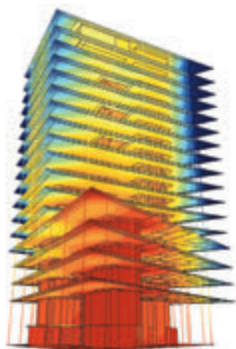


Centro d'esercizio FFS, Pollegio
Borlini & Zanini SA, Pambio Noranco



Dynamisch flexibel

Richti-Areal, Wallisellen ZH · JägerPartner AG Bauingenieure sia Zürich · Wiel Arets Architects Zürich



IngWare GmbH · CH-8703 Erlenbach · fon +41 (44) 910 34 34
www.ingware.ch · info@ingware.ch



Editor-in-chief:
Prof. György L. Balázs

Editors:
Prof. Géza Tassi
Dr. Herbert Träger

**Editorial board and
Board of reviewers:**
Assoc. Prof. István Bódi
Dr. Béla Csíki
Assoc. Prof. Attila Erdélyi
Prof. György Farkas
Gyula Kolozsi
Dr. Katalin Kopecskó
Dr. Károly Kovács
Ervin Lakatos
Dr. Éva Lublói
László Mátyássy
László Polgár
Dr. Salem G. Nehme
Antonia Teleki
Dr. László Tóth
József Vörös
Péter Wellner

Prof. Endre Dulácska
Dr. József Janzó
Antónia Királyöldi
Dr. Jenő Knebel
Prof. Péter Lenkei
Dr. Miklós Loykó
Dr. Gábor Madaras
Prof. Árpád Orosz
Prof. Kálmán Szalai
Prof. Géza Tassi
Dr. Ernő Tóth
Dr. Herbert Träger

Founded by: Hungarian Group of *fib*
Publisher: Hungarian Group of *fib*
(*fib* = International Federation for
Structural Concrete)

Editorial office:
Budapest University of Technology
and Economics (BME)
Department of Construction Materials
and Engineering Geology
Műegyetem rkp. 3., H-1111 Budapest
Phone: +36-1-463 4068
Fax: +36-1-463 3450
WEB <http://www.fib.bme.hu>
WEB editor: Olivér Czoboly

Layout and print:
Csaba Halmai
Navigar Ltd.

Price: 10 EUR
Printed in 1000 copies

© Hungarian Group of *fib*
HU ISSN 2062-7904
online ISSN: 1586-0361

Cover photo:
**Precast concrete elements of
Grupama FTC Stadium in
Budapest Hungary produced by
FERROBETON Co, CRH Group**



CONTENT

- 2** Gábor Madaras – Attila Várdai
BONDS BETWEEN DENMARK AND HUNGARY
- 10** György Farkas – István Völgyi – Péter Hegyi
**INNOVATIVE STRUCTURES OF ELI-ALPS RESEARCH
CENTRE IN HUNGARY**
- 18** Olivér Czoboly – György L. Balázs
**POSSIBLE MECHANICAL DETERIORATION OF FIBRES
INFLUENCED BY MIXING IN CONCRETE**
- 24** Rita Vajk – István Sajtos
**THE EFFECT OF AGGREGATE SIZE ON THE
BEHAVIOUR OF BEAMS WITHOUT SHEAR
REINFORCEMENT**
- 31** Viktor Hlavička – Éva Lublói
**EXPERIMENTAL AND NUMERICAL MODELING OF
FASTENING ELEMENTS**
- 38** Sándor Sólyom – György L. Balázs – Adorján Borosnyói
**MATERIAL CHARACTERISTICS AND BOND TESTS FOR
FRP REBARS**
- 45** Réka Anna Nagy
**REINFORCEMENT CORROSION IN ASPECT OF CRACK
WIDTH OF CONCRETE**
- 52** Zoltán Gyurkó – Adorján Borosnyói
**STATIC HARDNESS TESTING AND DEM MODELLING
OF HARDENED CONCRETE**
- 57** Emese Gál – Adorján Borosnyói
**FREEZE-THAW SALT SCALING RESISTANCE OF HPC
WITH COMBINED METAKAOLIN AND SILICA FUME
SLURRY USAGE**
- 62** Sándor Sólyom – György L. Balázs
BOND STRENGTH OF FRP REBARS

Sponsors:

Railway Bridges Foundation, ÉMI Nonprofit Ltd., HÍDÉPÍTŐ Co., Holcim Hungary Co.,
MÁV Co., MSC Consulting Co., Lábatlani Vasbetonipari Co., Pont-TERV Co.,
UVATERV Co., MÉLYÉPTERV KOMPLEX Engineering Co.,
SW Umwelttechnik Hungary Ltd., Betonmix Consulting Ltd., BVM Épelem Ltd.,
CAEC Ltd., Pannon Freyssinet Ltd., STABIL PLAN Ltd., UNION PLAN Ltd.,
DCB Consulting Ltd., BME Dept. of Structural Engineering,
BME Dept. of Construction Materials and Engineering Geology

BONDS BETWEEN DENMARK AND HUNGARY



Gábor Madaras – Attila Várdai

With this article the authors would like to highlight some cultural, economic and technical connections between the organizing country of fib Congress 2015 Denmark, and Hungary. During the preparation of this paper various links have been uncovered from well known facts to tiny, but exciting details.

Keywords: Denmark, Hungary, history, science, economics

1. INTRODUCTION

The aim of this article (by continuing the tradition of the past issues of Concrete Structures) is to highlight the links between the organizing country of the actual *fib* Symposium and Hungary. In 2015 the Symposium is held in Copenhagen; therefore the authors revealed historical, economic, cultural and technical connections between Denmark and Hungary.

Data survey and the preparation of this paper were pleasing as both authors had lived in Copenhagen in the past and have personal experience of the links between the two countries.

2. EXAMPLES OF HISTORICAL CONNECTIONS

2.1 THE FIRST LINK

The oldest remembrance in the written history about the Hungarian-Scandinavian connections originates from cca.1000 A.D. At those times the Viking warriors and tradesmen had lots of partnerships with people from South-East Europe and western part of Asia. Once, under not clarified circumstances a man from this region joined the Vikings, and with the Viking troops he arrived at Scandinavia. As the rumour says, the man's name was Tyrker, and he probably was Hungarian.

Later this man became a member of the expedition of Leif Eriksson (the son of Rød Erik) as a good friend of Erik and foster-father of Leif. Tyrker could be the first Hungarian who reached the land of America, together with the Vikings, some 500 years before Christopher Columbus. Also he might be the name-giving person of Vinland (the coast at the region of Boston today) where the expedition found a lot of wild grapes (the Vikings did not know this plant, but it was well-known in Tyrker's homeland).

2.2 MIDDLE AGES

In the Middle Ages both Denmark and Hungary was occupied with the affairs of their respective regions, Scandinavia and Central-Europe. The geographical distance between the two countries was too big to allow tight links. Only some records we know of, for example the funeral oration of Tycho Brache, Danish astronomer, was delivered by János Jeszeni court-physician in Prague.

2.3 THE 18TH AND 19TH CENTURIES

The Danish Royal Mounted Guards, a small regiment in the Danish Army serving as Royal Guards and a front line cavalry unit was founded in 1737. There were some Hungarian hussars in duty in this small troop. Later, in 1762 the root of the Danish cavalry was organised with the participation of five Hungarian officers.

The family of Kaas von Rewentlow (Danish noble family) was first mentioned in a document dated 1336. During the centuries they had lots of connections with Hungarians; and at the end of the 18th century one member of the family married a Hungarian woman and moved to Hungary. Their descendants were born as Hungarians and got the baron title. Ivor Kaas (1842-1910) (*Fig. 1*) was a famous publisher and politician and his son, Albert Niels Kaas (who had his studies in Hungary) worked in the Hungarian public administration.

Ádám János Hofstetter (Selmecebánya, 1667- Copenhagen 1720) was the son of a protestant priest in Hungary. After

Fig. 1: Baron Ivor Kaas



escaping religious persecution in Hungary, the family was granted asylum in Germany where Ádám János became a famous physician. King Frederick IV of Denmark (who supported the Austrian party between 1703 and 1711, in the Rákóczi's War of Independence) invited him to be his personal doctor.

Johann Jacob Stunder (Copenhagen, 1759 -Neusohl, Austro-Hungarian Empire – now Slovakia 1811) was a Danish painter who studied fine arts in Copenhagen. Answering the invitation of the Hungarian language reformer Ferenc Kazinczy he was working in several Hungarian cities. As he married a woman in Lőcse in 1797, he remained in the region until his death.

Dénes Széchényi, Earl of Sárvár (Pest, 1866- Stockholm 1934) was a diplomat and an emissary of the Austro-Hungarian Empire in Denmark and Norway from 1908 till 1917.

2.4 WWII

Interesting stories are linked to the Second World War in Denmark (riownag, 2012). In February 1945, some 12,000 Hungarian soldiers left Hungary, and went directly to Denmark. These troops acted there under the command of the invading German forces, but step by step they built better and better connections with the Danish population (and the local resistance). On the 22th of April, a poorly armed Hungarian troop commanded to the front rebelled against the Germans (who had numerical superiority) in Copenhagen, and a hopeless battle started. The story can be read in details in the book of Danish publicist Søren Peder Sørensen (*De ungarske soldater*, 2005). Unfortunately this document is not available in Hungarian, so the story is absolutely unknown in Hungary.

Besides photos and newspaper articles, there are two further “natural” souvenirs in Denmark today as a reminder of the Hungarian presence in Denmark during WWII. One is the so called “Hungarian tree” (*Fig. 2*) close to Holte in the Fredrikslund forest, with an engraved coat of arms of Hungary on the trunk. The other is a wooden sculpture of “The suffering Jesus” (*Fig. 3*), made of oak by an unknown Hungarian soldier at the home of the priest of Lønborg (West-Jütland).

After the Second World War, the diplomatic links were reformed in 1949. The first Hungarian ambassador was Vilmos Böhm from the Social Democrat Party. The relationship of the countries was considered normal in spite of the political differences. Although after the Hungarian revolution in 1956 the diplomatic links loosened, the Danish media showed a deep sympathy (*Fig. 4*) to the revolution.

Fig. 2: The Hungarian tree



Fig. 3: The sculpture of The suffering Jesus



Fig. 4: The cover of a Danish newspaper about the Hungarian revolution

3. ECONOMIC LINKS

The economic connections are dominated by the traditional trading with goods. Until the middle of the 1980s relevant industrial agreements are not known. The first step towards a modern cooperation was through a medical product (insulin)

with the NOVO/Nordisk Co. Later, the first Danish production site of VELUX (window factory) was built in Hungary (in 1988). Several Danish brands established offices in Hungary after the regime change in 1989. These companies were very careful with their investments, but increasing tendency was experienced over the coming years.

In 2000 49 Danish companies and joint-ventures existed in Hungary. 15 companies (31%) was involved in machinery and instrument industry, 14 companies (29%) in industrial goods, 10 companies (20%) in different services, education and all the others are involved in chemical, medical industry, foods and agriculture. The biggest Danish companies in Hungary was the world famous LEGO, the Grundfos group, and the Rockwool isolation company.

At the end of 2010 the total volume of the working Danish capital in Hungary was 371 M €, the Hungarian export to Denmark in 2011 was 530.4 M €, while the import reached 433.9 M €.

Today the most important Danish investors in Hungary are:

- Ib Andersen – steel cutting
- ISS- cleaning, guarding
- COWI- consulting
- Coloplast- medical products
- Grundfos- machinery
- Rockwool International- isolations
- JYSK- furnitures, household goods
- Nilfisk Advance- machinery
- LEGO- toys
- A.P. Moeller- Maersk-transporting
- Brdr. Hartman- packaging
- VELUX- windows
- TCC- telecommunications
- H. Lundbeck- medicines

Connected to the economic growth, cultural bonds are also being strengthened.

4. CULTURAL BONDS

4.1 TWIN-TOWNS

To enhance the cultural and social ties of the two countries, twin-town agreements have been made between Hillerød and Gödöllő, Kjellerup and Kiskunfélegyháza, Ringsted and Gyöngyös, Thisted and Baja, Viborg and Kecskemét.

Bent Hansen, chairman of Central Denmark Region received the Commander's Cross of the Hungarian Order of

Fig. 5: The Hungarian Ambassador to Denmark gives the Commander's Cross of the Hungarian Order of Merit to Bent Hansen



Merit (*Fig. 5*) in 2014 for his more than two decade activity in the improvement of the cooperation between the two countries.

4.2 MUSIC

The first modern trace, considering cultural connections is related to Emil Telmányi (*Fig. 6*), the Hungarian violinist-conductor (Arad, 1892 - Holte, 1988).

Telmányi had his studies in Budapest as a student of the Hungarian violinist, composer and music teacher Jenő Hubay. He arrived at Copenhagen in 1912, and in 1918 he married Anne Marie, the younger daughter of the Danish composer Carl Nielsen, who wrote his Violin Concerto, Op. 33 (1911) for his subsequent son-in-law.



Fig. 6: Emil Telmányi

From 1940 till 1969 he was a leading teacher of the Music Academy in Aarhus. In 1949, to provide authentic sounding when playing J.S. Bach violin sonatas he created a special, arched bow, so it can be assumed, that he had engineering instincts, too.

Until his death Emil Telmányi was an excellent ambassador of the Hungarian music, mainly with the constant propagation of the music of the Hungarian composer Béla Bartók, all over the world.

Nowadays the cultural bonds between the two countries are becoming stronger and stronger. With the Hungarian political opening after 1989 the possibilities are better in terms of conversation as well as and the exchange of cultural experience. The best Hungarian artists are welcome to Denmark, and the Hungarian audience is interested to get more and more from the Danish films, literature and design. The Hungarian literature became popular in Denmark, thanks to the excellent Péter Eszterhás (Budapest, 1940-) (*Fig. 7*), a Hun-



Fig. 7: Péter Eszterhás

garian writer, director and translator, who lives in Denmark.

The Danish P2 radio channel offers Hungarian music programmes daily, often from Hungarian musicians. A special tie is that in the person of Iván Fischer, the National Chamber Orchestra of the Danish Radio (DR Underholdnings Orkestret) has a Hungarian leading conductor.

Fig. 8: Andersen's children's book in Hungarian



Denmark created eleven Danish Institutes of Culture all over the world. One of these Institutes was founded in Kecskemét, Hungary, which has a very important position in the field of dissemination of culture and in the organisation in music education.

4.3 FAIRY TALES

The fairy tales of the renowned Hans Christian Andersen (Odense, 1805 - Copenhagen, 1875) were translated to Hungarian. His children's books (Fig. 8) can be found at almost all Hungarian households among the tales of "the great folk-tale teller", Elek Benedek (Kisbacon, 1859- Kisbacon, 1929).

4.4 SPORTS

Both nations are successful in handball (Denmark is the second, Hungary is the third in the Table of Medals of the Women's Handball European Championships) and had met several times in different international Championships. In the Summer Olympic Games in Sydney (2000) the Danish team conquered the Hungarian national team in a terrific battle and won the gold medal. In 2005 the two teams played for the third place in the Women's Handball World Championship. That tight game finally resulted with Hungarian success (HUN-DEN 27:24).

Also a very tight football match was played for the third place of UEFA European Championship in 1964. The result (HUN- DEN 3:1) could be set only after extra time. In 1992 Denmark won the first place of the European Championship.

In an interview (valogatott.blog.hu, 2014) retired Danish midfielder Morten Bisgaard mentioned that Hungarian trainers moved to Denmark (Frigyes Molnár, Lajos Szendrői, Géza Toldi) had great influence on Danish clubs in the past.

4.5 CHESS

Both in Denmark and in Hungary playing chess has become a part of culture. Both nations provided notable grandmasters such as Bent Larsen and Aron Nimzowitsch from Denmark, or Péter Lékó and the Polgár sisters (Zsuzsa, Judit and Zsófia Polgár) from Hungary. Also, several chess tactics have been developed in the two countries and named after the country or its grandmaster, such as the Danish Gambit (1. e4-e5, 2. d4-

Fig. 9: Danish Gambit



exd4, 3. c3) (*Fig. 9*); the Larsen's Opening (or Nimzo-Larsen Attack- 1. b3); the Hungarian Opening (or Benkő's Opening- 1. g3) or the Hungarian Gambit (which is a variation to continue the accepted King's Gambit: 1. e4-e5, 2. f4-exf4, with 3. Qf3).

It is noteworthy to mention that the ELO rating system (a method used to calculate the relative skill of players of board games, such as chess) was created by the Hungarian-American physicist Árpád Élő (Egyházaskesző, 1903-Brookfield, 1992).

4.6 FILMMAKING

Recently Hungary became a very famous spot for filmmaking; many movies were shot in Budapest and at the surrounding studios. Great Danish actors played in Hungarian scenes as well.

For example a part of Mads Mikkelsen's 'Move On' was shot in Sósokút. The Danish originated Viggo Mortensen (in 'Good') and Scarlett Johansson (in 'An American Rhapsody'- directed by the Hungarian director, Éva Gárdos) also starred in Hungary. The character of Scarlett Johansson (*Fig. 10*) is a young Hungarian girl in 'An American Rhapsody' and she speaks Hungarian in one scene.



Fig. 10: Scarlett Johansson in Budapest

Nowadays one of the most popular series on TV is HBO's 'Game of Thrones'. One of the main characters, Jamie Lannister is played by the Danish actor, Nikolaj Coster-Waldau. The stand-in of the actor is the Hungarian stunt man, Domonkos Párdányi (who was also replacing Mr. Coster-Waldau in the fighting scenes of 'Kingdom of Heaven' in 2005). Mr. Párdányi and his stunt-team received the SAG Award (fourth time in row, since 2012) for their performance in the 'Game of Thrones'.

5. TECHNOLOGY

5.1 PHYSICS

One of the most famous physicists of the world is the Danish Nobel Prize laureate Niels Henrik David Bohr (Copenhagen, 1885 - Copenhagen, 1962) (*Fig. 11*). His son, Aage Niels Bohr (Copenhagen, 1922 - Copenhagen, 2009) also received the Nobel Prize. Niels H. D. Bohr's researches with the atomic structure are considered fundamental in quantum mechanics. He was also the founder of the Institute of Theoretical Physics (or as it is called today, the Niels Bohr Institute), which became a focal point for theoretical physicists.

One of the first scientists who spent time at the Institute was the Hungarian radiochemist György Hevesy (Budapest, 1885 - Freiburg im Breisgau, 1966). In 1922 Hevesy co-discovered hafnium ($_{72}\text{Hf}$) with Dirk Coster, what was named after the home town of Niels Bohr (Hafnia, Latin name for Copenhagen).



Fig. 11: Niels Henrik David Bohr

During WWII Bohr was trusted with the Nobel Prizes of two of his Jewish colleagues (Max von Laue and James Franck) to keep them safe until the end of the war (npr, 2011). When the Nazis marched into Copenhagen, Bohr had to hide the medals because the names of the owners were displayed on them and if the Germans had found out that he was hiding the gold of German Jews, which would mean death penalty for him.



Fig 12: Hevesy dissolving the medals (drawn by Benjamin Arthur)

The German soldiers were only hours away from the building of the Institute and therefore, a sudden action was necessary. Finally György Hevesy was able to help his friend by dissolving the golden medals (*Fig. 12*). The liquefied metal was hidden in a flask and put on the shelf. Luckily the flask was not discovered and remained there during the war. When the war was over, Hevesy sent the raw metal to Stockholm, where the Swedish Academy recast the medals from the original material and re-presented them to their rightful owners.

5.2 THEORIES IN MECHANICS

One of the pioneers in engineering was the Hungarian Gábor Kazinczy (Szeged, 1889 - Motala, 1964) (*Fig. 13*). His tests with steel beams in 1913 are now considered as the fundamentals of plastic theories. He defined the term 'plastic hinge' (Kazinczy, 1914) and determined the plastic resistance of a structural element. He verified that his theory is valid for re-



Fig 13: Gábor Kazinczy

inforced concrete structures as well. He also claimed (in accordance with the current belief) that the safety of a structure properly can be determined only by probabilistic methods. He introduced the idea of partial safety factors. His results were adopted during many further researches. During WWII (at the end of 1944) he immigrated to Denmark.

Another well-known Hungarian researcher in the field of plasticity is Árpád L. Nádai (Budapest, 1883 - Pittsburgh, 1963), who (with Heinrich Hencky) developed the Hencky-Nádai deformation theory for plastic analysis. Tódor Kármán (Budapest, 1881- Aachen, 1963) was investigating the effect of confinement on the load bearing capacity of materials (Kármán, 1910). Both Professor Nádai and Professor Kármán received the Timoshenko Medal in 1958.

The Danish Harald Malcolm Westergaard (Copenhagen, 1888 - Cambridge, 1950) (*Fig. 14*) published many papers on the applicability of the recent theories of elasticity, plasticity and fracture mechanics. He focused on simple solutions; therefore his results became very popular worldwide. His theories to calculate stresses in slabs and concrete pavements are still part of the engineering practice. Based on his results József Jáky (Szeged, 1893 - Hévíz, 1950) proposed a method for concrete pavement design in Hungary (Jáky, 1937).

5.3 EARTHQUAKE ENGINEERING

The Hungarian Tamás Paulay (Sopron, 1923 - Christchurch, 2009) (*Fig. 15*) investigated the behaviour of Shear Walls and Coupling Beams for seismic loading at the University of Canterbury, New Zealand. He developed the application of capacity design and introduced the method into the first draft of Eurocode 8.

5.4 CONCRETE DESIGN

Reinforced concrete is traditionally a popular building material both in Denmark and in Hungary. As concrete is frequently used, intensive studies were carried out to better understand its complex behaviour.

The Danish Niels Saabye Ottosen proposed a constitutive model for concrete (Ottosen, 1979). His paper is very fre-



Fig. 14: Harald Malcolm Westergaard

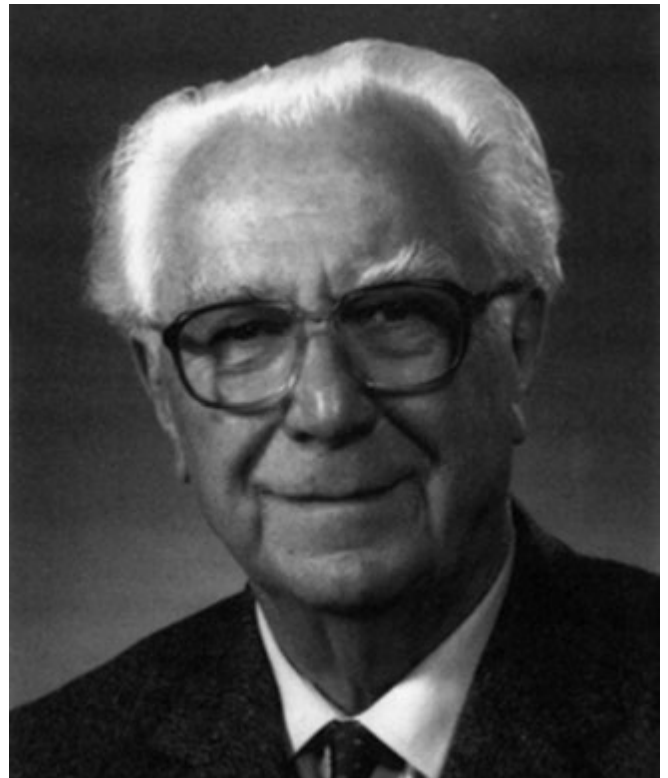


Fig. 15: Tamás Paulay

quently cited, even today. The Hungarian Sándor Popovics (Budapest, 1921 - Landsdowe, 2010) (*Fig. 16*), who were given the Palotás Award of the *fib* Hungarian Group in 2003, introduced a numerical approach to the complete stress-strain curve of the concrete (Popovics, 1973).

The experiments of Knud Windsturp Johansen in Copenhagen had great influence on the development of the yield-line theory. He also investigated the shear behaviour of reinforced concrete beams. Also, the equations in EC5, used for the design of shear dowels in timber-to-timber connections are based on his solutions (Johansen, 1949) (*Fig. 17*).

5.5 TECHNOLOGICAL PRODUCTS

During WWII many buildings in the Hungarian capital were destroyed and the rapid growth in the population after the war



Fig. 16: Sándor Popovics

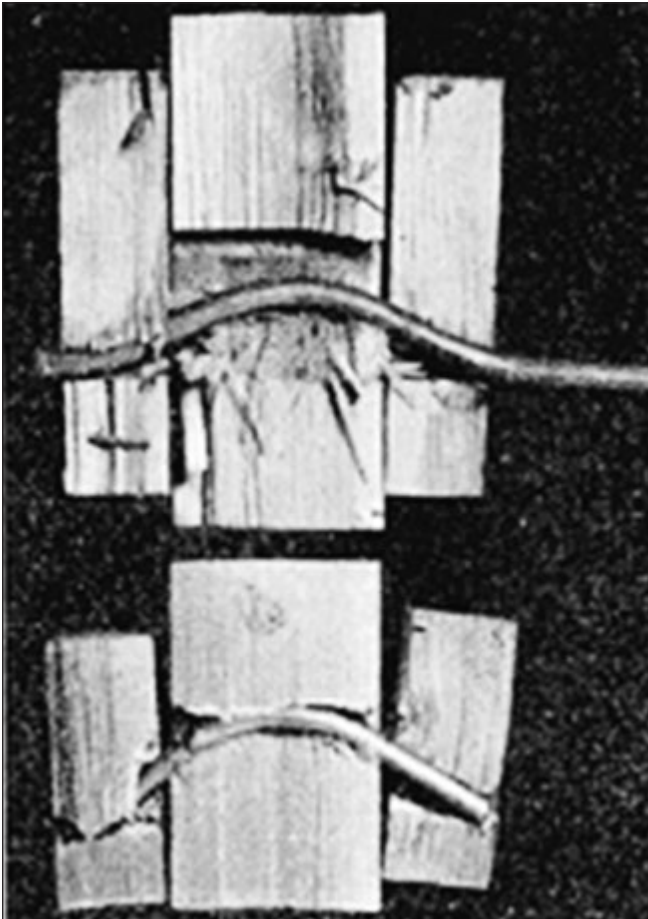


Fig. 17: Johansen's test with shear dowels

resulted in serious housing crisis. To provide accommodation for the inhabitants, the Hungarian government imported the large-panel systems both from Denmark and from the Soviet Union in the early 1960s. The Danish panel system was called Larsen-Nielsen system. Many building has been built with this technology in Hungary (Fig. 18).

This intervention proved to be successful to solve the housing crisis but these buildings were not able to continuously satisfy the demands. Recently the large-panel buildings are considered a serious issue what needs to be solved.

The ROCKWOOL International A/S, as the world's leading producer of stone wool has subsidiary company in Hungary as well. The company has been founded by H.J. Henriksen and V. Kähler in 1909, Denmark. ROCKWOOL offers high quality products for thermal insulation.

The VELUX also became a famous brand in Hungary. The company's roof windows are often installed into the roofs of the buildings all over the country. VELUX became a



Fig. 18: Buildings built with Larsen-Nielsen system

synonym of roof window in Hungary. VELUX has been also founded in Denmark (by Villum Kann Rasmussen, in 1941).

6. PERSONAL CONNECTIONS OF THE AUTHORS

The authors of this paper have some personal connections to Denmark.

6.1 GÁBOR

Not professional link, but nice to remember when in 1984 the former Hungarian basketball team, the team of the Technical University (MAFC) had a kind invitation from the University of Aarhus for a match. In the next year the Danish players requited the visit in Budapest. The biggest personal result of this friendship was later, when I had a scholarship in Denmark. I had the kind invitation to play as a guest-player in the team of the Aarhus University on an international tournament in Copenhagen...

And the professional ties?

With a Danish-Hungarian educational agreement I got a scholarship to visit the University in Lyngby to study some special technical questions concerning to punching of RC slabs. In that time the leader of the chair was Professor Mogens Peter Nielsen who organised me a very kind and friendly intro to the chair, and during my stay there he secured me every imaginable help in the university (and outside it), related to every professional and personal matters. With his help, a friendship started with Mikael W. Braestrup who is the head of the Organising Committee of our symposium in Copenhagen. This friendship in the *fib* family has existed for 30 years... I wish another 30 for both of us.

Also, my long term connection with Steen Rostam began during my Danish scholarship, who, to me till today is the "father of durability". We have spent a lot of time together in different *fib* Committees and Task Groups. I think he is a person who is able to teach and amuse everybody who is interested in the concrete profession.

Of course there are several other kind Danish colleagues behind this mentioned trio. I am grateful for all of them, and I am very glad to meet with them in Copenhagen.

6.2 ATTILA

I consider myself lucky to have the opportunity to spend a semester in Copenhagen during my BSc studies. In 2009 I

was an exchange student at the Copenhagen University College of Engineering (CUCE, or IHK in Danish), which is now merged with the Technical University of Denmark (DTU).

I am very grateful for all the support given by my Professors, Birte Rodevang, Lisbeth Lindbo Larsen and Jenny Rytter. Their lectures enhanced my motivation for this profession and the whole Danish atmosphere had a great influence on me. Also, the experience of that semester opened the horizon and this should be the purpose of connections between foreign nations.

7. REFERENCES

- Jáky, J. (1937): "The design of concrete pavements", (In Hungarian), *Magyar Mérnök- és Építész-Egylet Közlönye*, pp. 13-15.
- Kármán, T. (1910): "What influences the capacity materials?", (In Hungarian), *Magyar Mérnök- és Építész-Egylet Közlönye*, pp. 212-225.
- Kazinczy, G. (1914): "Test with clamped beams", (In Hungarian), *Beton-szemle*, 2, pp. 68-71, 83-87, 101-104.
- npr (2011): <http://www.npr.org/blogs/kulwich/2011/10/03/140815154/dissolve-my-nobel-prize-fast-a-true-story>

Ottosen, N.S. (1979): "Constitutive Model for Short-Time Loading of Concrete", *Journal of the Engineering Mechanics Division- ASCE*, Vol. 105, No. 1, pp.127-141.

Popovics, S. (1973): "A numerical approach to the complete stress strain curve for concrete", *Cement and concrete research*, 3(5), pp. 583-599.

riowang (2012): <http://riowang.blogspot.hu/2012/05/hungarian-soldiers-in-denmark.html>

valogatott.blog.hu (2014): http://valogatott.blog.hu/2014/03/18/a_real_madrid_olo_dan_magyar_edzok_nyomaban

Gábor Madaras (1950) Structural Engineer, PhD, Reinforced Concrete specialist, CEO of ÉMI-TÜV SÜD Ltd. He is a member of COM5 of *fib* and vice-president of the Hungarian Group of *fib*. His main fields of activities are reinforced- and prestressed concrete structures, lightweight concrete, durability and life-cycle analysis. His hobby is golf.

Attila Várdai (1985) Structural Engineer, MSc, Technical Expert at ÉMI-TÜV SÜD Ltd and part-time PhD student at the Department of Structural Engineering of Budapest University of Technology and Economics. He is a member of COM3 of *fib* and the Hungarian Group of *fib*. His main fields of activities are reinforced concrete design and structural strengthening.

INNOVATIVE STRUCTURES OF ELI-ALPS RESEARCH CENTRE IN HUNGARY

CHALLENGES AND SOLUTIONS FROM THE DRAWING INSPECTOR'S POINT OF VIEW



György Farkas – István Völgyi – Péter Hegyi

The most important information about the Extreme Light Infrastructure – Attosecond Light Pulse Source (ELI-ALPS) project are presented in this paper. The ELI-ALPS project is part of the Trans-European laser project (ELI), its facilities are currently being erected near Szeged. The special function of the research centre results in special requirements for the main building. After a short presentation of the research field and the requirements, the innovative structures of the main building are detailed. The design and construction procedure, the challenges occurred during the design and construction process, the questions and the answers are presented from the drawing inspector's point of view. The design of this rather complex facility was a real challenge for all participants. Innovative technologies are used, so far quite unknown in Hungary, which provided the participants valuable experiences.

Keywords: ELI, laser, innovative structures, vibration isolation, mass concrete

1. ELI RESEARCH FACILITIES IN CENTRAL EUROPE

The Extreme Light Infrastructure (ELI) will be the first large-scale scientific research facility network based on high-power laser realized with Trans-European cooperation, with coordinated management and research strategy. The investigation of the interaction between light and matter with the highest intensity, in the so-called ultra-relativistic range will be enabled by ELI. It will have strong impact on materials sciences, medicine and environment protection. New technical developments are expected to arise based on the new achievements of ELI.

Altogether three laser facilities will be constructed, each with different research fields, one in Romania, one in the Czech Republic and one in Hungary (Fig. 1). The projects in the countries have the following subtitles: Beamline (particles and X-ray experiments), Photonuclear applications and Attosecond. The first institute is built in Magurele, next to Bucharest, Romania. Photoinduced nuclear experiments will be performed at this facility.

The institute in Prague, Czech Republic is called as Beamline Facility. Mainly experimental projects using ultrahigh intensity light, like laser particle acceleration or laser generated X-ray radiation will be carried out there.

ELI Attosecond Light Pulse Source (ELI-ALPS) placed

Fig. 1: ELI facilities in Central Europe (ELI 2015)



Fig. 2: Facility of the ELI-ALPS (ELI 2015)

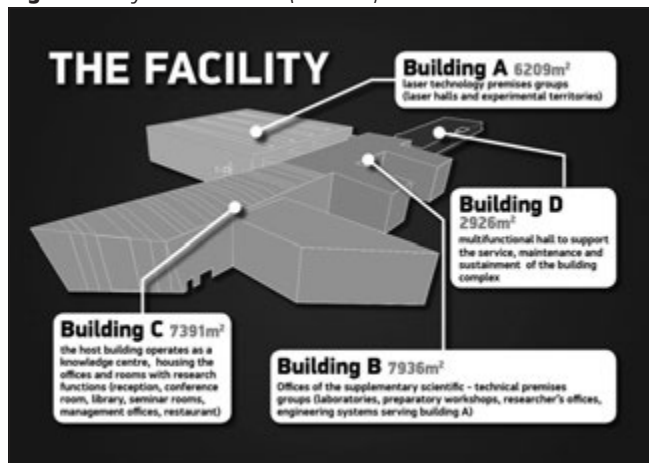




Fig. 3: 3D view of the ELI-ALPS research centre. (ELI 2015)

near Szeged, Hungary, is an attosecond laser facility. The main objective of this facility is to provide light sources between THz and X-ray frequency range in the form of ultra-short pulses with high repetition rate. The opening of a fourth research institute is planned, its main objective will be the non-linear quantum electrodynamics and laboratory astrophysics. Its laser tools will be able to generate 200 petawatt ($1 \text{ PW} = 10^{15} \text{ W}$) power pulses. The location of the fourth institute will be decided later (ELI 2015).

2. ELI-ALPS RESEARCH CENTRE IN HUNGARY

2.1 Research fields

The primary mission of the ELI-ALPS research facility is to make a wide range of ultrafast light sources accessible to the user groups of the international scientific community, with special consideration to coherent extreme-ultraviolet and X-ray radiations, and to attosecond pulses. In addition scientific and technological development will be carried out for the 200 PW peak intensity pulses. The results of the centre will be applicable for the users from the fields of scientific research and industrial applications likewise.

Main research and application fields of ELI-ALPS are as follows: valence electron science, core electron science, 4D imaging, relativistic interactions, biological, medical and industrial applications. (ELI 2015)

2.2 Technology – requirements (ÁKA 2015)

The laser technology implemented to the facility requires the housing of the laser equipments, secondary sources, target areas, laser preparation areas and other special laboratories. Clean rooms with total area of 8000 m^2 and special radio-protection experimental halls (Low / Medium / High Shield Secondary Source and Target Area, LTA, MTA, HTA) will be constructed. As the facility will be equipped with state of the art experimental apparatus, it has to meet special conditions. (ÁKA 2015)

The most important requirements for the experimental areas are as follows:

- temperature stability with maximum allowed variance of $\pm 0.5 \text{ }^\circ\text{C}$;
- stability of the relative humidity;
- extreme stability of the building during the experimental period with extremely low allowed angular velocity;
- quasi vibration-free experimental areas with maximum $6 \text{ } \mu\text{m/s}$ velocity.

2.3 Architecture – functional design

The coordination of the preparation and implementation of the project is managed by ELI-HU Nonprofit Ltd. The facility was designed by a group of Hungarian designers. The general designer of the research centre is the ÁKA 2012 Consortium. The architectural design is the product of the Artonic Design Architectural Ltd. The geotechnical documentation was made by the Taupe Ltd. The superstructures were designed by the Földvári Ltd. The vibration-free basement of the Building “A” was designed by the Konzulterv LP, with participation of the Taupe Ltd and the Földvári Ltd. The independent drawing inspector was the Budapest University of Technology and Economics. The experts of the inspector team represent the Faculty of Civil Engineering, Mechanical Engineering, Architecture and Electrical Engineering. The team was managed by Attila Joó from the Department of Structural Engineering.

The research centre has to provide sufficient space for the experimental areas, offices for about 150 researchers and administrative personnel, and additional seminar and conference rooms, workshops, library and meeting rooms. To make the facility fulfil its function all the requirements mentioned in the previous section had to be taken into account during the design procedure. To meet these requirements the different functions are separated in four buildings as *Fig. 2* shows. Building „A” is the main building of the research centre. As the most important building, it houses clean rooms, laser halls and experimental areas. No significant machinery will be installed in it since the strict criterion of vibration could not be achieved otherwise. The complex and innovative solutions of the structural system of this building will be detailed in the next section. The main role of Building „B” is the serving of building „A”. Laboratories, preparation workshops, researchers’ offices, and the machinery rooms will be installed here. The highly attractive Building „C” is a host building for offices and additional research functions (*Fig. 3*). Reception, conference hall, library, several seminar rooms, management

offices and cafeteria will be placed here. Building „D” is a multifunctional building for storage, servicing and maintenance of the research centre. The total net building area of ELI-ALPS is 24 462 m² (ELI 2015).

3. INNOVATIVE STRUCTURAL CONCEPT OF BUILDING “A” IN SERVICE OF THE FUNCTION

To be able to construct a structure which can meet the above mentioned extra requirements a special “house-in-the-house” structural system was adopted (Fig. 4). An external shell was designed with 80×80 m dimension. This is to provide the isolation of the internal structures from the environmental effects. The internal structure contains the scientific areas. This internal structure acts completely separately from the external one, to reduce the environmental effects on the research zones. The experimental areas are designed within the internal structure, either as steel truss frames (LTA) or as concrete bunkers (MTA, HTA), depending on the amount of radiation occurring during experiments (ÁKA 2015).

3.1 External structure

The external structure covers the inner part of the facility. To minimise the interaction between the two structures only one internal support was designed with special care (Fig. 5). The



Fig. 5: Excavation pit of Building “A” with diaphragm walls and piling under the basement. Erection of a 45 m long central pile using the bentonite-coating technology. The coating avoids the friction along the surface of the pile. The large reaction of the central pile is moved from the reaction zone of the stabilization piles of the basement. (ELI 2015)

other supports were placed well outside the internal structure. The foundation is made of piles which act as support for concrete columns. The central column (cross-section 1x1 m) has a special foundation since it should not interact with the internal structure. It is supported by four 45 meter long piles with a diameter of 1.8 meter (Fig. 5). These piles were constructed using a special bentonite-coating technology. Applying this

Fig. 4: Section of Building “A”.

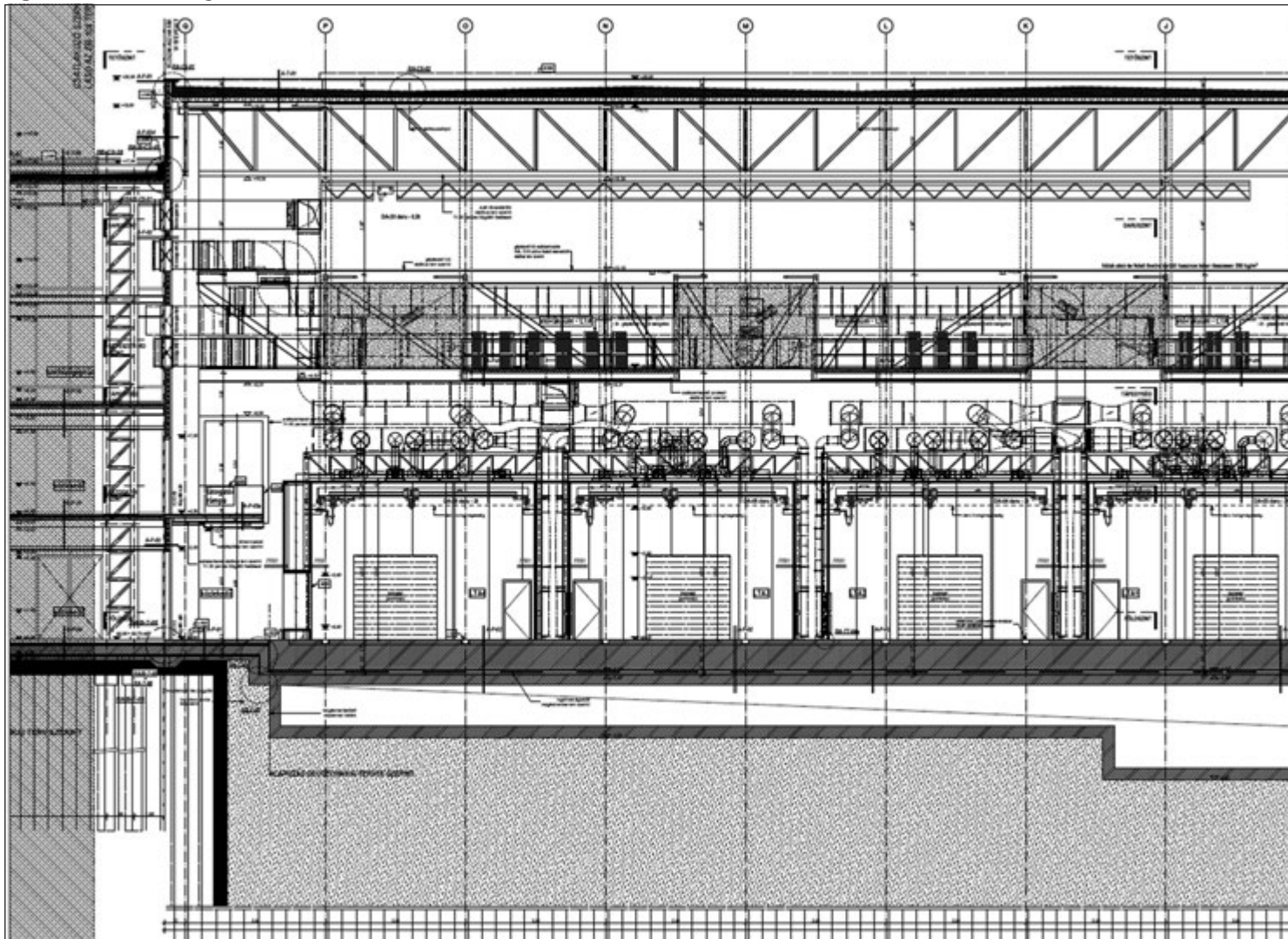




Fig. 6: The first pair of main truss girder with a length of 40 m (grey painting) is placed onto the columns of the external structure. (ELI 2015)

method, the end bearing of the piles remains active but the friction is inactivated by the coat. However the coating ensures horizontal support of the piles against buckling. This innovative technology was never used before in Europe. The pile cap is under the basement. Due to the length of the piles the soil zone loaded by the central column is deeply under the internal structure, therefore the central piles effect the settlement of the basement imperceptibly (ÁKA 2015).

The total height of the external structure is about 20 meters. Concrete columns support the hierarchical structure. Simply supported truss girders with 40 meter span are connected to two pairs of truss main girders with the same span and perpendicular direction (Figs. 6 and 7). These trusses will carry the load of the platforms of the machinery placed onto them.



Fig. 7: 40 m span truss girders (yellow) are supported by the main truss girders (grey). (ELI 2015)

Another set of truss girders are also constructed to carry the load of the sheathing. The main truss girders are supported by square columns with dimensions of 1 meter. The external structure is braced by RC walls at the perimeter of the building (ÁKA 2015).

3.2 Internal structures

The ELI-ALPS laser research centre is being built close to the northern city borders of Szeged on a site, which used to be an old Soviet military base next to highroad no. 5. The mechanical properties of the soil with layers of clay and silt are poor. This resulted in a quite complicated foundation system. The foundation of the external structures and of the internal structures were separated with diaphragm walls (background

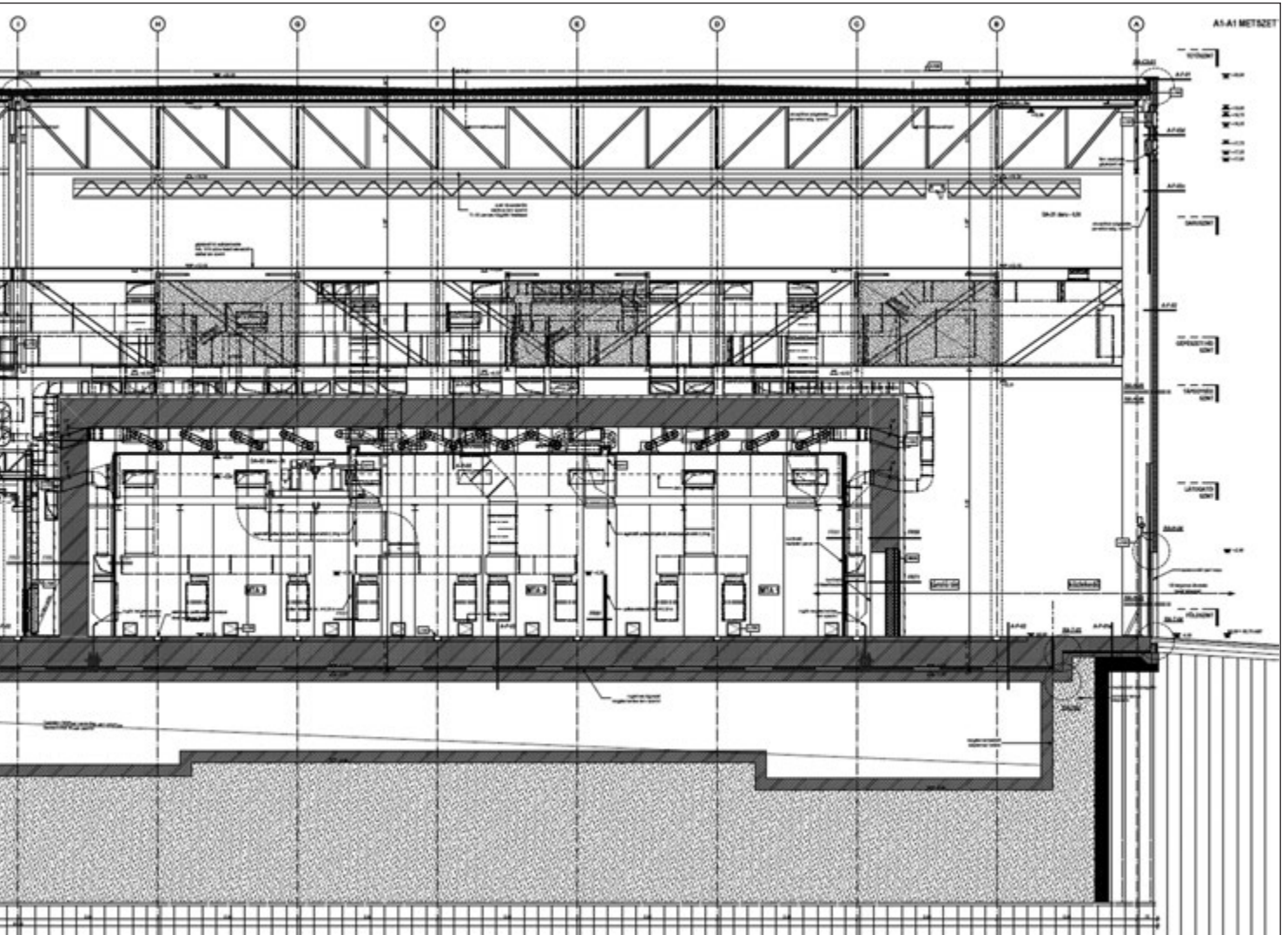




Fig. 8: Construction of the basement with varying height. The top and bottom slabs of the basement are connected with groups of honeycomb walls. The height of the basement depends on the weight of the zone above. The weight of the removed soil is close the weight of the superstructure. This method avoids significant settlement and tilt of the building. (ELI 2015)

of Fig. 5). The diaphragm walls rim the basement of Building „A”, consequently the level of the groundwater under the basement can be observed and controlled. The upper silt and clay layers are stabilized using 215 pieces of 31 meter long piles. The piles transfer the loads to deeper soil layers with more advantageous mechanical properties. This way the clay layer is not overloaded, and settlement can be decreased. Piles also reduce the differences in settlement caused by the inhomogeneous soil. The soil is changed to gravel in the pile-top-zone. A special basement is being built on the top of the gravel layer without connecting it to the top ends of the piles.

The aim of the special, rigid basement with variable height is to reduce the inhomogeneity of the reactions. Two experimental areas will be surrounded with concrete bunkers (see later). The weight of these bunkers is very high, which results in a rather inhomogeneous reaction distribution. To minimise the differences in settlement varying height of the basement is used (maximum height about 7 meters). To increase the stiffness of the basement, honeycomb-shaped columns were placed between the top and bottom slabs (Figs. 8 and 9).

On the top of the basement a 5500 m² large and 0.9 meter thick vibration-free slab is being built. To reduce the effect of vibration the slab rests on special corkboards. The size and distance of the boards depend on the weight distribution of

the structure above. The desired compression stress of the boards is about 0.2 MPa. The small changes in live load of the vibration-free slab can be compensated by active load distribution springs connecting the basement to the vibration-free slab.

The internal superstructures will be built on the top of the vibration-free slab. The most important parts of building “A” are the three experimental areas, LTA, MTA (~25×30 meters) and HTA (~35×35 m). The wall and slab thickness of the MTA bunker is 1 meter. In case of the HTA 2 meter thickness will be used to achieve the required radiation protection level. Several steel frames with cranes will be installed in the building for further functions. The variability in the structural type causes the extreme inhomogeneity in gravity load (ÁKA 2015).

4. INSPECTORAL WORK - NUMERICAL MODELLING

As it was described above, two independent structures were designed to minimise the environmental effect on the experiment area. The inspectoral work was also divided into two separate stages, firstly the independent modelling of the shell structure, and secondly the internal structure.

4.1 External structure

The external shell structure is composed of mainly steel trusses, with additional concrete columns and bracing walls. The modelling of the foundation of the external structure was outside our task. Based on the structural type, an adequate finite element model was made in ANSYS (ANSYS, 2011), using mainly beam elements to model the trusses (Fig. 10). These elements have two nodes and six degree of freedom per node. Each structural element (i.e. chord and web) was modelled using its ideal properties, the eccentricity between structural elements were also taken into account. The concrete columns were beam elements also, while the bracing walls were modelled using a four node shell element with six degrees of freedom at each node. The loads were taken into account as nodal forces including the self-weight of the structure and machinery, additional live loads. Linear material behaviour based on

Fig. 9: Construction of the upper slab of the basement and the columns. (ELI 2015)



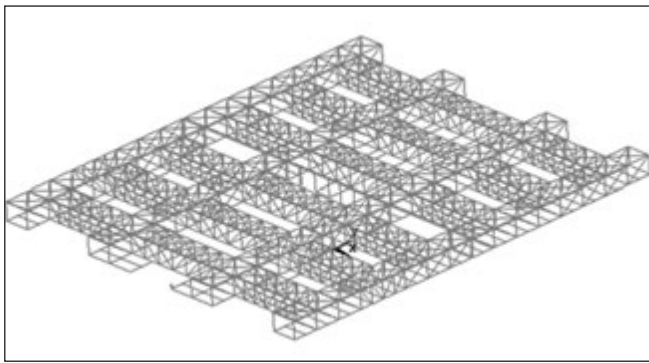


Fig. 10: Numerical model of the roof structure

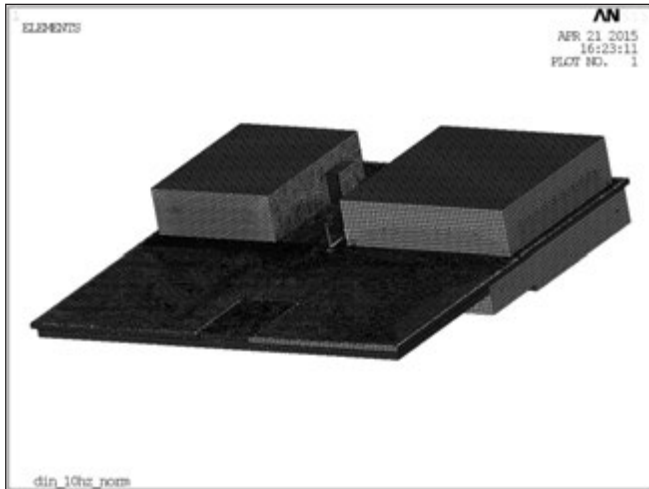


Fig. 11: Numerical model of the internal structure

S235 steel and C30/37 concrete material class was assumed for the analysis. The challenge in the modelling was the complex geometry, boundary condition and excessive amount of structural elements (Lovas A., Dunai L., et al 2013).

4.2 Internal structure

The modelling of the internal structure was far more difficult and complex. The FEM model was made again using ANSYS software, containing the basement, the honeycomb columns, the corkboards, the vibration-free slab and the HTA/MTA bunkers as well (Fig. 11). All the structural elements were modelled with shell elements (four nodes, 6-6 DOF). Linear material behaviour as of C30/37 concrete was assumed, similarly to the previous model. The dominant load case of this structure was the self-weight (sum of 520000 kN) with a rather uneven distribution. Additionally the self-weight of the walls, slabs and the steel frames of the LTA frames were considered along with a predicted overall live load of 10 kN/m² acting on the vibration-free slab.

The corkboards were modelled as linear springs acting in all three dimensions. As a simplification in the numerical model these spring were “smeared” over the surface of the vibration-free slab. To be able to take into account the different corkboard distribution, eight zones were defined (Fig. 12). Within each zone the stiffness of the corkboard springs were constant, between the zones varying, according to the actual situation.

During modelling the complex foundation system (soil changing + piles) was neglected and the effect of the foundation was modelled with linear springs. Similarly to the modelling of corkboards, three zones were defined to set the spring coefficients. These coefficients were calculated by the Department of Geotechnics. The initial numerical values were

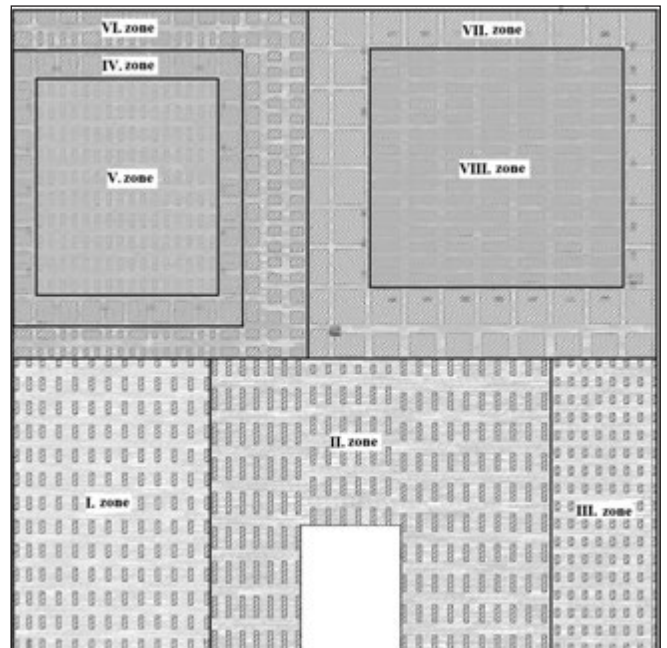


Fig. 12: Corkboard zones

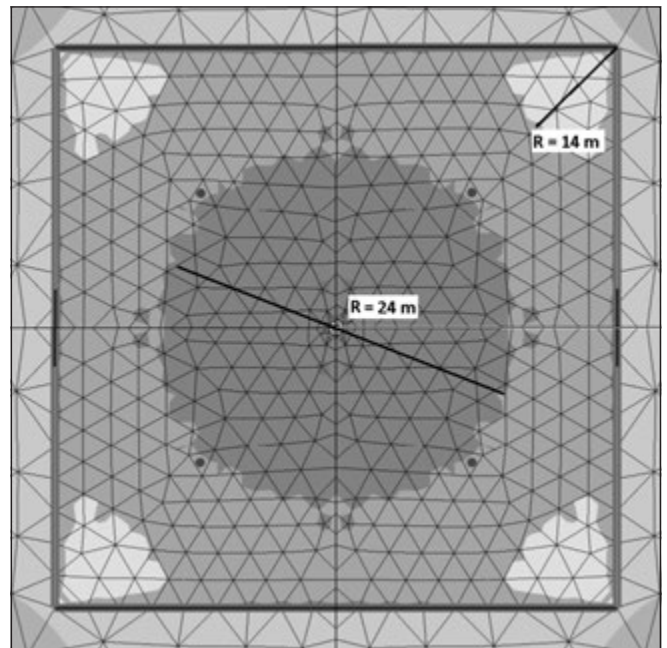


Fig. 13: Foundation zones

1.2 MPa/m, 1.4 MPa/m and 1.75 MPa/m which were later modified according to the in-situ measurements (see Fig. 13).

The geometry of the basement was rather complex because of it's the original shape and the honeycomb columns inside. This resulted in that the meshing process could be done rather difficultly. The mesh size was 70 cm for the shell elements (spring elements does not need meshing). The total number of shell elements was above 90000, the number of linear springs (including both the corkboards and the foundation) was almost 30000.

Continuous consultations with the design team helped to improve the details of the model for both parties. As the construction started several changes were made to the original plans. This also meant that the model has to be modified, improved to keep it updated. The modelling of such a complex structure was a real challenge for both the designer and the inspector's team.

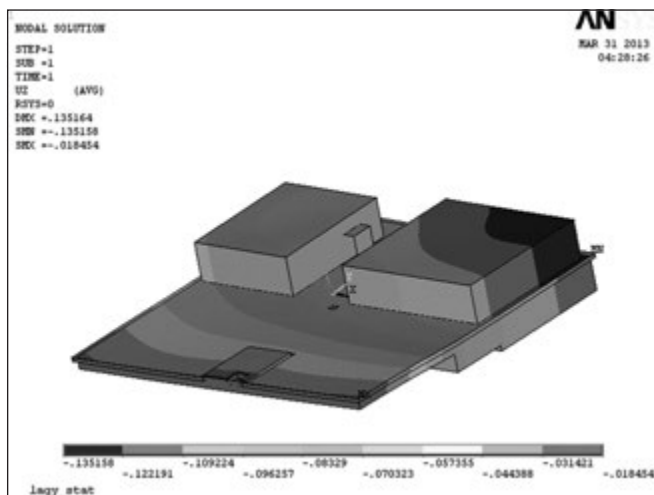


Fig. 14: Total displacement of the internal structure in [mm]

4.3 Analyses

All analyses performed were both material and geometrical linear. A simple static analysis was performed to check the load bearing capacity of the structures. For the internal structure, which has to fulfil several additional requirements, detailed investigations were performed. Deflections due to settlement, difference of deflection due to internal load redistribution were studied (Fig. 14). Detailed earthquake analysis was carried out to investigate the potential collision of the central column and the inner structure among others. Since the extremely complex structural behaviour, consultation with the designer was needed several times to set the ac-

ceptable parameter values. Finally all criterion regarding the static and earthquake requirements were met.

The strictest criterion was connected to vibration. For this a modal analysis was performed to investigate the eigenfrequencies and eigenshapes of the internal structure. Because of the extremely low criterion and the uncertainty of input parameters (such as vibration frequency, direction, damping coefficient, material behaviour), the vibrations were further studied. Time-history analyses were performed for different input records to show the behaviour of the structure. To be completely certain about the vibration behaviour of the structure, a monitoring system will be built after the construction works finished. Based on the measurements of this monitoring system the actual behaviour will be visible, and direct vibration control can be achieved during experiments.

5. CONCLUSION

This paper introduced the ELI project, a new international scientific cooperation in the field of laser research. The Hungarian element of the project, the ELI-ALPS is right now under construction near Szeged (Fig. 15). The extremely strict requirements are based on the function of the facility, the precision of the planned experiments. This led to innovative structural solutions, never before used in Hungary or Europe. These requirements were outlined, and the structural system was introduced briefly. The independent numerical modelling was described. The continuous consultations helped in the improvement and modification of the model. Nevertheless a vibration monitoring system has to be built, to get certain information how the extremely strict requirements are met.

Fig. 15: View of the building site with the facility and with the rain reservoir (ELI 2015)



6. ACKNOWLEDGEMENT

The authors wish to express their gratitude to the ELI-HU Non-Profit Ltd. and to the designers of the ELI-ALPS facility for the information about the ELI project.

7. REFERENCES

- ANSYS Inc. (ANSYS) (2011), «Structural Analysis Guide, Online Documentation»
- ÁKA 2012 Consortium (ÁKA) (2015), “Technical contract documentation of the ELI-ALPS” (In Hungarian), Artonic Design Architectural Ltd., Taupe Ltd., Földvári Ltd., Konzulterv LP. (In Hungarian)
- ELI-HU Non-Profit Ltd. (ELI) (2015), “www.ELI-hu.hu”.
- Lovas, A., Dunai, L., et al (2013), „ELI Laser Research Center Drawing Inspection Document” (In Hungarian), BME,.

Prof. György Farkas (1947) civil engineer (MSc), PhD, Dr. habil, professor at the Department of Structural Engineering, Budapest University of Technology and Economics. *Main fields of interest:* construction and design of prestressed concrete structures, Member of the Hungarian Group of *fib* and the Hungarian Academy of Engineers.

Péter Hegyi (1988) civil engineer (MSc), PhD student of the Structural Engineering Department, Budapest University of Technology and Economics. *Main fields of interest:* thin-walled steel structures, bracing effect of ultra-lightweight concrete, time dependent behaviour.

Dr. István Völgyi (1979) civil engineer (MSc), PhD, assistant professor at the Department of Structural Engineering, Budapest University of Technology and Economics. *Main fields of interest:* design methods for reinforced concrete girders, shear behaviour of RC girders, spun-cast concrete structural elements. Member of the Hungarian Group of *fib*.

POSSIBLE MECHANICAL DETERIORATION OF FIBRES INFLUENCED BY MIXING IN CONCRETE



Olivér Czoboly – György L. Balázs

Favourable experience with fibre reinforced concrete (FRC) resulted in its increasing use worldwide. The properties of fibre reinforced concrete are mostly influenced by the fibre type and the amount of fibres. Fibre properties (tensile strength, length, surface characteristics, shape and density) are normally defined by the fibre producers. However, the properties of hardened FRC are influenced by the properties of fibres existing after mixing.

The question is whether the properties of fibres can be significantly influenced by the mixing procedure. Herein we studied how the 2 to 30 minute mixing time in concrete influences the fibre properties of different fibre materials and fibre shapes. According to our experimental study some of the fibres were deteriorated during the mixing in concrete. The type and degree of deterioration significantly depends on the properties of the fibre. The typical deterioration types of the tested fibres were summarized in our article.

Keywords: fibre, mechanical deterioration, tensile strength of fibre, FRC, Fibre Reinforced Concrete, CMOD, residual flexural strength

1. INTRODUCTION

Since 1874 A. Bernard used to strengthen concrete by the help of addition of steel splinters (Maidl, 1995). Porter in 1910 mentioned the possibility of applying short wire in concrete (Katzner, 2006). In 1965, J. P. Romualdi (USA) applied a patent on steel wire reinforced concrete already reported by him in 1963 (Palotás, 1977).

More and more fibre types were developed with better and better properties because of the good experiences. There are a large number of different fibre materials (steel, polymer, glass, carbon, basalt, natural fibres) which can be used in practice (Fig. 1).

The homogeneous dispersion of the fibres is very important to achieve the best performance of FRC. The manufacturers of the fibres specify the type of mixing (dry or wet) and the minimum mixing time after addition of fibres in concrete.

The main question is whether the properties of fibres can be significantly influenced by the mixing procedure. Herein

Fig. 1: Some typical fibres used in concrete

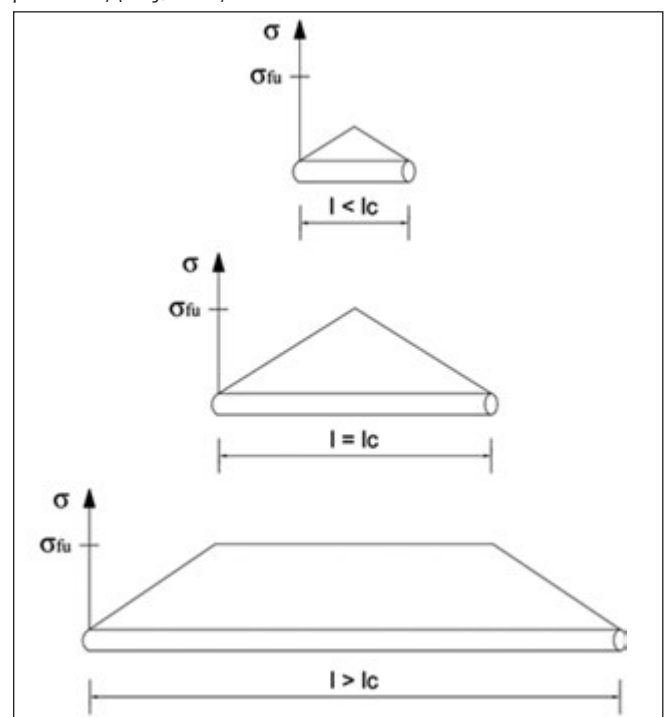


we studied how the 2 to 30 minute mixing of concrete influences the fibre properties of different fibre materials and fibre shapes.

2. LITERATURE REVIEW

Almost all the properties of FRC depend on the bond of fibres (Naaman, Najm, 1991). Several researches (Feng, Sun, Wang,

Fig. 2: Tensile stress of the fibres with different lengths (l_c - critical length=fibre length at which the fibre first breaks instead of being pulled out) (Kelly, 1973)



Shi, 2014; Halvax, Lubl6y, 2013; Kopecsk6, 2002; Zile, Zile, 2013) dealt with the bond of different fibres.

The bond of fibres mainly depend on material, shape, surface of fibres and the mechanical properties of the matrix, the amount of fibres and the loading rate (Bal6zs, Polg6r, 1999; Kov6cs, Bal6zs, 2003). Consequently, almost all properties of FRC changes with the changing of the surface and the shape of fibres.

The appropriate fibre length is very important for effective usages of fibres. If the fibre lengths are too short the fibres will pull out from the mixture and the whole load bearing capacity of the fibres cannot be utilized (Fig. 2).

As written in the introduction, the homogeneous dispersion of the fibres is particularly important. Fibres may even negatively influence the properties of concrete if quality of casting is poor (Fig. 3). Too many fibres will concentrate at certain locations; therefore, the slurry cannot totally surround the fibres. Bond of these fibres will not be appropriate. At other parts of the mixture there will be less fibre than planned. As a result, the manufacturers of the fibres determine the minimum mixing time after addition of fibres into the concrete.

Fig. 3: Possible changing of properties of FRC depending on the volume fraction of fibres (Schematic curve: A, B, C, D curves mean different fibres types and different quality of casting) (Naaman, Paramasivan, Bal6zs et al., 1996)

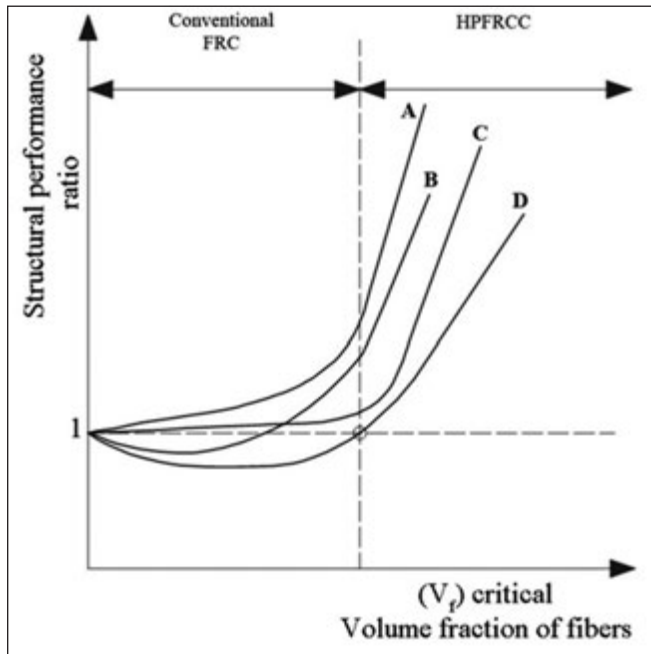


Fig. 4: Three-point bending test set-up (dimensions are in mm)(fib Model Code 2010, 2013)

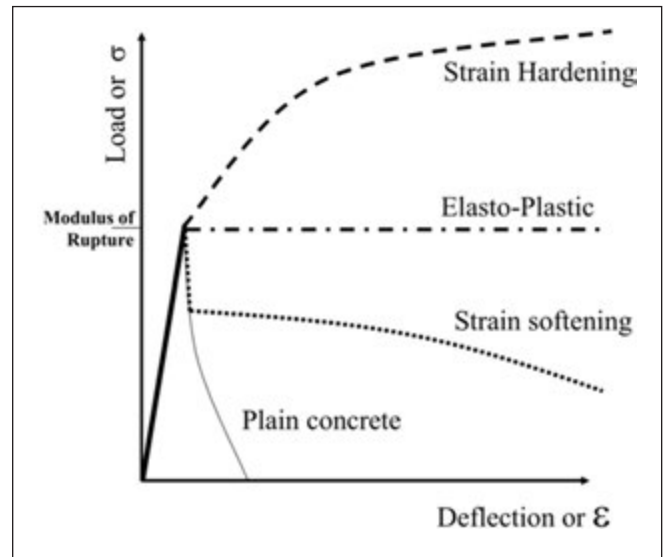
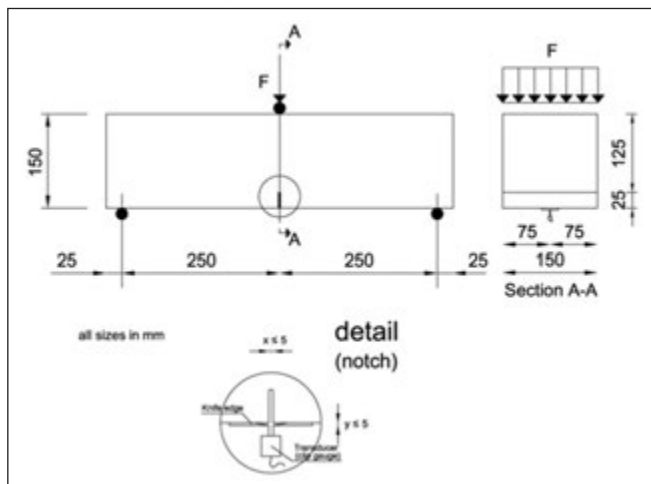


Fig. 5: Typical load/ deflection (stress/ strain) diagrams of fibre reinforced concrete (Cement and Concrete Association of New Zealand, 2009)

Several researchers tested the durability of FRC. Those showed that some types of fibres (different glass fibre types) could deteriorate in the concrete because of the high pH of concrete (Kopecsk6, 2004). We have got only a few information about the influence of the mixing procedure on the properties of fibres.

Herein we studied how the 2 to 30 minute mixing of concrete influences the fibre properties of different fibre materials and fibre shapes. We tested the tensile strength of fibres and performed three-point bending tests on notched FRC beams according to EN 14651:2005+A1:2007.

FRC has residual flexural strength after cracking. The residual post-crack flexural strength of FRC depends on the fibre type and the fibre dosage. The post-cracking flexural strength of FRC beams can be even higher than the flexural strength caused by the cracking moment (Fig. 5).

3. EXPERIMENTAL PROGRAMME

We tested two types of steel fibres (a fibre without coating and another with brass-coating), three types of macro polymer fibres and two basalt fibres (with different lengths) (Tab. 1). (Macro polymer fibres are designated as polymer fibres with higher than 0.3 mm diameter (EN 14889-2:2006)).

During our tests similar mix composition (Tab. 2) and same consistence (flow class: F4) were used. Quartz aggregates ($d_{max}=16$ mm, fineness modulus = 5.6) were used for all mixtures. The particle size distribution curve of the aggregate is included in Czoboly and Bal6zs (2014). The fibre type, the fibre content (0,3V%, 0,5V%) and the quantity of superplasticizing admixture (Glenium C300) were different in the different mixtures. The fibres were added to the fresh concrete. The mixing process was done with forced type concrete mixer. After removing the specimens from the formwork they were stored in water for 7 days then kept at laboratory conditions until testing. 28 days old specimens were tested in three-point bending test.

We developed a procedure to isolate the fibres (even the fibre diameter is only a few μ m) from the fresh concrete without further deterioration, consequently we could test the fibre properties before and after mixing.

Table 1: Properties of tested fibres

	Material	Fibre length [mm]	Fibre diameter [μm]	Density [kg/m^3]	Tensile strength [N/mm^2]
S-1	Steel	50	1000	7850	1000-1200
S-2	Steel (Brass-coated)	12	200	~ 7850	3000
P-1	Polymer (Modified olefin)	48	~ 800	900-920	640
P-2	Polymer (Polyolefin)	50	500	910	510
P-3	Polymer (Polypropylene)	54	320	910	> 500
B-1	Basalt	12	13-20	~ 1900	
B-2	Basalt	24	13-20	~ 1900	

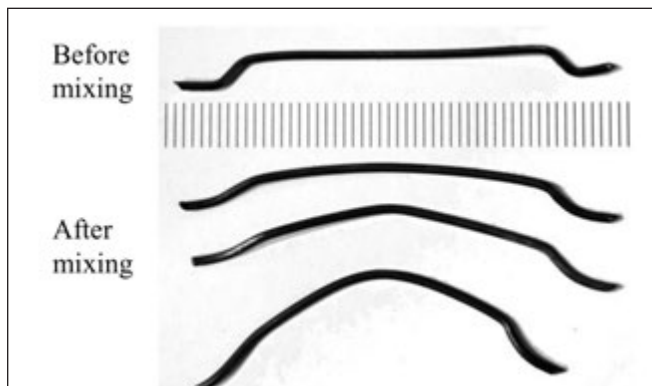
4. CHANGING OF FIBRE PROPERTIES DURING MIXING IN CONCRETE

Our laboratory tests indicated different changes of fibre properties for different fibres due to mixing. Different ways of mechanical deterioration was observed depending on the material, production technology, coating, size and surface of fibres. The mechanical deterioration methods depended mainly on the fibre material. We summarized the typical mechanical deterioration for different fibre materials in *Tab. 3*.

We did not experience significant change of properties of fibres in case of non-coated steel fibre (S1 fibre in *Tab. 1*) caused by mixing in concrete. Shape deformation was observed for some fibres during mixing (*Fig. 6*). The shape deformation probably does not significantly influence the properties of FRC. Abrasion of coating and also shape deformation were observed in case of coated fibres (S2 fibre in *Tab. 1*) during mixing.

The surfaces of macro polymer fibres were changed during the mixing (P1, P2 and P3 fibres in *Tab. 1*). The surface pattern of the polymer fibres abraded and the surface started to nap during mixing (*Fig. 7*). The nap of surface was increased as mixing time increases. The nap of surface was observed in all macro polymer fibres which were tested. The degree of the nap of surface depended on the material of fibre, the diameter and the surface of the fibre. The abraded fibre materials were isolated from the fresh concrete (*Fig. 8*).

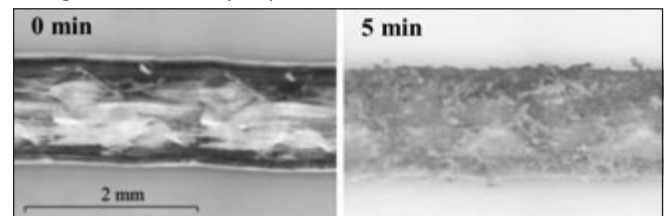
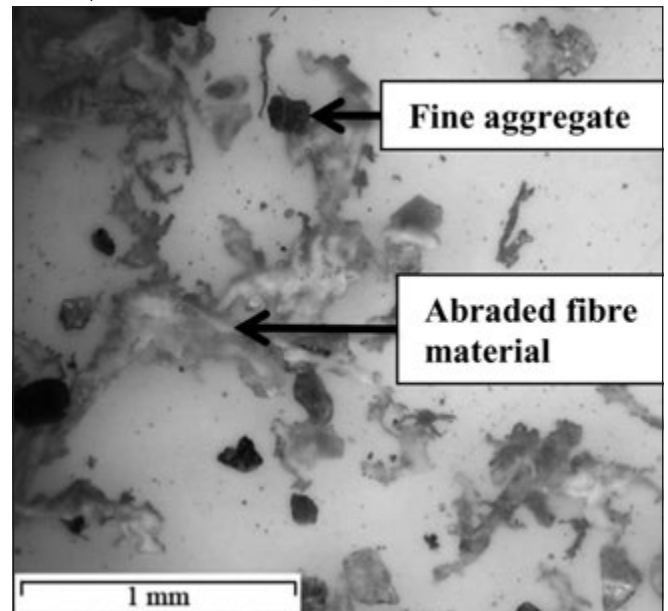
Some typical mechanical deterioration modes can be seen in *Fig. 9*. These deterioration modes were observed already after 2 minutes long mixing of concrete and the number of deteriorated fibres increased as mixing time increases.

Fig. 6: Shape deformation of steel fibres [S1 fibre in *Tab. 1*]**Table 2:** Concrete composition

Material	Type		Mass [kg/m^3]	Volume [litre/m^3]
Aggregate	0/4 mm fraction	45%	824	311
	4/8 mm fraction	55%	1008	380
	Σ	100%	1832	691
Cement	CEM I 42,5 N		380	123
Fibre
Water	$m_w/m_c =$	43,0%	163	163
Admixture cem. m%		0,70%	2,66	2,66
Air				15

The slurry was stuck on the napped surface of the fibre and some aggregate penetrated into the fibre (*Fig. 10*). The density of some fibres increased during the mixing of concrete. The macro polymer fibres floated on the water before mixing (density of fibre was cca. 890 kg/m^3) and some fibre sunk in the water after mixing (density of these fibres was more than 1000 kg/m^3) (*Fig. 11*).

The fibres were added to fresh concrete. The mixing times were measured from the moment of addition of fibres. Samples were removed from the fresh concrete after 5 and 30 minutes. The fibres were isolated from the fresh concrete. Tensile tests were carried out on the P2 type (*in Tab. 1*) fibres without mixing, after 5 minutes mixing and 30 minutes mixing in concrete. The tensile tests were carried out on 30 pieces of fibres per mixing times (0 min, 5 min and 30 min) with

Fig. 7: Abrasion of surface pattern of the macro polymer fibre (the mixing time is on the top of pictures) (P1 fibre in *Tab. 1*)**Fig. 8:** Microscope picture about the abraded fibre material (P2 fibre in *Tab. 1*)

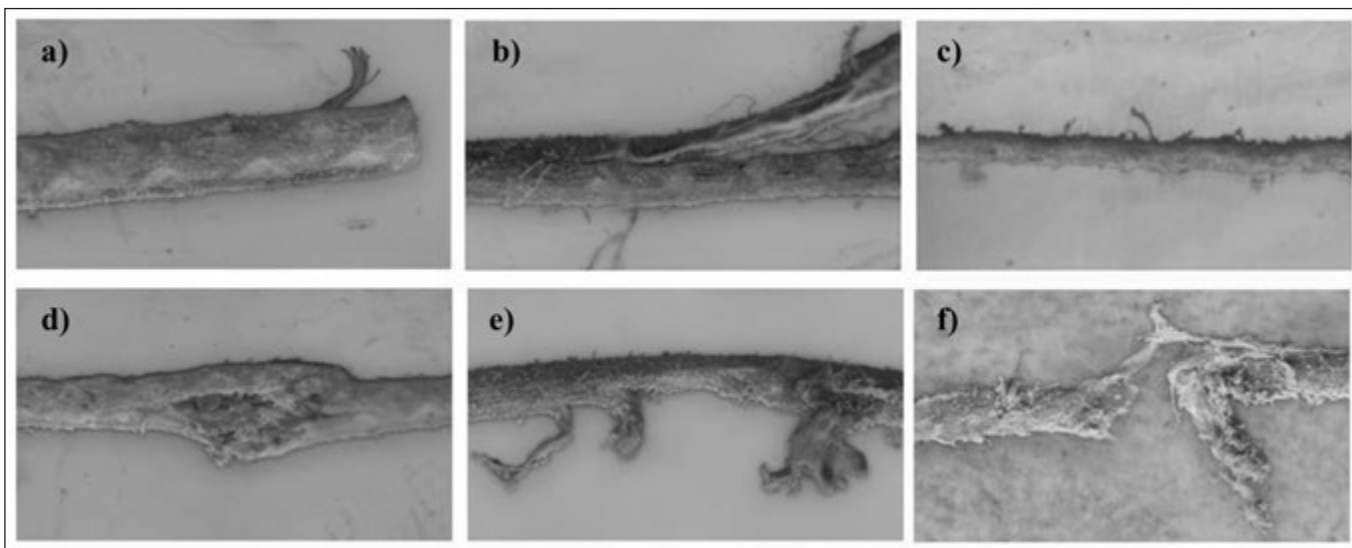


Fig. 9: Mechanical deterioration of polymer fibres (P1 fibre in Tab. 1)
a) disintegration of fibre end, b) opening of fibre end, c) splitting of fibre, d) bruise of fibre, e) notch in fibre, f) shortening of fibre length

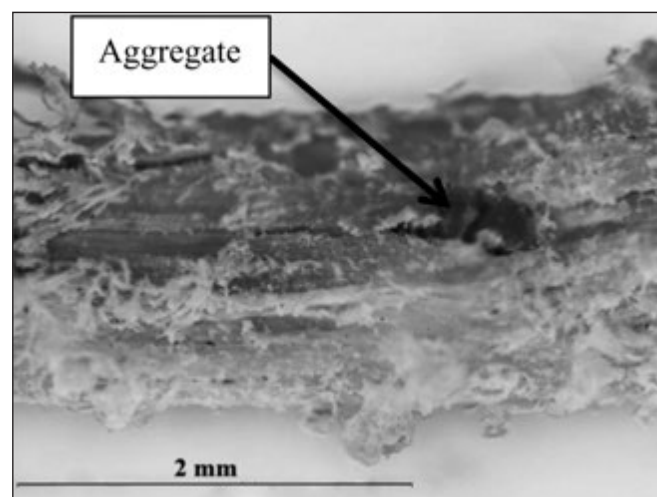


Fig. 10: Aggregate penetration into the fibre during mixing in concrete (P1 fibre in Tab. 1)

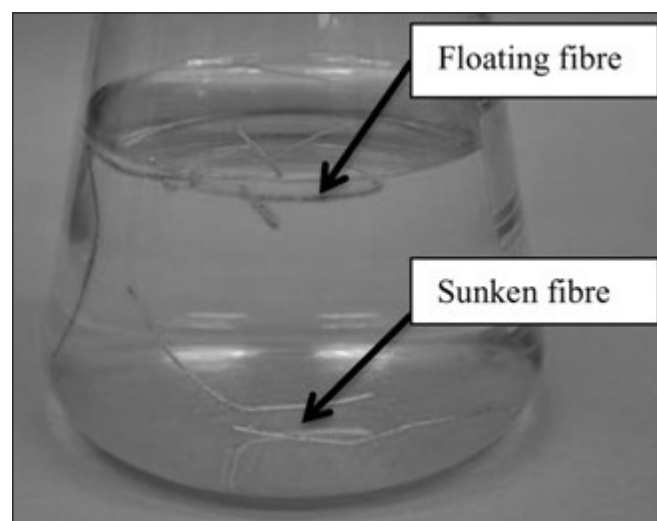


Fig. 11: Behaviour of macro polymer fibres in water after mixing in concrete (P1 fibre in Tab. 1)

10 mm/min loading rate according to EN 14889-2:2006 standard. The results of tensile tests can be seen in Fig. 12. The thick lines show the 2nd order fitting curve to the average of the results of 30 pieces of fibres. Mixing time increased scatter of results as indicated in Fig. 12.

The tensile forces of the macro polymers fibres (P1 fibre in Tab. 1) decreased as the mixing time increases. In Fig. 12

Table 3: Possible mechanical deterioration of fibres influenced by mixing in concrete

Fibre type	Type of fibre deterioration		See
Steel fibre	deformation of shape		Fig. 6
	abrasion of coating (if exist)		
Macro polymer fibre	abrasion	abrasion of surface pattern	Fig. 7
		abrasion of fibre material	Fig. 8
		nap of surface	Fig. 10
	deterioration starting from the end of fibre	disintegration of fibre end	Fig. 9/a
		opening of fibre end	Fig. 9/b
		longitudinal splitting of fibre	Fig. 9/c
	destruction of fibre	local damage of fibre	Fig. 9/d
		opening of fibre in its middle portion	
		notch in fibre	Fig. 9/e
		shortening of fibre length	Fig. 9/f
	aggregate penetration into the fibre	Fig. 10	
Mono basalt fibre	shortening of fibre length		Fig. 14

it can be seen that the deviation of the Force vs. Strain curves increased as the mixing time increased. The inclination of the curves decreased as the mixing time increased. The decrease of the inclination of the curves might be explained by the abrasion of fibre material, and also by the smaller diameter of the fibres and by the different type of mechanical deterioration of the fibres.

We observed that the mechanical deterioration of the fibres and the decrease of tensile forces of the fibres significantly depend on the properties of the applied fibres (material, tensile strength, surface characteristics, shape and size of fibres). The mechanical deterioration of the fibres might be explained also by the properties of fresh concrete (grain of aggregate, ratio of fraction of aggregate, density of aggregate, consistence of fresh concrete), mixing method, abrasion of mixing paddles, mixed volume, adding moment of fibres (to fresh concrete or to dry components).

Three-point bending tests were made on notched FRC

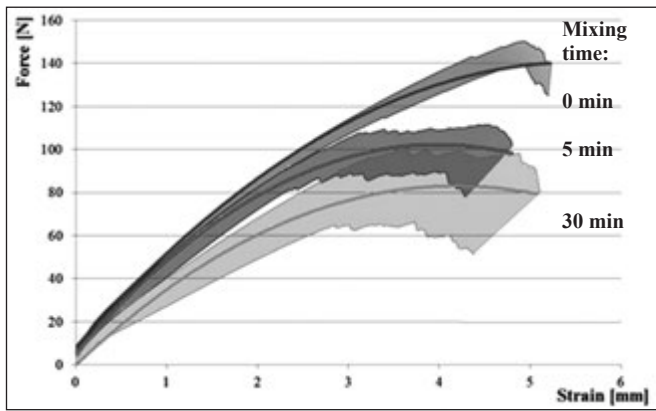


Fig. 12: Average and distribution of Force vs. Strain diagram of tensile test of P2 fibres (in Tab. 1) without mixing, after 5 min and 30 min mixing in concrete (The tensile tests were made on 30 pieces of fibres for each mixing times (0 min, 5 min and 30 min) with 10 mm/min loading rate.)

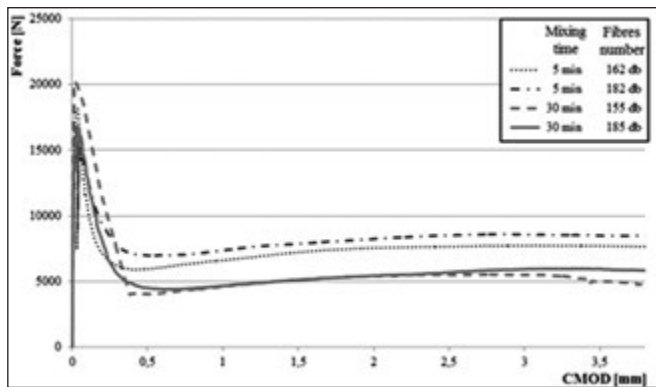


Fig. 13: Force-CMOD curves of Three-point bending tests of FRC beams with P2 fibres (in Tab. 1), (each curve shows a measurement, the number of fibres was counted in the cracked cross-section)

beams according to *EN 14651:2005+A1:2007*. In *Fig. 13* can be seen the results of three-point bending tests of FRC beams with the P2 fibres (see in *Tab. 1*). The post-cracking residual flexural forces of FRC beams decreased by the longer mixing times (for same fibre numbers). The decreasing of the post-cracking flexural forces might be explained by the decrease of tensile forces of fibres in case of longer mixing times.

We also tested the mechanical deterioration of mono basalt fibres. The shortening of fibre length of mono basalt fibres (B1 and B2 fibres in *Tab. 1*) were observed after mixing (*Fig. 14*).

The fibres were isolated from the fresh concrete after 5, 10, 15 and 20 minutes mixing times. The lengths of fibres were measured on pictures taken by digital microscope. In *Fig 15*, the mean length of fibres can be after of different mixing times in concrete. (Each value is the average of 100 measurements.) *Fig. 15* indicates that the mean value of fibre length decreased as the mixing time increased. The intensity of decrease of mean fibre length was higher in the first 5 minutes

Fig. 14: Shortening of fibre length of mono basalt fibres (B2 fibre in Tab. 1) during mixing in concrete (at the top of the pictures mixing time after the adding of fibres can be seen)

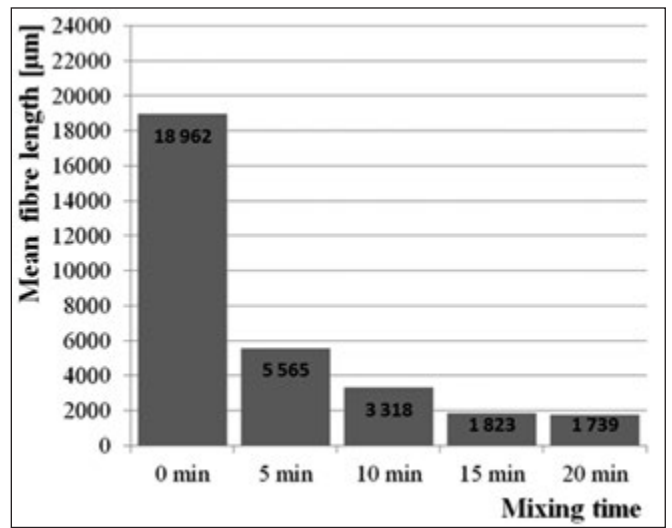
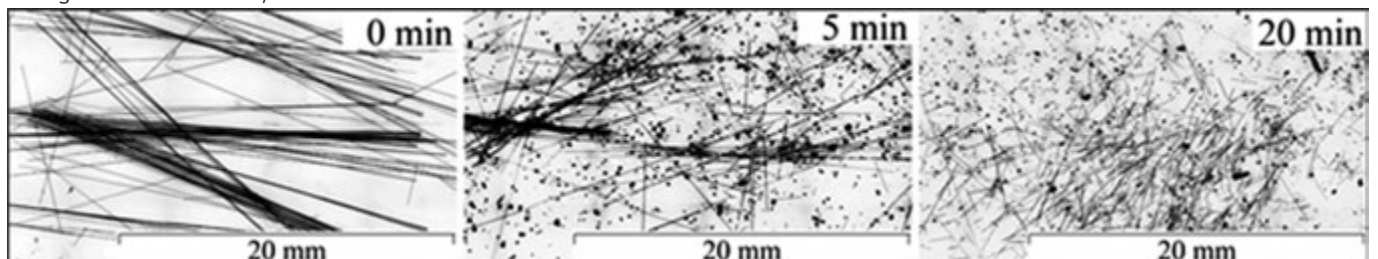


Fig. 15: Mean fibre length of mono basalt fibres (B2 fibre in Tab. 1) without mixing and 5, 10, 15, 20 min mixing in concrete (Each value is an average of 100 measurements.)

than later. The intensity of the decrease of mean fibre length continuously decreased until 20 minutes mixing time.

5. CONCLUSIONS

Main purpose of our experimental study was to determine the effect of mixing time (2 min to 30 min) on the properties of fibres FRC, respectively. We tested two types of steel fibres (one without coating, and another with brass-coating), three type macro polymer fibres and two basalt fibres (having different lengths).

A procedure was developed to isolate the fibres (even if the fibre diameter is only a few μm) from the fresh concrete without further deterioration. We tested the fibre properties both before and after mixing.

According to the results of our experimental study some of the fibres were deteriorated during mixing in concrete. The type of deterioration and the degree of deterioration significantly depended on the material, production technology, coating, size and surface of fibres. Deterioration types of the tested fibres were summarized in our article.

Shape deformation was observed in case of some steel fibres during mixing. This shape deformation probably does not influence significantly the properties of FRC. Abrasion of coating and also shape deformation were observed for coated fibres during mixing.

In case of the macro polymer fibres abrasion, deterioration that started from the end of fibres and destruction of fibres occurred.

The tensile forces of the tested macro polymer fibres decreased as the mixing time increased. The deviation of the Force-Strain curves increased as the mixing time increased.

The steepness of the curves decreased as the mixing time increased. The decrease of the steepness of the curves might be explained by the abrasion of fibre material, by the smaller diameter of the fibres and by the different types of mechanical deterioration of the fibres.

The post-cracking flexural forces of FRC beams decreased as the mixing times increased (for same fibre type and fibre numbers). The decrease of the post-cracking flexural forces might be explained by the decrease of tensile forces of fibres in case of longer mixing times.

Shortening of mono basalt fibres were observed after mixing in concrete. The fibre length decreased as the mixing time increased.

Type and degree of mechanical deterioration of the examined fibres were different for the same mixture and mixing time because the fibres had different impact at different locations in the concrete. Some fibres spent longer time near the mixing paddles and the others contacted only with the aggregates. Sometimes the degree of mechanical deterioration of fibres was different along the fibre length.

Mechanical deterioration of fibres also can be seen after 2 minutes, but the degree of deterioration and the number of deteriorated fibres increased as the mixing time increased.

6. ACKNOWLEDGEMENT

The authors gratefully acknowledge the possibility of using the digital microscope at the Department of Polymer Engineering (BME). We acknowledge specifically to dr. Bálint Morlin, dr. Salem G. Nehme, dr. Katalin Kopeckó, Viktor Hlavíčka and Sándor Sólyom for their help and advices.

7. REFERENCES

- Balázs, G. L., Polgár L. (1999): „Past, present and future of fibre reinforced concrete” (A szálerősítésű betonok múltja, jelene és jövője), *Vasbetonépítés*, Vol. 1., No. 1., pp. 3-10.
- Cement and Concrete Association of New Zealand (2009): „Fibre Reinforced Concrete, Information Bulletin IB 39, 19 p.
- Czoboly, O., Balázs, G. L. (2015): “Possible deterioration of fibres influenced by mixing in concrete” (Szálak lehetséges károsodása betonban való keverés során), *Vasbetonépítés*, ISSN 1419-6441, online ISSN: 1586-0361, Vol. XVI., No. 4., pp. 91-95., http://www.fib.bme.hu/folyoirat/vb/vb2014_4.pdf
- EN 14651:2005+A1:2007 (2007): “Test method for metallic fibre concrete – Measuring the flexural tensile strength (limit of proportionality (LOP), residual), European Committee for Standardization, 17 p.
- EN 14889-2:2006 (2006): „Fibre for concrete - Part 2: Polymer fibres – Definitions, specifications and conformity” European Committee for Standardization, 27 p.
- Feng, J., Sun, W. W., Wang, X. M., Shi, X. Y. (2014): „Mechanical analyses of hooked fibre pullout performance in ultra-high-performance concrete”, *Construction and Building Materials*, Vol. 69, pp. 403–410.
- fib* Model Code 2010 (2013): “*fib* Model Code for Concrete Structures 2010”, Ernst & Sohn, ISBN 978-3-433-03061-5, 402 p.
- Halvax, K., Lublőy, É. (2013): „Pull-out behaviour of steel fibres”, *Fibre Concrete 2013*, Czech Republic, Prague, 2013 September 12-13., pp. 1-10.
- Katzer, J. (2006): „Steel Fibers and Steel Fiber Reinforced Concrete in Civil Engineering”, *The Pacific Journal of Science and Technology*, Vol. 7. No. 1., 2006 May, pp. 53-58.
- Kelly, A. (1973): „*Strong Solids*”, 2nd edn, Clarendon Press, Oxford, 285 pp.
- Kopeckó, K. (2002): „Bond of Glass Fibres in Concrete”, In: Balázs, G. L., Bartos, P. J. M., Cairns, J., Borosnyói, A., *Bond in Concrete; from research to standards: Proceedings of the 3rd International Symposium*, Budapest, pp. 799-808.
- Kopeckó, K. (2004): „Durability of Glass Fibres”, In: di Prisco M., Felicetti R, Plizzari G. A., *Fibre-Reinforced Concrete, BEFIB 2004: Proceedings of the 6th RILEM Symposium on Fibre Reinforced Concrete (PRO 39)*. Varenna, Italy, 2004. 09. 22-24., pp. 583-592.
- Kovács, I., Balázs, G. L. (2003): „Structural behaviour of steel fibre reinforced concrete”, *Journal of Structural Concrete*, 2003/2, pp. 57-63.
- Maidl, B. R. (1995): „Steel Fibre Reinforced Concrete”, *Ernst & Sohn, ISBN-10: 3433012881*, 292 p.
- Naaman A. E., Najm H. (1991): „Bond-Slip Mechanism of Steel Fibers in Concrete”, *ACI Materials Journal*, 1991 March-April, pp. 135-145.
- Naaman, A. E., Paramasivam P., Balázs, G. L. et al. (1996): “Reinforced and prestressed concrete using HPRCC matrices” *Proceedings of the 2nd Int. RILEM/ACI Workshop*, Ann Arbor USA, June 11-14, 1995. (eds. Naaman and Reinhardt), E & FN Spon London, pp 291-347.
- Palotás, L. (1977): „Design and crack prediction of steel wire reinforced concrete”, *Steel wire reinforced concrete*, pp. 69-79., www.pp.bme.hu/ci/article/download/4148/3253 (download: 2014. 12. 11.)
- Rácz K. (2008): „Machines of concrete technology” (Betontechnológia gépei), teaching material for Structural Engineers to Concrete technology training, 156 p.
- Wischers, G. (1974): „Fibre Reinforced Concrete” (Faserbewehrter Beton), *Beton* 24, Heft 3, pp. 95–99 and Heft 4, pp.137–141.
- Zile, E., Zile, O. (2013): „Effect of the fibre geometry on the pull-out response of mechanically deformed steel fibers”, *Cement and Concrete Research*, Vol. 44, pp. 18-24.
- Olívér Attila Czoboly** (1988) Civil Engineer, PhD student (Department of Construction Materials and Technologies, Budapest University of Technology and Economics). His main fields of activities are experimental investigation and modelling of FRC structures, HPC, structural diagnostics, reconstruction of structures, fire resistance of concrete. He is member of *fib* and Hungarian Group of *fib*. He is the secretary of *fib* Commission 9 „Dissemination of knowledge”.
- György L. Balázs** (1958), Civil Engineer, PhD, Dr.-habil., professor of structural engineering, head of Department of Construction Materials and Technologies and Deputy Dean of the Civil Engineering Faculty of Budapest University of Technology and Economics (BME). His main fields of activities are experimental investigation and modelling of RC, PC, FRC structures, HSC, fire resistance of concrete. He is chairman of several commissions and task groups of *fib*. He is president of Hungarian Group of *fib*, Editor-in-chief of the Journal “Concrete Structures”. He was elected as President of *fib* for the period of 2011-2012.

THE EFFECT OF AGGREGATE SIZE ON THE BEHAVIOUR OF BEAMS WITHOUT SHEAR REINFORCEMENT



Rita Vajk – István Sajtó

In this paper an engineering model is presented to calculate the load bearing capacity and the ductility of reinforced concrete beams without shear reinforcement. The applied numerical model takes into account the real, size dependent stress-strain diagram of concrete and the localization of the deformation in both the compression damage and the cracking due to tension.

The recent shear resistance calculation methods, which consider the interaction between bending and shear, are also used to get good estimation for the shear resistance and the ductility of the beams.

The calculation method is compared to experimental results of a series of 18 beams with two type of reinforcement ratio and 3 type of aggregate composition. Good agreement was found between theory and experiment.

Keywords: shear resistance, aggregate composition, cohesive crack

1. INTRODUCTION

Design of outstanding and innovative structures requires precise and real information about behaviour of structures for both ultimate- and serviceability limit state. This paper investigates how the beam size and aggregate composition of concrete influences the behaviour of RC beams.

Most of the civil engineers in Europe use the methods of Eurocode 2 to calculate the load-bearing capacity and ductility of RC structures. The calculations can be refined to get more precise answers if one would consider more complicated calculation model which requires more properties of the beam and the material it is made of. Commonly used parameters are strength of the concrete and the steel, the size of the concrete beam, and the number and size of the reinforcing steel bars. Less known is that aggregate composition also influences the load bearing capacity and the type of behaviour of RC beams. The aggregate composition will be characterized by the largest aggregate size, d_{max} . Its effect is considered through aggregate size dependent, engineering type material laws. A firm basis of this type of models may be found in the literature (Bažant, 1998; MC1990; Fantilli, 2002, 2007; Karihaloo, 1997; Rodrigues 2010).

The important parameters should be used in the calculation of RC beams depend on the model used and the question asked. The main question now is how the type of behaviour/failure depends on aggregate and beam size.

1.1 CALCULATION OF SHEAR RESISTANCE IN BEAMS WITHOUT SHEAR REINFORCEMENT

In Eurocode 2 (2004) the suggested calculation method for beams without shear reinforcement is based on experimental investigations. Recently several researcher work on the real

physical model of the RC beam without shear reinforcement. The common in these researches is that the load carrying capacity and the deformation ability are calculated based on bending dependent shear behaviour of the beam. Interestingly, the same conclusion can be drawn based on experiments (Muttoni, 2008), and also based on theoretical considerations. The conclusion based on theory is independent of whether applying fracture mechanics (Carpinteri, 2011/1) or traditional theory of reinforced concrete (Bogdándy-Hegedűs, 2014).

The possible future refinement of the European calculation standard is published in the Model Code 2010 (MC 2013). Three possibilities are given for calculating beams without shear reinforcement. Level of Approximation II. is based on the Collins's model (1986), which is called the Simplified Modified Compression Field Theory. Level I. is the conservative simplification of Level II. A third possibility for the calculation recommends using non-linear finite element methods. The Critical Shear-Crack Theory by Muttoni (2008) is proposed by Model Code 2010 to calculate punching shear, however it can also be applied to calculate shear in beams without shear reinforcement, as it has a common physical modelling philosophy to the Modified Compression Field Theory. Fracture mechanics based Bridged Crack Model by Carpinteri (2011/1,2) also gives good estimations for the type of behaviour/failure, even for the location of the critical crack of reinforced concrete beams compared to experimental results.

In this paper the methods published in the Model Code 2010 (MC 2013) and the Critical Shear Crack Theory (Muttoni, 2008) are used.

1.2 AGGREGATE COMPOSITION

When designing a concrete mixture the aggregate composition is characterized by the maximum aggregate size and the weight fractions of the aggregate passing through the standardized

sieve system. Concrete is a strain softening material for both tension and compression. The strain softening branch is influenced by the concrete composition and also the size of the structure itself (Bazant, 1998; Karihaloo, 1997).

In case of tension the fracture energy is used as a material parameter to characterize the strain softening phenomena. Fracture energy is increased as the maximum aggregate size is increased for normal strength concrete (e.g.: Karihaloo, 1997).

In case of compression the slope of the strain softening part defines the stress-strain curve. However this slope is depended on the size of the examined structure (Fantilli, 2007).

When modelling the normal strength concrete subjected to tension using theory of fracture mechanics tools considering the aggregate composition, the hypothesis is that the interface between the cement matrix and the maximum diameter aggregate is the weakest link. This weakest link can be modelled as a penny-shaped crack with diameter equal to the maximum diameter of the grains inside the specimen.

For normal strength concrete the cracks are developed on the interface of the cement matrix to the aggregate. For high strength concrete the aggregate breaks at lower stress than the cement matrix, so the interface between the cement matrix and the aggregate is no longer the weakest link. This phenomenon is considered in the Model Code 2010 too when the shear resistance is calculated.

So while for normal strength concrete the maximum aggregate size is a suitable parameter to characterize aggregate composition then for high strength concrete it is not.

In this paper the models we use are for normal strength concrete and the concrete composition will be characterized by the maximum aggregate size.

2. NUMERICAL MODEL

An RC beam, loaded in three-point bending, is examined in the vicinity of the middle cross section. Since the self-weight of the beam is much smaller compared to the load the beam can resist, this middle cross section can be estimated to give the maximum moment and maximum shear effect of the beam.

In the calculations it was assumed that Bernoulli-Navier's hypothesis is valid, in addition to that the connection between the concrete and the reinforcement is rigid i.e. there is no slip. The simple equations, as usual in the engineering practice, are used to the calculations: equilibrium-, geometrical equations, and non-linear real, grain size, and size dependent material laws.

2.1 MATERIAL MODELS

The following material laws are applied:

a) Behaviour of concrete for tension:

In the calculation the tensile strength of the concrete is not neglected.

After reaching the tensile strength of concrete micro cracks develops, but the specimen has not yet fallen into two parts as between the two sides of the cracks there are still connections by concrete parts and aggregates. These bridging parts are damaged gradually so as the tensile stress gradually decreasing.

The strain softening behaviour can be described as a function of the crack opening, while before cracking the strain is the driving parameter. We adopted smeared crack approach to convert crack opening for strain.

The behaviour model of concrete for tension is linear until f_t , afterwards the so called extra-long tail softening curve (Bazant, 1998) is used, with the grain size dependent fracture energy (Hillerborg, 1976; Karihaloo, 1997):

$$\frac{\sigma_c}{f_t} = 0.075 - 0.00652w' + 0.9250e^{-1.614w'} \quad \text{for } w' \leq 11.5 \quad (1a)$$

$$\text{and } \sigma_c = 0 \quad \text{for } w' > 11.5 \quad (1b)$$

where w' is the non-dimensional crack width, and can be calculated as:

$$w' = w f_t / G_f = \varepsilon_c 3d_{max} f_t / G_f \quad (2)$$

and where f_t is the tensile strength of concrete, and G_f is the d_{max} dependent fracture energy (MC1990).

The crack opening is changed for strain using the size of the crack band size. The crack band size is the function of the maximum aggregate size, and it was estimated as $3d_{max}$. The crack band size is the width of the micro cracked zone around the line of macro crack.

b) The behaviour of concrete for compression:

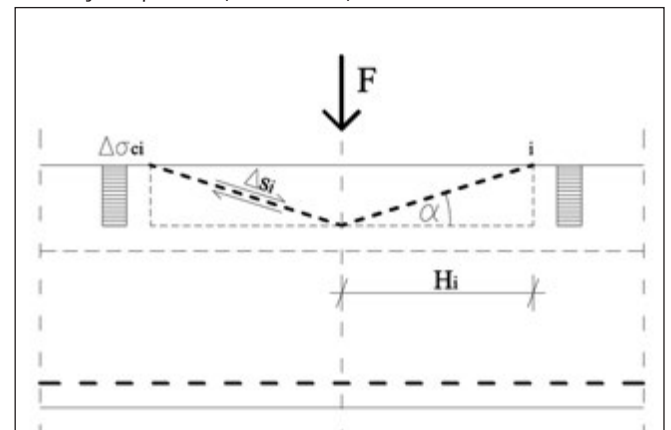
The concrete for compression is modelled based on the Model Code 2010 up to the stress reaches the peak stress f_c :

$$\sigma_c = \frac{\frac{E_c \cdot \varepsilon_c}{E_{c1} \cdot \varepsilon_{c1}} - \left(\frac{\varepsilon_c}{\varepsilon_{c1}}\right)^2}{1 + \left(\frac{E_c}{E_{c1}} - 2\right) \cdot \frac{\varepsilon_c}{\varepsilon_{c1}}} \cdot f_c \quad (3)$$

As soon as the compressive stress of the concrete reaches the peak value f_c localized damage develops along sliding planes (Fig. 1). The sliding plane angle was taken 17.5° which was confirmed by both experimental observation and theoretical consideration too (Fantilli, 2002, 2007). The sliding along the damage planes produces inelastic shortening which determines the post peak average compressive strain. According to the experimental results the slope of the softening branch for compression increases in larger concrete specimen. Therefore longer specimens behave in a more brittle manner, i.e. possibility of longer slip planes results more brittle behaviour. Sliding displacement along the crack due to compression was converted into compressive strain considering the size of the beam part affected by compressive damage. The model proposed by Fantilli et al (Fantilli, 2002, 2007) was adopted to describe the behaviour of concrete for compression after the stress peak.

Following Fantilli (2007), after the peak stress, f_c , is reached, the softening part of the stress-strain diagram is curvature, μ and size dependent:

Fig. 1: Longitudinal sliding of the reinforced concrete element due to failure by compression (Fantilli, 2007)



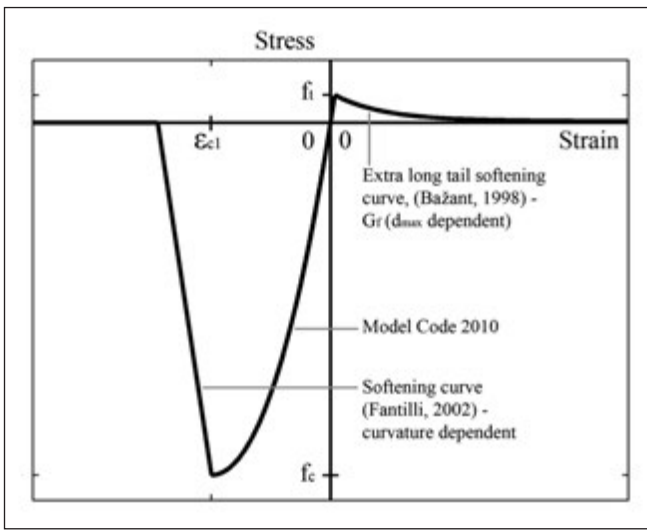


Fig. 2: Material model of concrete for tension and compression

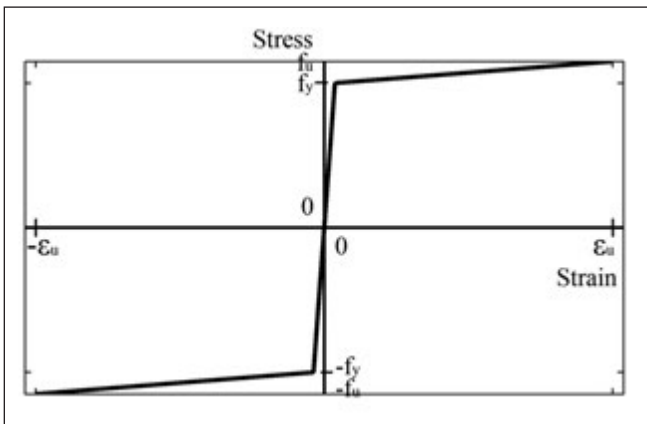


Fig. 3: Material model of steel

$$\sigma_c = f_c - \frac{E_c^2 \cdot \mu \cdot \sin \alpha}{K} \cdot \ln \left[\frac{\mu \cdot (E_c \cdot \sin \alpha - y_{c,max} \cdot K) + K \cdot \varepsilon_c}{\mu \cdot (E_c \cdot \sin \alpha - y_{c,max} \cdot K) + K \cdot \varepsilon_{c1}} \right] + E_c \cdot (\varepsilon_c - \varepsilon_{c1}) \quad (4)$$

In the equations (3) and (4): σ_c is the compressive stress of concrete; f_c is the compressive strength of concrete; E_c is the modulus of elasticity at $\sigma_c=0$; E_{c1} is the modulus of elasticity at $\sigma_c=f_c$; ε_c is the compressive strain; ε_{c1} is the compressive strain at $\sigma_c=f_c$; μ is the curvature of the beam at the cross section examined; $y_{c,max}$ is the location of the neutral axis measured from the compressed extreme fibre; $\alpha \approx 17.5^\circ$ is the sliding slope, position of crack caused by compression measured from horizontal axis; and parameter $K=0.1f_c \cdot \cos \alpha$.

The complete concrete material model for concrete can be seen on Fig. 2.

c) The behaviour of the reinforcement:

A bilinear material law is used to characterize the behaviour of reinforcing bars which is suggested also e.g. in the Eurocode 2 (Fig. 3).

2.2 BENDING FAILURE OF BEAM

The moment – curvature diagram of the cross section is calculated using the equilibrium equations, material laws and the Bernoulli-Navier's hypothesis. The value of the moment is calculated to a chosen curvature value. The chosen material laws make possible consider the effect of tensile strength of concrete, yielding of steel bars for tension and compression failure of concrete. Three parts of the moment curvature

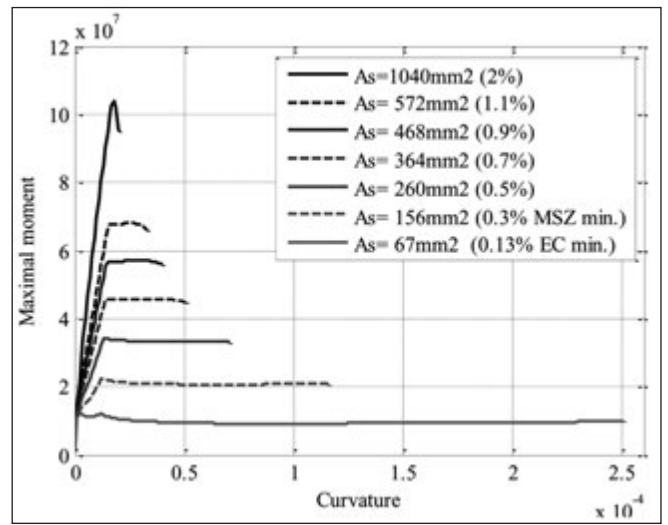


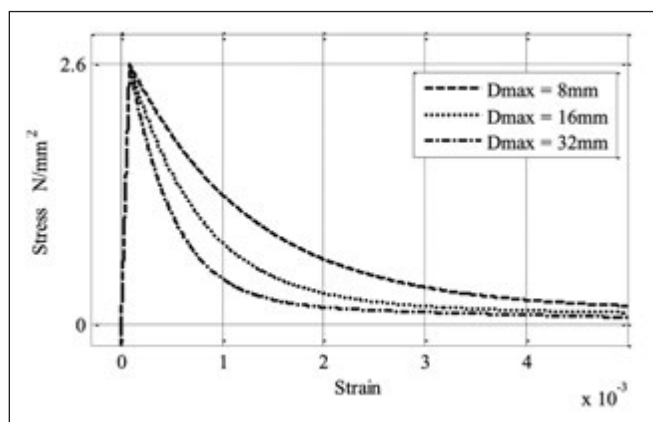
Fig. 4: The effect of reinforcement ratio to moment capacity of the cross-section according to proposed calculation model (cross section size: 200×300mm, C25/30)

diagram can be distinguished. The beginning part represents the state where both the concrete and the reinforcement are in elastic state, meaning, the concrete in tension has not yet cracked. As the first peak or change in stiffness is reached, macro crack developed in concrete by tension, but the steel is still in elastic state (Fig. 4). (The moment when the tensile stress is equal to tensile strength and the moment for the macro crack appear are not the same. The tensile strength indicates the beginning of the cracking process and fully developed the macro crack appears at the end of strain softening curve for tension.) Sometimes, depending on the reinforcement ratio, brittle behaviour is experienced after the first peak in moment, but it is changed for strain hardening path after small deflection for beams having larger reinforcement ratio than the minimum. After the second, more remarkable change in stiffness the steel yields, and a plateau can be seen on the moment curvature diagram of the beam. The deformation (now curvature) is limited by the breaking of the reinforcement or by compression failure of concrete.

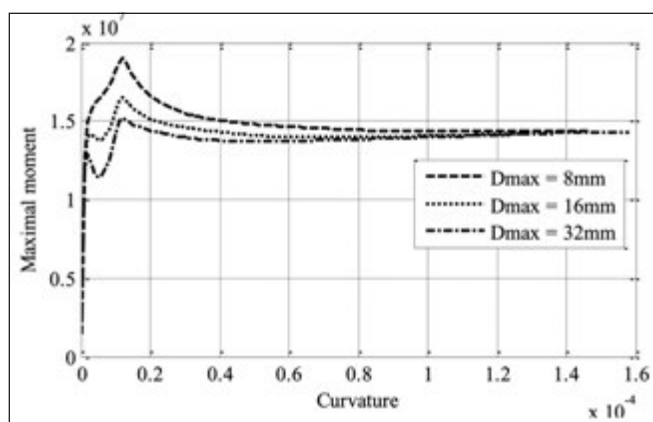
To determine the minimum reinforcement ratio one have to compare the maximum moment corresponding to first macro crack appearance to the moment of the plateau where the steel yields. If the later one is larger than the reinforcement ratio is larger than the minimum. So the minimum reinforcement ratio avoids possible brittle behaviour.

Moment curvature diagrams on Fig. 4 are showing how the steel content changes the type of behaviour and deformation ability according to proposed calculation method. Increasing the reinforcement ratio reduces the deformation ability, and so the ductility, and the ductile behaviour is slowly changed for rather brittle one.

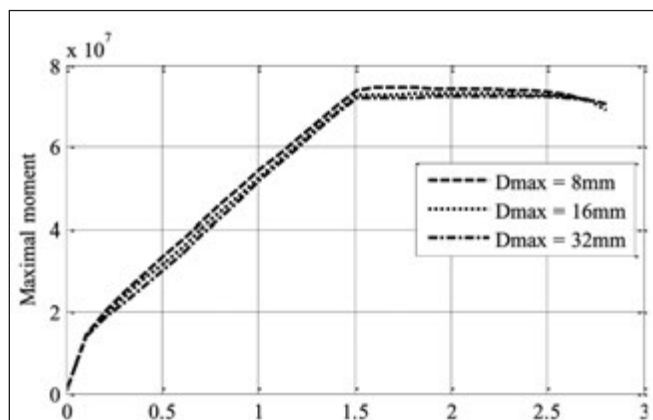
Fig. 5b presents the effect of the maximum aggregate size to beams with around minimum steel reinforcement ratio based on the proposed calculation method. The strain softening part, i.e. the fracture energy as a function of d_{max} , has pronounced effect on the “cracking moment”. The cracking moment can have different definition related to Fig. 5b. It could be related to the first or second peak moment, although the moment, when the stress at the bottom extreme fibre is equal to the tensile strength, is the common branching point of the three curves. First peak is the maximum moment during the cracking yielding process, while the second peak corresponds to the sudden yielding of longitudinal steel bars after the macro crack appeared. For steel content larger than the minimum



a)



b)



c)

Fig. 5: The effect of different maximum aggregate size for bending according to proposed calculation model a) model of concrete for low steel percentage b) moment-curvature diagram for low steel percentage c) and for higher steel percentage (cross section size: 200×300 mm, C25/30, $A_s = 100 \text{ mm}^2$ (0.167%) and $A_s = 600 \text{ mm}^2$ (1%))

one the effect of the maximum aggregate size is diminished after the crack due to tension is developed and the moment-curvature diagram is basically determined by yielding of steel bars (Fig. 5c).

Using the moment – curvature diagram of the cross section the load – deflection diagram of the beam can be constructed as usually done in the engineering practice.

2.3 SHEAR FAILURE OF BEAM

For the calculation of shear without shear resistance several calculation models are known. In this paper two calculation models have been used and compared. These methods give limits to the moment curvature diagram which is determined for bending. The limits are for both moment value and curvature too. So the shear failure limits both load-bearing capacity and deformation ability too.

The critical shear-crack theory (CSCT) (Rodrigues, 2010) was originally established for the calculation of punching shear, however it can be used to determine the shear resistance of one-way members such as beams without shear reinforcement. The shear resistance is calculated as the function of the deformation state. The method was verified experimentally for both failures of members by shear before yielding of the flexural reinforcement and failures of members by shear after yielding of flexural reinforcement. In the former case both load-bearing capacity and deformational ability is limited, while in the latter case “only” the deformational ability is limited.

The shear resistance of a beam without shear reinforcement by (Rodrigues, 2010):

$$\frac{V_{Rc}}{b d \sqrt{f_c}} = \frac{1/3}{1 + 120 \frac{\varepsilon_d}{16 + d_{max}}} \quad (5)$$

where ε_d is the longitudinal strain of the cross section at $0.6d$ from the compressed extreme fibre. For high strength concrete ($f_{ck} \geq 60 \text{ MPa}$) d_{max} have to be taken as 0.

This calculation method gives a conservative result for short beams, where $a/d \leq 3$. Where a is the shear span.

Model Code 2010 Level II of Approximation is based on the Simplified Modified Compression Field Theory (Collins, 1986). The shear resistance is given by the following equations:

$$V_{Rd,c} = k_v \frac{\sqrt{f_{ck}}}{\gamma} z b \quad (6)$$

$$k_v = \frac{0.4}{1 + 1500\varepsilon_x} \cdot \frac{1300}{1000 + k_{dg}z} \quad (7)$$

$$k_{dg} = \frac{32}{16 + d_{max}} \geq 0.75 \quad (8)$$

where ε_x is the longitudinal strain calculated at the mid-depth of the effective shear depth and must not exceed 0.003; $\sqrt{f_{ck}} \leq 8 \text{ MPa}$; z is the effective shear depth what is calculated as the maximum of $0.9d$ and the distance between the centroids of compressed and tensioned part of the cross section.

Since for each cross section of the beam the shear resistance may be found as a function of the deformation state of the cross section for bending therefore it is possible to estimate the possible location of the shear crack. However it must be remarked that for three point bending case it is always next to the mid cross-section.

3. VERIFICATION BY EXPERIMENT

3.1 PRESENTATION OF THE EXPERIMENT

All together 18 simply supported RC beams were tested with a span of 1000 mm and cross-section size 100×140 mm, loaded at mid-span on a 100×100 mm steel plate (Fig. 6). Two kind of reinforcement ratios ($2\phi 8 \text{ mm}$ and $3\phi 8 \text{ mm}$) and three kind of maximum aggregate size ($d_{max} = 8, 16 \text{ or } 32 \text{ mm}$) were used however the compressive strength of the concrete was tried to be kept the same (Tab. 1). In each beams 5 pieces of $\phi 4 \text{ mm}$ stirrups were used to hold in place the longitudinal steel-bars. This means that these stirrups were positioned about 250 mm from each other which is a larger distance than the effective cross sectional size, so according to shear calculations they

Tab. 1: Tested RC beams

Specimens	A_s (mm ²)	d_{max} (mm)	Average f_c (N/mm ²)	F_{max} (kN)
RC-8-2-8-A, RC-8-2-8-AB, RC-8-2-8-B	101	8	22	24.4, 26.4, 24.4
RC-16-2-8-A, RC-16-2-8-AB, RC-16-2-8-B	101	16	29	37.3, 32.9, 42.6
RC-32-2-8-A, RC-32-2-8-AB, RC-32-2-8-B	101	32	29	31.8, 31.2, 32.4
RC-8-3-8-A, RC-8-3-8-AB, RC-8-3-8-B	151	8	22	38.1, 25.6, 27.0
RC-16-3-8-A, RC-16-3-8-AB, RC-16-3-8-B	151	16	29	37.3, 31.8, 32.8
RC-32-3-8-A, RC-32-3-8-AB, RC-32-3-8-B	151	32	29	37.6, 39.5, 46.6

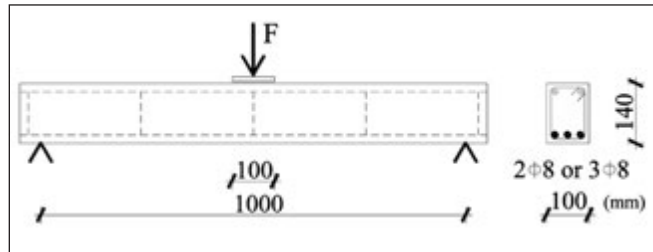


Fig. 6: Experimental setup

may be neglected. The steel type was B 500.

The experimental tests were carried out under force control using hydraulic loading system. The force and the vertical displacement of the mid cross-section were measured.

Most of the beams showed shear failure. Comparing the test results one can come to the conclusion that specimens with larger maximum aggregate size has larger shear resistance. It is also evident from the force – displacement curves that the shear failure reduced load-bearing capacity and deformational ability too (Fig. 7).

3.2 COMPARISON OF THE THEORETICAL AND EXPERIMENTAL RESULTS

Fig. 8-13 presents the comparison between the theoretical and the experimental results for beams in Tab. 1. On these figures the following lines can be distinguished: three dotted black lines represents the experimental results, fine grey line represents the behaviour based on calculated bending resistance, two dotted fine grey lines represent the shear limits as the function of the beam deflection, and the bold black line represents the behaviour of the beam limited by the CSCT shear resistance.

There is quite good agreement between the experimental results and the calculated ones using CSCT predicting shear resistance.

Comparing the theoretical and the experimental results the following conclusions can be drawn:

a) The characteristic points of the experimental load-deflection diagrams match quite well to the theoretically determined ones. The change in the stiffness of the curves can be seen at the about the same moment where the concrete tensile strength is expected to be reached.

b) At each figures results of two kind of shear calculation are shown. One of based on the Critical Shear-Crack Theory (CSCT) limits the bending resistance at similar level as it was found in the experiments. These beams are failed by shear in experiments too. The shear resistance calculation based on the Model Code 2010 gave a much conservative limit on the bending resistance.

c) In the case of specimen with 2φ8 of reinforcement

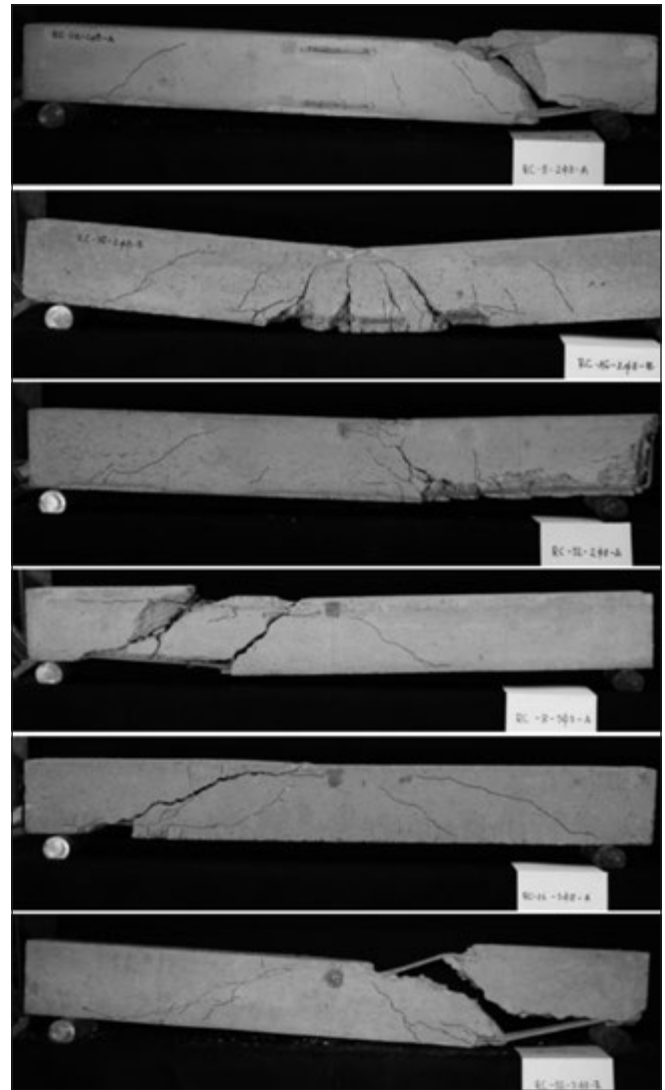


Fig. 7: Photos of the beams: a typical photo was chosen from the three similar beams. From above: 2φ8 $d_{max} = 8$ mm; 2φ8 $d_{max} = 16$ mm; 2φ8 $d_{max} = 32$ mm; 3φ8 $d_{max} = 8$ mm; 3φ8 $d_{max} = 16$ mm; 3φ8 $d_{max} = 32$ mm.

and $d_{max} = 16$ mm, and 32 mm the experiments showed bending failure at the latter case with limited deflection. For $d_{max} = 32$ mm prediction of CSCT match quite well with the experiment. For $d_{max} = 16$ mm case one possible explanation could be that the stirrups, which were used to keep the longitudinal reinforcements in place increased the shear resistance (Fig. 9).

d) Both the experiments and also theoretical calculation showed that the shear resistance is depended on concrete composition i.e. depended on maximum aggregate size for normal strength concrete. It is also a conclusion, that the concrete composition influences the failure mode although the quality of the concrete kept constant i.e. the compressive strength of concrete kept constant.

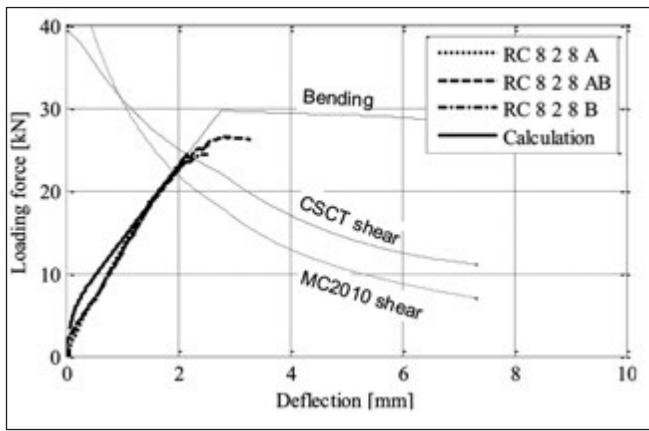


Fig. 8: Specimen 2φ8 $d_{max} = 8$ mm

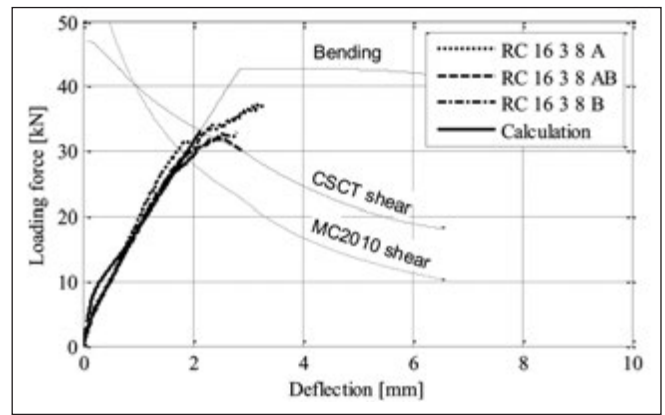


Fig. 12: Specimen 3φ8 $d_{max} = 16$ mm

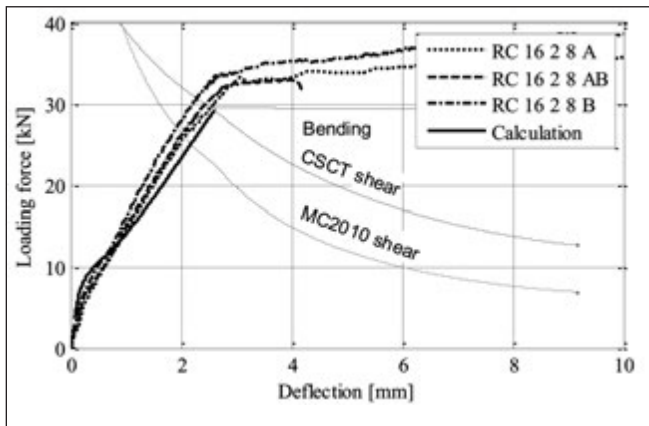


Fig. 9: Specimen 2φ8 $d_{max} = 16$ mm

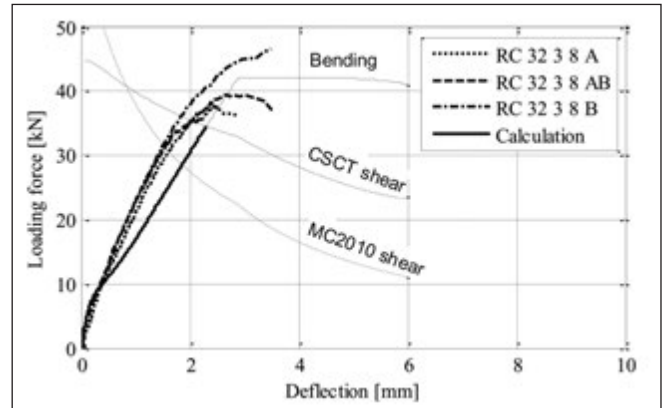


Fig. 13: Specimen 3φ8 $d_{max} = 32$ mm

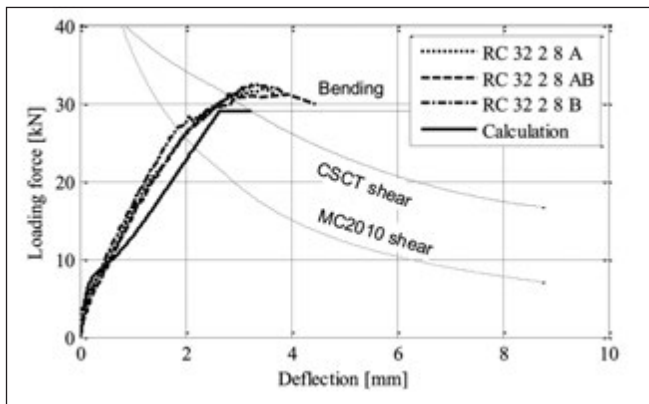


Fig. 10: Specimen 2φ8 $d_{max} = 32$ mm

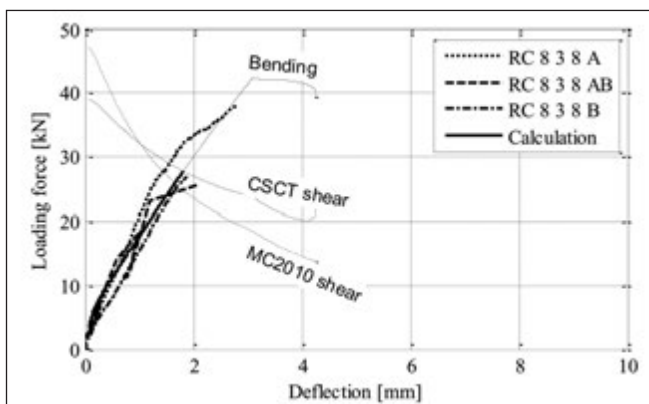


Fig. 11: Specimen 3φ8 $d_{max} = 8$ mm

4. CONCLUSIONS

In the paper three point bending beams were examined both experimentally and theoretically.

The main question was how the concrete composition, characterized by maximum aggregate size for normal strength

concrete, influences the load-bearing capacity, deformational ability and failure mode.

In the experiments the same quality of concrete was used but the aggregate composition was variable.

In the theoretical calculations the behaviour model of concrete was chosen such a way that the effect of aggregate composition on the material behaviour, and so on the behaviour of the beam, could be taken into account. The shear resistance calculation model took into account the deformation state due to bending. The necessity of that could be confirmed either by considering principles of fracture mechanics or principles of traditional engineering methods.

Good match was found between theory and experiment comparing load-bearing capacity, deflection and failure mode.

It seems to be a conclusion having firm basis that change in concrete composition alone may also change the failure mode too.

Improvement of the shear model is necessary in the future in order to extend the application limits of the used models.

5. NOTATIONS

- b width of the cross section
- d effective depth of the cross section
- d_{max} maximum aggregate diameter
- E_c modulus of elasticity at $\sigma_c = 0$
- E_{c1} modulus of elasticity at $\sigma_c = f_c$
- f_c concrete compression strength
- f_{ck} characteristic value of the concrete compressive strength
- f_t tensile strength of concrete
- f_u tensile strength of reinforcement
- f_y yield strength of reinforcement
- G_f d_{max} dependent fracture energy
- $K = 0.1 f_c \cos \alpha$ parameter

k_v	parameter
V_{Rc}	shear resistance without shear reinforcement
$V_{Rd,c}$	shear resistance for design
y_{cmax}	location of the neutral axis measured from the compressed extreme fibre
w	crack width
w'	non-dimensional crack width
z	effective shear depth
$\alpha \approx 17.5^\circ$	sliding slope measured from a horizontal line
ε_c	compressive strain
ε_{c1}	compressive strain at $\sigma_c = f_c$
ε_d	longitudinal strain at $0.6d$ from the extreme compressive fibre
ε_u	strain at maximum force of reinforcement
ε_x	longitudinal strain calculated at the mid-depth of the effective shear depth
μ	curvature of the cross section
γ_M	partial safety factor
σ_c	normal stress for concrete

6. REFERENCES

- Bazant, Z. P., Planas, J. (1998): "Fracture and Size Effect in Concrete and Other Quasibrittle Materials", *CRC Press LLC*
- Bogdándy, B., Hegedűs, I. (2014): „A nyomott öv nyírási teherbírása és az Eurocode szerinti nyírási ellenállás kapcsolata” („Relationship between the shear resistance of the concrete compression zone and the shear resistance according to Eurocode 2”), *Vasbetonéptés*, pp. 62-67
- Carpinteri, A., Carmona, J. R., Ventura, G. (2011): "Mode Transition in Reinforced Concrete Beams – Part 1: Theoretical Model", *ACI Structural Journal*, pp. 277-285
- Carpinteri, A., Carmona, J. R., Ventura, G. (2011): "Mode Transition in Reinforced Concrete Beams – Part 2: Experimental Tests", *ACI Structural Journal*, pp. 286-293

- CEB-FIP Model Code 1990 (1991): "Bulletin d'information 203-205", *Lausanne*
- Collins, M. P., Vecchio, F. J. (1986): „The Modified Compression-Field Theory for Reinforced Concrete Elements Subjected to Shear”, *ACI Structural Journal*, pp. 219-213
- Eurocode 2. (2004): EN 1992-1-1: 2004. "Design of concrete structures – Part 1-1 General rules and rules for buildings", *CEN*
- Fantilli, A. P., Iori, I., Vallini, P. (2007): "Size effect of compressed concrete in four point bending RC beams", *Engineering Fracture Mechanics* 74, pp. 97-108
- Fantilli, A. P., Ferretti, D., Iori, I., Vallini, P. (2002): "Mechanical Model for Failure of Compressed Concrete in Reinforced Concrete Beams", *Journal of Structural Engineering*, May, pp. 637-645
- fib** Model Code for Concrete Structures 2010 (2013): *Ernst and Sohn, Berlin*
- Hillerborg, A., Modéer, M., Petersson P.-E (1976): "Analysis of Crack Formation and Crack Growth in Concrete by Means of Fracture Mechanics and Finite Elements", *Cement and Concrete Research*, Pergamon Press Inc. pp. 773-782
- Karihaloo, B. L. (1997): "Fracture Mechanics and Structural Concrete", *Longman, London*
- Muttoni, A., Ruiz, M. F. (2008): „Shear Strength of Members without Transverse Reinforcement as Function of Critical Shear Crack Width", *ACI Structural Journal*, pp. 163-172
- Rodrigues, R. V., Muttoni, A., Ruiz, M. F. (2010): „Influence of Shear on Rotation Capacity of Reinforced Concrete Members without Shear Reinforcement", *ACI Structural Journal*, pp. 516-525

Rita Vajk (1981), received her M.Sc. architect degree from the Budapest University of Technology and Economics in 2006. She is a PhD student at the Department of Mechanics, Materials and Structures.

István Sajtos (1961), civil engineer, PhD, associate professor and head of the Department of Mechanics, Materials and Structures at Budapest University of Technology and Economics. His main interests are structural mechanics of reinforced concrete-, masonry-, and shell structures, and also retrofitting of historical masonry structures. He is the member of Hungarian Chamber of Engineers, American Concrete Institute and Hungarian Group of **fib**.

EXPERIMENTAL AND NUMERICAL MODELING OF FASTENING ELEMENTS



Viktor Hlavička – Éva Lublóny

This research mainly focused on the load bearing capacity, failure mode and possible numerical simulation of fastening systems. Laboratory tests were carried out and results were evaluated. Resistances of two different fastening systems were investigated (mechanical joint: torque controlled expansion anchor, bonded anchor: with epoxy resin and threaded rod). Main goals of our tests were the determination of numerical model parameters and identification of relations between material properties and resistance of joints. Finite element models of the two fastening systems were introduced. Linear and bilinear material models and static analysis were used in the numerical models.

Keywords: concrete, fastening systems, bonded anchor, expansion anchor, finite element modeling

1. INTRODUCTION

1.1 Overview of post-installed fastenings

Two types of anchors are used in fastenings: cast-in-place and post-installed anchors (Fig. 1). There are several types of cast-in-place anchors pigtail and all-thread anchors, steel rebars, L-bolts, J-bolts, headed studs, anchor channels, etc.. These

connections are installed at the same time as the base material (concrete) is manufactured. Most of cast-in-place anchors have a special head, and placed into the concrete before it hardens (Eligehausen, Hofacker, Lettow, 2001; Eligehausen, Malleé, Silva, 2006; Fuchs, 2001). In this study, only post-installed anchors with drill installation were investigated.

Several post-installed anchors are available with different way of load-transfer. The commercially available fastenings can transfer the load to the host material via the following mechanisms: mechanical interlock, friction or bond (Fig. 2). Furthermore, the most recent techniques use combined bond and friction (e.g. bonded expansion anchors). In case of expansion anchors the load is transferred by friction. Generally, an expansion sleeve is expanded by an exact displacement or torque applied on the anchor head during the installation process. The chemical fastenings are anchored by bond. In addition, bonded anchors can be divided into two subgroups: capsule or injection systems. The bond material can be either organic, inorganic or a mixture of them. The loads are transferred from the steel (normally a threaded rod, rebar) into

Fig. 1: Fastening methods in concrete (Fuchs, 2001)

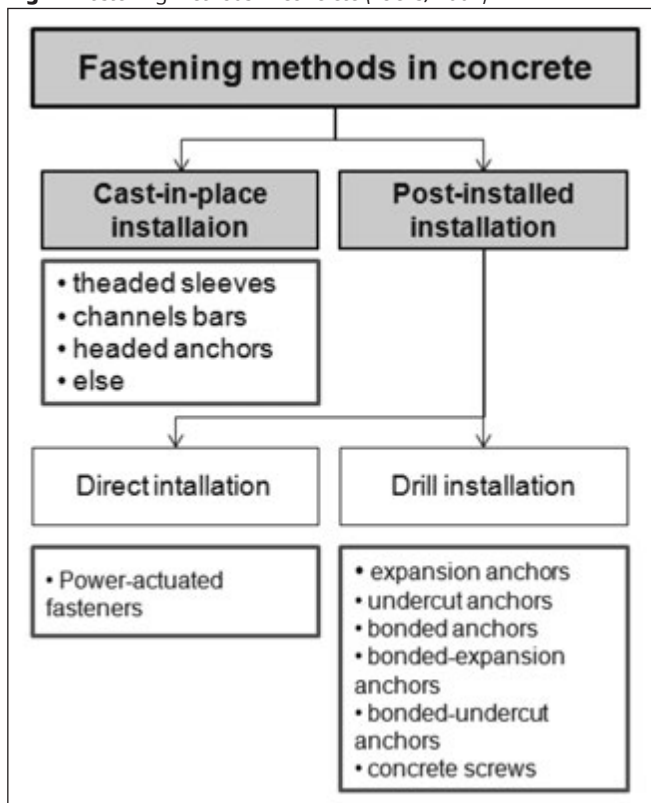
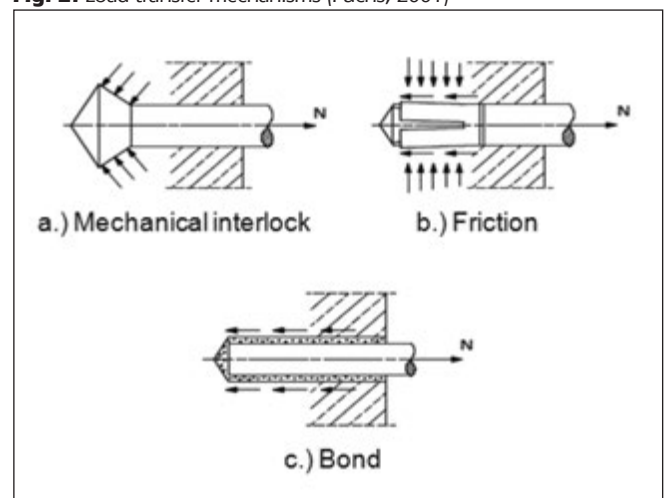


Fig. 2: Load transfer mechanisms (Fuchs, 2001)



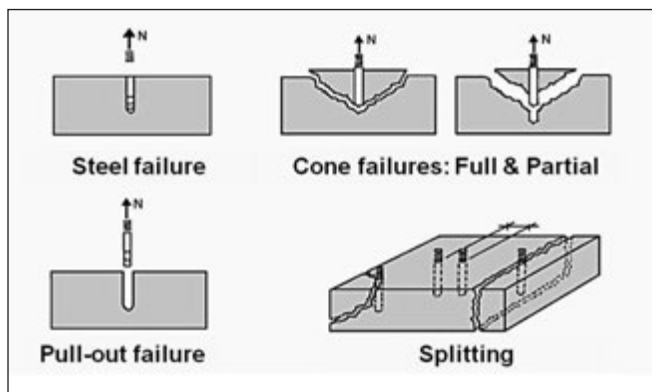


Fig. 3: Failure modes (Fuchs, 2001)

the bonding material and are anchored by bond between the bonding material and the sides of the drilled holes (Fischer, 2010; fib MC 2010; Fuchs, 2001).

1.2 Failure methods

The following types of failures were observed in case of the anchorages under tension: steel failure, concrete cone, pull-out of anchor and concrete splitting (Fig. 3).

The steel failure depends on tensile strength of steel, from the ultimate steel strength (f_u) and the cross-sectional area (A_s). The steel capacity can be calculated (Fischer, 2010; Fuchs, 2001; fib MC 2010; Simon, Eligehausen, Kirzakis, 2005).

Properties of concrete cone failure mostly depend on the embedment depth (h_{ef}) and the concrete strength (f_c). According to the Concrete Capacity Design the cone failure is the optimal failure type, because concrete strength is completely utilized. Concrete cone failures can be either full cone type or partial cone type. Partial cone failure is considered to be the failure of the connection, but there is a residual capacity that is the consequence of the resistance of the bonding agent (Fischer, 2010; Fuchs, 2001; fib MC 2010; Simon, Eligehausen, Fuchs, Sippel, 2000, Spieh, Eligehausen, 2002).

Pull-out failure has to be discussed separately for bonded and expansion anchors. Pull-out failure of mortar bonded anchors means bond failure between mortar and concrete, while pull-out failure excluding mortar means bond failure between the steel fastening and the bonding material. The bond strength (τ_u) depends on the certain product, but its value is included in the corresponding approvals (Fischer, 2010; Fuchs, 2001; fib MC 2010; Simon, Eligehausen, Kirzakis, 2005).

Pull-out failure in case of expansion anchors is possible under tension, including or excluding the expansion sleeve (pull-out/pull-through).

Splitting failure is caused by the critical edge-, spacing distances. This failure mode is not within the scope of this paper, since all the performed specimens failed by splitting were excluded during the evaluation of the results (Fischer, 2010; Fuchs, 2001; fib MC 2010; Simon, Eligehausen, Kirzakis, 2005, Nemes, Lublóy 2011).

2. MATERIALS

2.1 Tested anchors

A torque controlled expansion anchor (Fischer FBN II 8/50 gvz) and a bonded anchor system were tested (Fischer FIS EM epoxy) (Fig. 4). Both expansion and bonded anchors were installed according to the MPII (Manufacturer's Printed

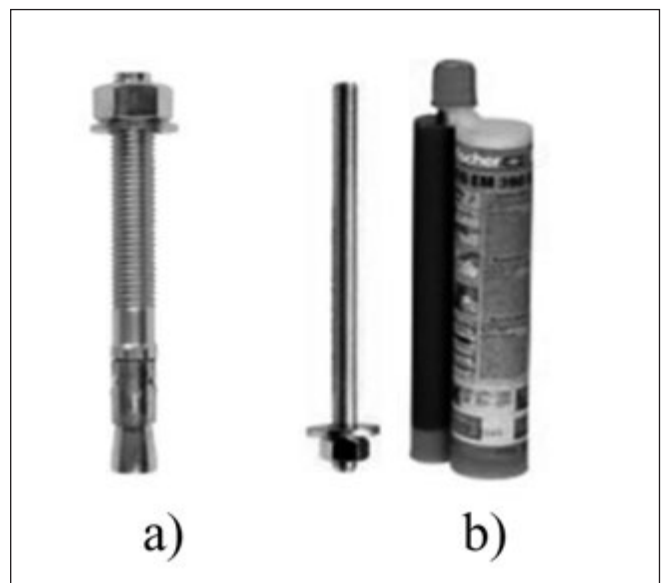


Fig. 4: Tested anchors: torque controlled expansion anchor (a), bonded anchors with epoxy resin (b) (Fischer, 2010)

Installation Instructions). The embedment depth was $h_{ef}=50$ mm in all cases ($\sim 6d$, where "d" is the diameter of the anchor), and the diameter of the anchors and threaded rods was 8 mm, their material was 8.8 (Fischer, 2010).

2.2 Concrete mixtures

The composition of the tested concrete mixtures is shown in Table 1. All mixtures were made by using Portland cement (CEM I 42.5 N). The aggregates were natural quartz sand and quartz gravel and a superplasticiser of BASF Glenium C323 Mix was also used. The specimens were held under water for 7 days, then kept at laboratory temperature (20 °C) for additional 21 days (Fig. 6). Compressive and flexural strength properties of each mixture were tested on additional 4 cubes of 150x150x150 mm and 3 specimens of 70x70x250 mm, respectively. The geometry of concrete specimens was chosen with minimum needed dimensions that allow the occurrence of all potential failure modes during the tests. The minimum sizes could be calculated as a function of the embedment depth.

3. TESTS METHODS

3.1 Pull-out tests

The unconfined test setup is shown in Fig. 7. The size of the specimens was 300x300x100 mm. The loading devices were a displacement controlled test apparatus, which allowed the recording of residual stress after the failure. This setup enabled the formation of all possible failure modes, the results were not affected by the geometry of investigated samples (thickness of the test member, critical edge, placing). The measuring setup was capable to measure, record and show the applied load and the related displacement of the anchor in real-time. The perpendicular pin-joints ensured the centrality of the acting force. The displacement was measured by two electronic transducers. Three additional independent displacement transducers were used to record the deformation of the surface. The load was measured by a calibrated load cell. All channels were recorded simultaneously with CATMAN® software through a Spider8 data acquisition device. The tests were carried out in accordance with the instructions given in

Table 1: Composition of concrete mixtures

No.	Aggregates [kg/m ³]			Cement	Water	Super-plasticiser
	0/4 mm	4/8 mm	8/16 mm	[kg/m ³]	[kg/m ³]	[kg/m ³]
I.	833	463	555	410	152	6.2
II.	833	463	556	390	160	3.9
III.	833	463	555	365	170	2.6
IV.	834	463	556	310	189	0.62
V.	833	463	556	290	196	0.58
VI.	844	469	563	300	180	0.6
VII.	812	451	542	380	180	1.5
VIII.	776	431	517	380	211	0.8
IX.	878	488	585	300	150	2.1



Fig. 6: Concrete specimens for pull-out tests

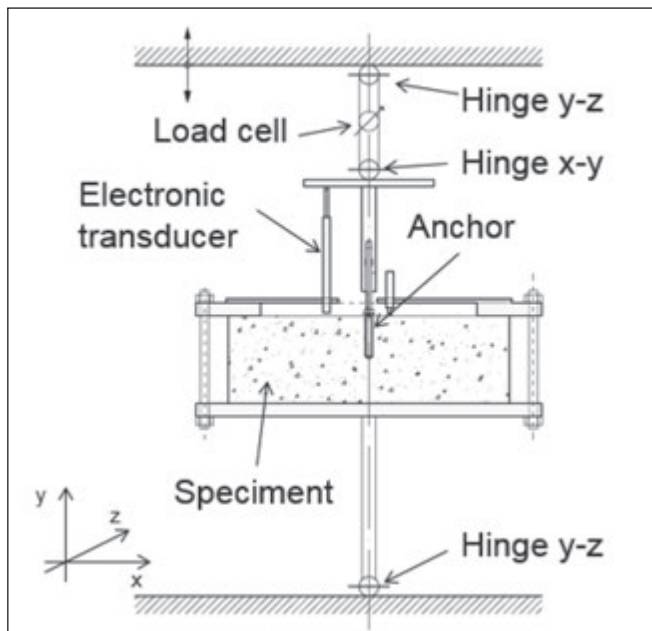


Fig.7: Arrangement of pull-out tests

ETAG 001 Annex A. The support distance was greater than 4 h_{ef} (ETAG, 2006; ETAG, 2008).

The tested number of specimens for the pull-out testes are given in Table 2.

3.2 Porosity test

The test is based on the water-absorption capacity of the specimens. The volume of absorbed water depends on the volume

Table 2: Summary pull-out-tests

No.	Tested anchors		SUM
	Torque controlled expansion anchor	Bonded anchor - epoxy + M8.8	
I.	3	3	6
II.	3	3	6
III.	3	3	6
IV.	3	3	6
V.	3	3	6
VI.	-	5	5
VII.	-	5	5
VIII.	-	5	5
IX.	-	5	5
SUM	15	35	50

Table 3: Properties of concrete mixtures

No.	Porosity [V%]	Flexural strength [N/mm ²]	Compressive strength [N/mm ²]
I.	5.96	8.15	68.52
II.	9.74	7.58	56.31
III.	7.82	7.54	51.17
IV.	11.46	5.61	31.49
V.	11.93	5.59	22.23
VI.	8.05	7.23	47.40
VII.	6.94	8.51	56.94
VIII.	9.44	6.48	43.22
IX.	6.9	7.78	53.76

of air contained in the specimens. At first concrete samples had been dried in an oven until constant weight and then were stored under water. Weight measurements were repeated after 1, 24, 48, 72 hours. Finally, the apparent porosity was calculated according to EN 13755:2008 (Table 3).

3.3 Compressive strength

Compressive strength is the primary parameter for the determination of capacity of the anchor. Uniaxial compressive

strength tests were carried out on concrete cubes 28 days after casting. The results were evaluated in accordance with EN 12390-3:2009 for concrete (Table 3).

3.4 Flexural strength

The purpose of these measurements was to establish the boundary between the partial and full cone failure as a function of flexural strength. The determination of flexural strength under bending moment was carried out on 3 samples of 70x70x250 mm taken from each concrete mixture. The tension resistance was calculated. The results were obtained and evaluated according to EN 12390-5:2009 (Table 3).

4. RESULTS

4.1 Load-displacement curves

The load-displacement curves in case of steel failure are shown in Fig. 8. This failure mode was dominant for torque controlled expansion anchors. These load-displacement curves have three different parts. In the first part the external load exceeds the prestress force in the bolt. In the second part the cone is gradually pulled further into the sleeve, allowing increased displacements for each further increment of load

Fig 8: Load-displacement curves in case of steel failure

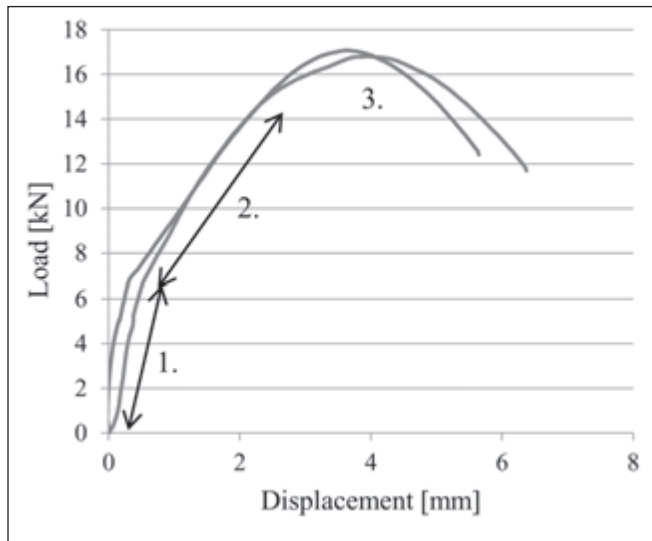
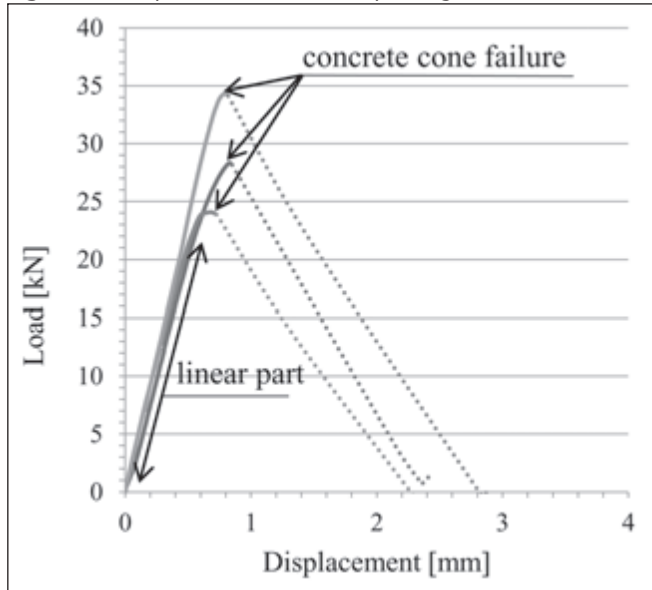


Fig. 9: Load-displacement curves corresponding to cone failure



(CEB, 1991). The third part shows the non-linear decreasing (necking) behavior of steel. It was observed that this failure occurred in case of expansion anchors when the compressive strength of concrete was at least 50 MPa. The mean value of the resistance was 16.8 kN.

The curves are shown in Fig. 8 belong to the expansion anchors. However this failure type could also be noticed in case of the tested bonded anchors. The failure mode was steel failure - using unconfined test setup - when the bond stress and the tensile strength on the idealized concrete-cone was higher than the tensile strength of the steel.

The load-displacement curves of cone failure are shown in Fig. 9.

The curves represent full cone failure. Full cone starts at the deepest point of the embedment depth, and the cone angle is approximately 35°. This angle is general for NPC (Eligehausen, Sawage, 1989). This failure means that the tension resistance of the base material reached its maximum on the cone surface so the concrete tensile strength was fully utilized. This failure type is fast and brittle, the curves are mainly linear, only a short ductile period can be seen before the failure.

This failure could also be noticed in case of expansion anchors, when the compressive strength of material was at less than 50 MPa.

5. RELATIONSHIP BETWEEN THE ULTIMATE LOAD AND THE PROPERTY OF CONCRETE

Fig. 10 represents the load bearing capacity as a function of compressive strength of concrete in case of expansion anchors.

In case of mixtures V., mixtures IV. cone failure, while in case of mixtures III., mixtures II., mixtures I. steel failure was the typical failure type. It can be stated that over 50 N/mm², compressive strength of concrete is high enough to prevent cone failure. The dot-dashed line on Fig. 10 represents the ultimate load for steel failure.

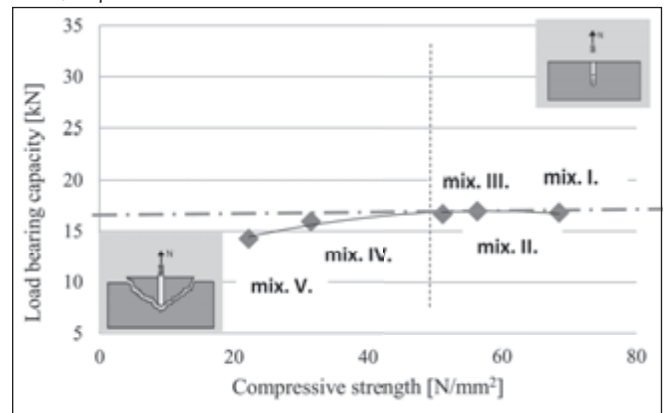
In Fig. 11 load bearing capacity as a function of compressive strength of concrete in case of epoxy mortar can be seen.

In case of epoxy mortar cone failure was typical. It is visible that higher compressive strength causes higher load bearing capacity. This relation is approximately linear.

Fig. 12 represents the load bearing capacity as a function of porosity of concrete in case of using epoxy mortar.

It can be stated that higher porosity causes lower load bearing capacity. The reasons of this trend are that the po-

Fig. 10: Load bearing capacity vs. compressive strength of concrete curve, expansion anchors



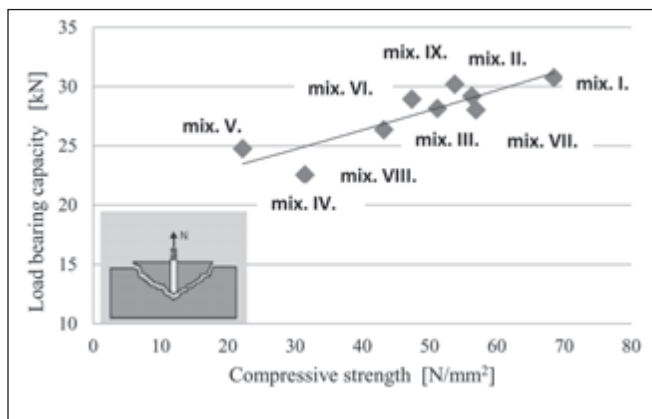


Fig. 11: Load bearing capacity vs. compressive strength of concrete, epoxy mortar

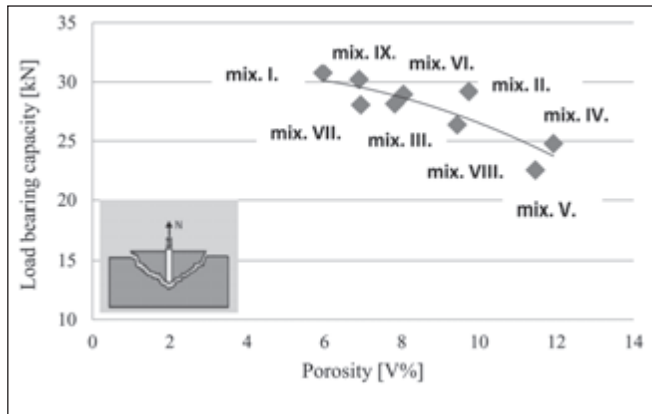


Fig. 12: Load bearing capacity vs. porosity of concrete, epoxy mortar

osity reduces the compressive strength and also effects the adhesion of epoxy mortar (Hlavička, Lublůy, Balázs, 2014).

6. NUMERICAL ANALYSIS

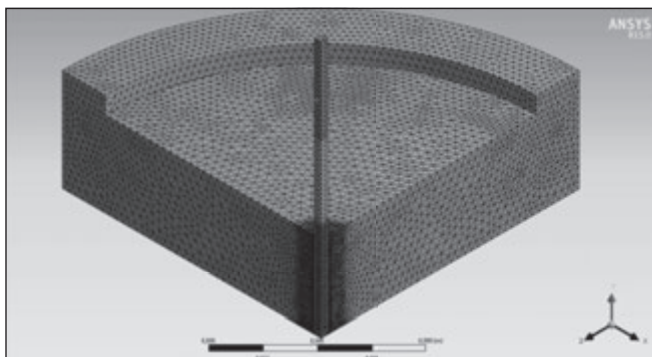
Beside the experiments numerical analysis were also carried out. The object of the numerical models was to reproduce the results and failure types of our experiments. For the two different fixing systems two different finite element models were created. Analyses were made in ANSYS Workbench 15 software.

6.1 Finite element models

Full-size finite element models of ¼ of the specimens were created by using axis-symmetric boundary conditions (Fig. 13).

In the models tetrahedron elements were used and the mesh was refined around the bond. The bonded anchor model had

Fig. 13: Finite element model for bonded anchor



4 parts (steel anchor, epoxy mortar, concrete, steel frame) and the expansion anchor model had 3 parts (steel anchor, concrete, steel frame). Between the parts we had to define contact elements. Between the anchor and epoxy “bonded”, between the epoxy and concrete “bonded” and between concrete and steel frame “frictionless” contact elements were applied. For the expansion anchor model we did not have epoxy mortar, in this model between the head of anchor and concrete we used “bonded” contact elements.

The fixed support was at the top of the steel frame. Displacement type load was applied, which acted at the vertical front of the steel anchor. The velocity of displacement load was 1 mm/min that was the same load used for the experiments.

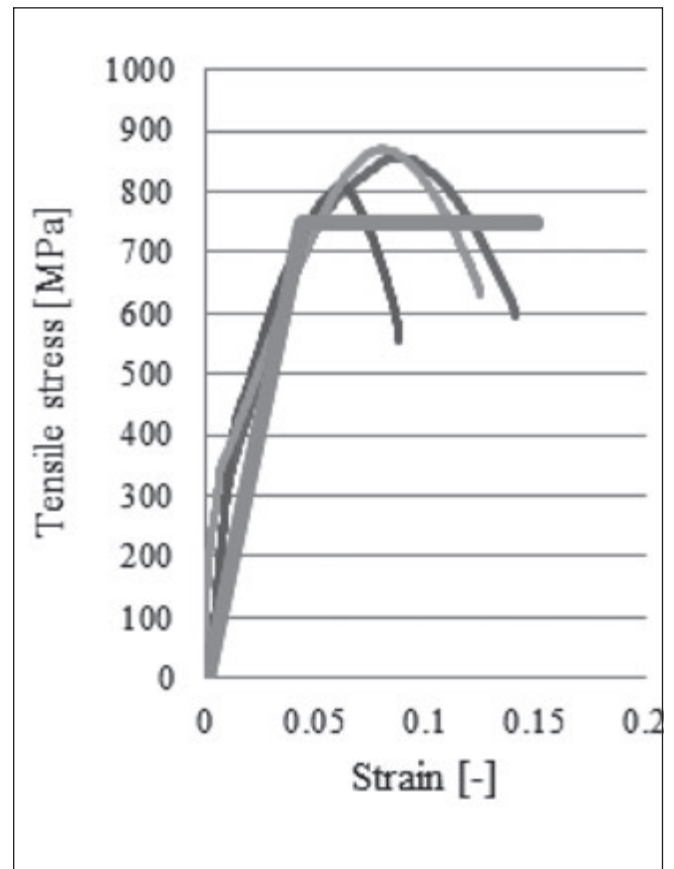
6.2 Numerical model of expansion anchor

Two material models were used for modeling of expansion anchor. At first we supposed linear elastic material models for all materials. Initial data were taken from engineering data library of the software, which were later modified according to the experiments. Secondly non-linear (bilinear) material models were applied and we used the result of the materials tests (Fig 14, Fig 15).

The results of these numerical analyses were force-displacement curves. These curves were compared to experiments results (Fig. 16).

It can be stated that the difference between the test and numerical analysis is significant in case of linear elastic materials models. This difference is approximately 28-30% unconservatively. In case of bilinear materials the model took account the yield strength of steel anchor. Therefore the difference in this case was only 11-12 %.

Fig. 14: Bilinear material model for expansion anchors



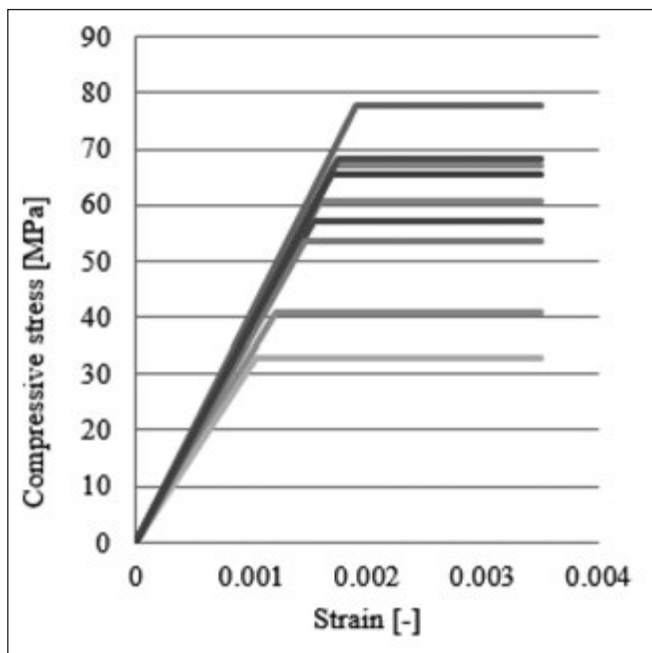


Fig. 15: Bilinear material model for concrete mixtures

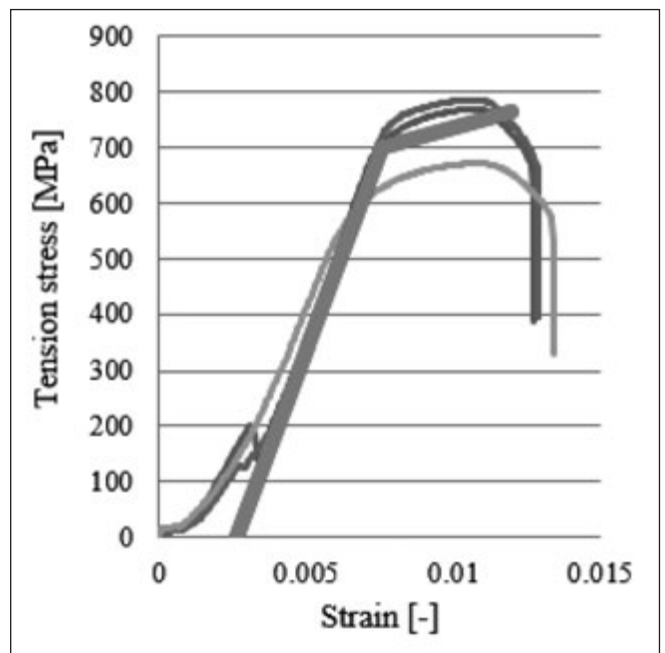


Fig. 17: Bilinear material model for steel anchors (M8 8.8)

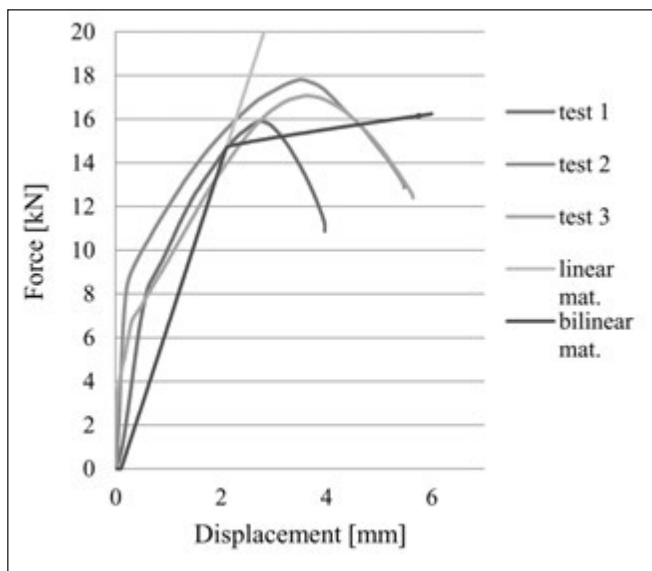


Fig. 16: Force-displacement curves for expansion anchors (II. mixtures)

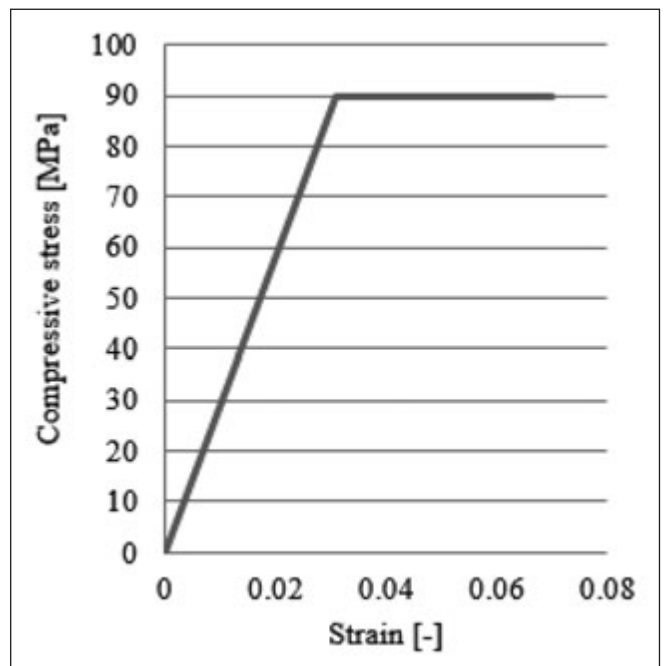


Fig. 18: Bilinear material model for epoxy mortar

6.3 Numerical model of bonded anchor

In this case we also used two types of material models (linear-elastic, bilinear). Fig. 17 represents the bilinear material model of steel anchors and Fig. 18 shows the bilinear material model of epoxy mortar.

Fig. 19 presents the first principal stress values of the model. It can be stated that the critical stress is in the anchor. This stress is less than the tensile stress, but the stress in the concrete is higher than the tensile stress of concrete. Therefore failure occurred in the concrete.

Fig. 20 represent the force as a function of displacement in case of bonded anchors. It is visible that the curve of the linear material model and the curve of the bilinear material model are the same. It means that the stress was less than the yield stress of steel and the steel remained linear elastic.

7. CONCLUSIONS

This research mainly focused on the resistance, failure modes and possible numerical simulation of fastening systems. An

own test method was developed in order to measure force and displacement of fastening subjected to pure tension. 50 tests were carried out for two fastening systems and 9 different mixtures of concrete. Main goals of tests were the determination of numerical model parameters and identification of relations between material properties and resistance of joints. Based on test results it can be stated that resistance of torque controlled expansion anchor is much smaller than resistance of bonded connection with threaded rod that has the same diameter. Moreover, in the connections with expansion anchors (diameter M8) shear cone failure occurs if concrete compressive strength is below 50 N/mm² and steel anchor fails in case of higher concrete strength. In addition to this resistance of fixing systems with epoxy resin and M8 8.8 steel rod linearly increases with higher concrete strength. Finite element models of the two fixing systems are introduced next to the experiments. Firstly linear and bilinear material models and static analysis were used for numerical tests and later explicit dynamic solutions were also applied for detailed mod-

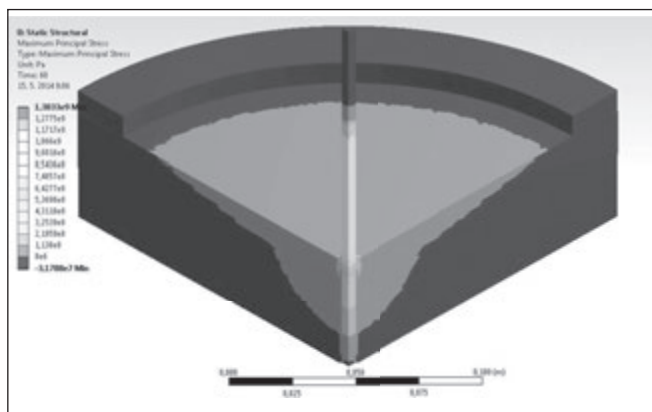


Fig. 19: First principal stresses for bonded anchor

elling of material failure. Finite element model calculations show that application of linear material model is adequate if shear cone failure occurs. On the other hand, if failure of steel rod is possible then bilinear material model is recommended. What is more, static calculations give results only indirectly (via stresses and strains) so application of dynamic analysis can be advantageous.

8. ACKNOWLEDGEMENT

The authors wish to thank Szabolcs Kovács-Sebestény (Fischer Hungary LPs.) for providing the necessary anchors, dr. Salem Georges Nehme (Department of Construction Materials and Technology, BME) for designing the concrete mixtures, and dr. László Attila Joó (Department of Structural Engineering, BME) for consultation of the finite element models.

9. REFERENCES

- CEB (Comité Euro-International du Béton) (1991): "Fastening to reinforced concrete and masonry structures", Bulletin D'Information N° 206, ISBN: 2-88394-011-8
- Eligehausen, R., Fuchs, W., Sippel, T. (2000): "Anchorage to Concrete", *TARTOK 2000*, Budapest, pp. 261–270. ISBN: 963-420-640-9
- Eligehausen, R., Hofacker, I., Lettow, S. (2001): "Fastening technique – current status and future trends", *International Symposium on Connections between Steel and Concrete*, Volume One, pp. 11-27.
- Eligehausen, R., Mallee, R., Silva, JF. (2006): "Anchorage in Concrete Construction", *Ernst&Sohn*, ISBN-13 978-433-01143-0
- Eligehausen, R., Sawade, G., (1989): "A fracture mechanics based description of the pull-out behavior of headed studs embedded in concrete", *RILEM report on Fracture Mechanics on Concrete – Theory and Application*, Chapman Hall Ltd, London
- ETAG 001. "Guideline for European Technical Approval of Metal Anchors for use in concrete", Annex A: *Details of test*. November. (2006).

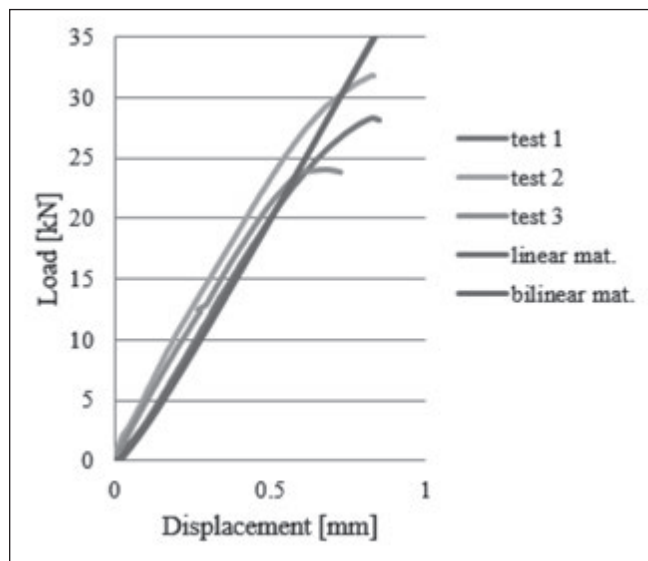


Fig. 20: Force vs. displacement curves for bonded anchors (VII. mixtures)

- ETAG 001. "Guideline for European Technical Approval of Metal Anchors for use in concrete", Part 5: *Bonded anchors*. November. (2008).
- fib MODEL CODE 2010. *Concrete to steel*. Volume One. 282-285. ISBN: 978-3433-03061-5
- Fuchs, W. (2001): "Evolution of fastening design methods", *Proceedings of International Symposium on Connections between Steel and Concrete* (Eds.: Eligehausen, R.), Volume One, Stuttgart, Germany, pp. 45-60.
- Hlavička, V., Lublőy, É., Balázs, L. Gy. (2014): "A beton porozitásának hatása a tapadásos csapok tönkremenetelére", *VASBETONÉPÍTÉS*, 2014/3, pp. 55-61.
- Nemes, R., Lublőy, É. (2011): "Application of anchors under special concrete conditions", *Periodica Polytechnica - Civil engineering 55/1*, pp. 73-79. ISSN 1587-3773
- Simon, I., Eligehausen, R., Kirtzakis, V. (2005): "Behaviour of Post-Installed Rebars in Uncracked and Cracked Concrete", *Keep Concrete Attractive*, Hungarian Group of fib, pp. 669-674.
- Spieth, H., Eligehausen, R. (2002): "Design of post-installed rebar connections", *Proceeding of the 3rd International Symposium held at the Budapest University of Technology and Economics. Hungary*, pp. 439-446. ISBN 963 420 714 6
- Technical Handbook - Europe*. fischerwerke GmbH.. Stuttgart. (2010). 13-186.
- Viktor Hlavička (1987)** structural engineer (MSc), PhD student of Department of Construction Materials and Technology at the Budapest University of Technology and Economics. His main fields of interest are: fastening to concrete, fastening systems, finite element modeling. Member of the Hungarian Group of fib.

Éva Lublőy (1976), PhD, Senior lecturer in structural engineering, at the Budapest University of Technology and Economics. Her main fields of interest are: fire design, behaviour of constructions materials at elevated temperature. Member of the Hungarian Group of fib.

MATERIAL CHARACTERISTICS AND BOND TESTS FOR FRP REBARS



Sándor Sólyom – György L. Balázs – Adorján Borosnyói

This paper intends to summarize the behaviour of the FRP rebars in concrete for direct pull-out and beam type test conditions, furthermore it also gives a brief overview of the material characteristics and the bond mechanism between FRP rebars and concrete. In normal strength concrete, the mode of bond failure of FRP rebars was found to differ considerably from that of deformed steel rebars, most importantly due to damage of the resin rich surface of the rebar when pull-out failure takes place. The bond strengths developed by FRP rebars appear to be rather similar to what is expected from deformed steel rebars under similar experimental conditions, however, there are some considerable differences, too. The failure modes and the bond-slip curves indicate some of the fundamental differences between steel and FRP materials. Two types of test methods are considered to measure the bond strength of rebars: pull-out test and beam test, both of which give different values, owing to their test arrangements. This paper reports in detail on the influence of testing arrangement to the bond strength, due to the wedging effect of the rebars and different stress states in concrete specimens.

Keywords: FRP (Fibre Reinforced Polymer), bond behaviour, pull-out test, beam test

1. INTRODUCTION

Over the last century steel reinforced concrete was the most widely used structural material in construction. Nevertheless, it is well known that, under certain environments, the corrosion of steel reinforcement can lead to the deterioration or even collapse of structural elements, requesting expensive repairing and strengthening or reconstruction works whenever deterioration starts. This disadvantageous attribution of the steel reinforcement has contributed, that researches started to focus on alternative solutions (Lublóy et al., 2005).

FRP (Fibre Reinforced Polymer) materials offer a promising solution since for many years they are successfully used in other industries (such as the automobile and sports manufacturing industries) and more recently in construction. There are many examples of structural applications indicating the speed and convenience of strengthening and repairing of concrete structures using advanced composites as cost effective solutions (Borosnyói, Balázs, 2001; Szabó, Balázs, 2007). Furthermore, there are structures reinforced with FRP rebars that have been in service in aggressive environments in various parts of the world, for more than 20 years, without considerable structural problems.

The widespread adoption of any new type of reinforcement, such as fibre reinforced polymers, requires the development of product specification, testing standards and codes of design practice, which is usually a process that can take many years to be completed. One of the fundamental aspects of structural behaviour is the bond development, since the bond stress transfer between reinforcement and the surrounding concrete is the basis of the theory of reinforced concrete (Borosnyói, 2015). Without a proper transfer of stresses between concrete

and rebar, reinforced concrete structures would not be viable (Borosnyói, Balázs, 2001; Sólyom, Balázs, 2015b).

Bond of steel reinforcement to concrete has been extensively studied in the last 40 years and a huge amount of experimental and analytical work has been published on this subject (CEB Bulletin 151, 1982; *fib*, 2000). However, the design formulae of the most current design codes of practice do not incorporate enough provisions for the use of alternative reinforcing materials other than steel. Publication of *fib* Model Code 2010 (*fib*, 2013) was an important step in this respect. In order to introduce of FRP rebars, new design specifications are needed, which will allow engineers to apply these materials in the near future.

To manufacture fibre reinforced polymers different fibres (glass, carbon, aramid and recently also from basalt) are used. Fibres are bound together with diverse resins (polyester, vinyl ester and epoxy). Mechanical properties of FRP rebars can be considerably different from that of the conventional steel reinforcements, as well as their surface characteristics. FRP rebars provide excellent resistance to environmental factors such as freeze-thaw cycles, chemical attack etc.

Tensile strength and Young's modulus of FRP rebars depend mainly on: the shape and size of the cross section of the rebar, the type of fibre and resin, the volumetric ratio of fibres (usually 60-70 V%), the angle between the fibres and the longitudinal axis of the rebar. Tensile strengths of FRP rebars are in the range of 450 to 3 500 N/mm², between 35 000 and 580 000 N/mm² in terms of Young's moduli and in the range of 0.5 to 4.4% in terms of failure strains (Balázs, Borosnyói, 2000; *fib*, 2007). The most important difference between FRP and steel rebars is that FRP rebars have linear elastic behaviour up to failure without any plasticity and

considerable release of elastic energy. FRP rebars can be engineered to have the desired mechanical and physical properties (Sólyom, Balázs, 2015a).

There are two basic types of test methods for investigating of bond behaviour of FRP rebars in concrete: *pull-out tests* and *beam tests*. Pull-out tests are the most widely used. These tests offer the simplest approach to determine the bond strength of rebars in concrete, even though, it is well known that, the stresses developed in the concrete during pull-out tests rarely occur in practice, and the bond values developed under these tests differ substantially from those developed in reinforced concrete elements under practical conditions (Achillides, Pilakoutas, 2004).

Beam tests address some of the disadvantages of the pull-out tests offering the advantages of representing the bond stress fields more accurately (Tighiouart, Benmokrane, Gao, 1998).

Herein a brief overview is presented on the material properties as well as on the interaction between FRP rebar and concrete for internal FRP rebars.

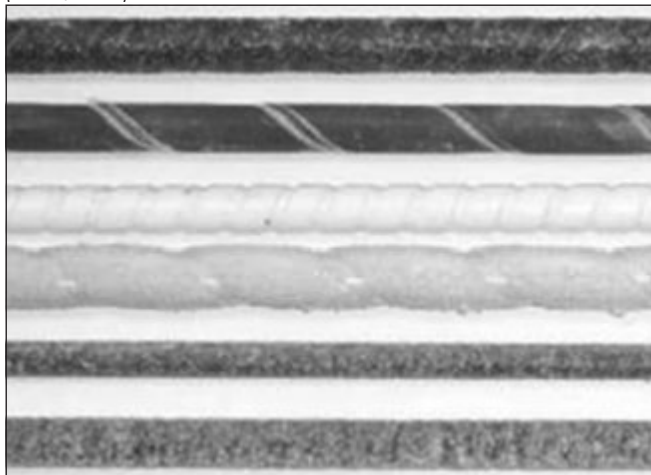
2. REINFORCEMENT CHARACTERISTICS

In the technical report prepared by *fib* Task Group 9.3 (*fib*, 2007) there is a comprehensive description about fibre reinforced polymer rebars as internal reinforcement for reinforced concrete structures. FRP rebars are made of continuous fibres impregnated with polymeric resins. Low modulus polymeric matrix is used to bond together continuous fibres with high strength and high stiffness. In the case of FRP composites the reinforcing fibres constitute the backbone of the material and they determine its strength and stiffness in the direction of the fibres.

The polymeric matrix has the following roles in the composite material: to bind together the fibres and protect their surface from damage during handling, fabrication and service life of the composite; to separate the fibres; to transfer stresses from the surface of the FRP rebar to the fibres. The matrix should be chemically and thermally compatible with the fibres.

The most widespread manufacturing process is the *pultrusion process*. Fibres are pulled and impregnated before curing takes place in a heated die. The mechanical properties of FRP rebar can be tailored by different fibre arrangements

Fig. 1: FRP rebars: carbon (top two), glass (middle two), basalt fibre reinforced polymer rebars (bottom two) with various surface preparations (Szabó, 2013)



or a combination of two or more types of fibres. Appropriate selections of the surface deformation: sand coating, over-moulding a new surface on the rebar or indentation can contribute to achieve high bond strength of FRP rebars in concrete.

Typical FRP rebar products for construction are shown in *Fig. 1*.

2.1 Fibres

Properties of FRP rebars in longitudinal directions depends mainly on fibres. They are stiff enough for handling, are lightweight and have high tensile strength. Fibres are stronger than the bulk material that constitutes the fibres due to their preferential orientation of molecules along the fibre direction and because of the reduced number of defects present in fibre compared to the bulk material. The most important fibres used to make FRP rebars are glass, carbon, aramid and basalt. All these fibres exhibit a linear elastic behaviour under tensile loading up to failure without showing any yield. Glass and basalt fibres are isotropic, having the same values of mechanical and thermal properties in the main directions, while carbon and aramid fibres are anisotropic.

2.2 Polymeric matrices

Matrices can be considered both a structural as well as a protection component. Matrix is a polymeric composite and it is called resin system during processing the FRP rebars. Composite material fabrication and properties are fundamentally affected by the resin, its chemical composition and physical properties. Therefore, the choice of matrix will affect both the mechanical and physical properties of the final product, special care should be taken when designing a composite system.

FRP rebars are produced using two basic types of polymeric matrices: thermosetting and thermoplastic resins. Thermosetting resins are polymers which are irreversibly formed from low molecular weight precursors of low viscosity. They cannot be melted after curing. If they are heated, their shape remains unchanged until thermal decomposition at high temperature. Typical thermosetting resins are epoxy, polyesters and vinyl ester.

Thermoplastics resins are capable of being reshaped by subjecting them to temperature reaching values above their forming temperature. Most common thermoplastic resins are polyether ether ketone (PEEK), polyphenylene sulphide (PPS) and polysulfone (PSUL).

3. BOND MECHANISM OF FRP REINFORCEMENT TO CONCRETE

In order to develop new design guidelines, and hence facilitate the faster acceptance of FRP materials by the construction industry, a better understanding of the composite action of FRP reinforced concrete is essential. Bond between concrete and FRP rebars is crucial to develop the composite action of FRP reinforced concrete. To achieve composite behaviour, proper bond must be activated between reinforcement and concrete for the successful transfer of forces from one to the other (*fib*, 2007).

Owing to the different material characteristics, manufacturing processes and surface treatments bond of FRP

rebars differ from that of conventional steel reinforcement in many ways. The most fundamental differences between the two reinforcing materials (steel and FRP) are that steel is isotropic, homogeneous and elasto-plastic material, whereas FRP is anisotropic, non-homogeneous and linear elastic.

In spite the fact that differences in bond mechanism of FRP and steel rebars exist, there are also similarities such as: an increase in bond strength can be achieved either from a decrease in rebar diameter or a decrease in embedment length, furthermore the position of rebar during casting has the same effect in both cases.

3.1 FRP rebar-concrete interaction

Description of the bond mechanism between rebar and concrete is presented in *fib* Bulletin 10 (2000). Bond action of plain FRP rebars is attributed only to the adhesion at zero slip. As soon as the adhesion breaks down, owing to the plain surface of the rebar, bond slip occurs. Due to the surface characteristics, no tensile cracking is likely to occur and splitting bond forces are unlikely to develop. Plain rebars (smooth rebars without any surface treatment) are allowed as internal reinforcements only if they are used together with other anchoring solutions such as bends, hooks and transverse rebars. In case of the surface treated smooth rebars, the bond stress has two main components: the adhesion at zero slip and the friction as slip is developed. When deformed rebars are considered, there is a third component: the mechanical interlock (also known as bearing), playing the most important role in developing high bond strength, among the three components of bond stress. In this article the authors will study only surface treated and deformed FRP rebars.

In case of the deformed or surface treated FRP rebars, the interaction between concrete and FRP rebar is described in *Fig. 2* by using the bond versus loaded end slip response curve.

Section OA: At the beginning of loading, the main mechanism resisting the external load is the chemical adhesion between the two materials. At this stage, no measurable slip is observed.

Section AB: For higher bond stress values (as the load increases) the chemical adhesion breaks down and a different bond mechanism is set. The slip at the loaded end of the rebar increases and the deformations of the rebar and induce large bearing stresses in the concrete, thus originating microcracks at the tips of the rebar deformations allowing the rebar to slip. It is believed that the onset of the microcracks is delayed because of the “softer” surface deformations of the FRP rebars when compared to that of steel rebars.

Section BC: As the slip of the rebar increases, the bearing

stresses increase considerably and the radial component from the bond forces is balanced against the rings of tensile stresses developed in concrete. If the rebar is not adequately confined and the value of the tensile hoop of stresses exceeds the tensile strength of concrete, splitting cracks may appear along the length of the rebar.

Section CD: If sufficient resistance to splitting can be provided by the surrounding concrete the bond stress can reach the maximum bond strength (τ_b^*). Once the maximum bond stress has been reached, the bearing mechanism breaks down. The residual bond strength is mainly dependent on the frictional resistance as both ends of the rebar (loaded and unloaded) are slipping.

3.2 Failure modes

Depending on the concrete strength and shear strength of surface deformations, four different modes of bond failure can take place (*fib*, 2000):

Shearing off part or all the surface deformations of the rebar. In this case the concrete strength is high enough, so the bond strength of FRP rebars is controlled by the shear strength between successive layers of fibre or by the shear strength of rebar deformations. Therefore, an increase in concrete strength will not be necessarily followed by an increase in bond strength of the FRP rebar. This type of bond failure yields the highest possible bond strength.

Concrete shear failure. For lower concrete grades, the concrete is crushed in front of the rebar deformations; therefore the bond strength is mainly controlled by the concrete shear strength. This failure mode is similar to that of deformed steel rebars.

Combined mode. With intermediate levels of concrete strength, a combined mode of the above failures is likely to occur.

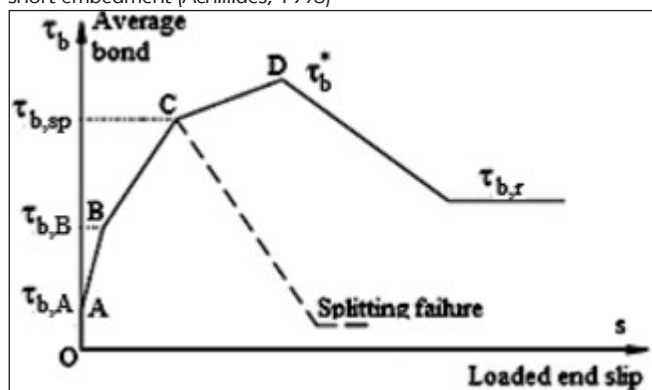
Squeeze through. Due to the low stiffness in the radial direction, the rebar can squeeze through the concrete. In this case bond is provided by the friction between the deformations of the rebar and the concrete. The bond is much more ductile in this case.

4. TEST METHODS

Baena Muñoz (2010) and Szabó (2013) in their researches have drawn attention to the importance of test method on final results. Usually, in a testing program the test setup is not considered a variable although its influence on the test results should be known in order to compare to results of different studies. Effect of testing method on the test results should be minimized in any case (Szabó, 2013).

Another possible source of error, when calculating the bond strength, is presented in a study done by Soong, Raghavan, Rizkalla (2011). In the study the result of two previous researches were compared to illustrate the influence of loading rate and inconsistency in the definition of contact surface area used in the calculation of interfacial bond strength. Since the dimensions and the properties of the rebar and the concrete were the same, the difference in the maximum pull-out load is believed to be due to the differences in the loading rates used by the two groups of researchers. Despite the fact that, the pull-out loads reported by Al-Zaharani (1995) were lower than the ones reported by Benmokrane et al. (1999), the bond strengths were higher with same rebar dimensions. In addition to the effect of loading rate, another reason for this is believed to be the difference in the definition and calculation of the

Fig. 2: Typical average bond stress versus loaded end slip curve of FRP short embedment (Achillides, 1998)



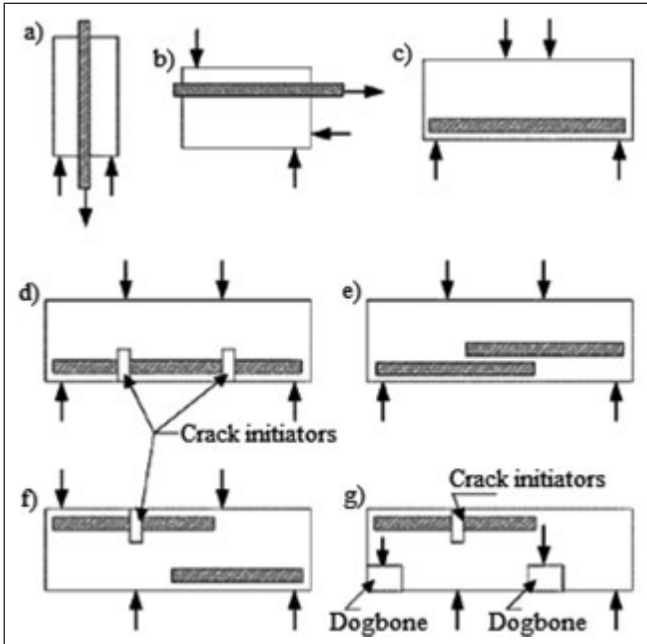


Fig. 3: Types of test methods for different bond values of FRP rebars in concrete: a) pull-out specimen; b) beam-end specimen; c) simple beam specimen; d) hinged beam-end specimen; e) splice specimen; f) cantilever beam specimen (without dogbones); and g) cantilever beam specimen (with dogbones). (ACI, 2004)

contact surface area. While Benmokrane et al. (1999) have calculated the contact surface area using the average diameter of the rebar. Al-Zahrani (1995) has calculated the contact area using the actual diameter of the rebar and the dimensions of the lugs. Above discussion suggests that the interfacial bond strength could be very much dependent on test parameters and surface geometry of the rebar, whereas the interfacial bond strength should be a unique value independent of the test parameters and surface geometry of the rebar.

There are two basic types of test methods for investigating of bond behaviour of FRP rebars in concrete: pull-out tests (Fig. 3.a) and beam tests (Fig. 3.b, Fig. 3.c, Fig. 3.d, Fig. 3.e, Fig. 3.f, Fig. 3.g). Bond strength from beam tests is typically found to be lower than from pull-out tests (ACI, 2003). In case of the pull-out tests, the splitting of the concrete is avoided due to the absence of local bending on the rebar, the confining action of the reaction plate on the concrete specimen and the higher thickness of the concrete cover. In the beam tests setup, the concrete surrounding the rebars is in tension, and leads to cracking under low stresses and reduction of the bond strength. As a consequence, the pull-out tests provide higher bond stress values which can be considered as an upper-bound value for the bond stress-slip performance of FRP rebars. Beam test are offering the advantages of representing the bond stress fields more accurately (Tighiouart, Benmokrane, Gao, 1998).

4.1 Pull-out test

Advantages of pull-out tests are: reduced material use, easily manageable specimen size and the ability to perform high number of tests. Disadvantages are: friction induced at bearing plates, concrete is in compression around the FRP rebar, and difficulties with gripping of the reinforcement (in case of higher applied loads), because the FRP materials are usually weak in transverse direction compared to the longitudinal direction.

Even though pull-out tests are the most common tests for bond analysis, they present some drawbacks too. The most

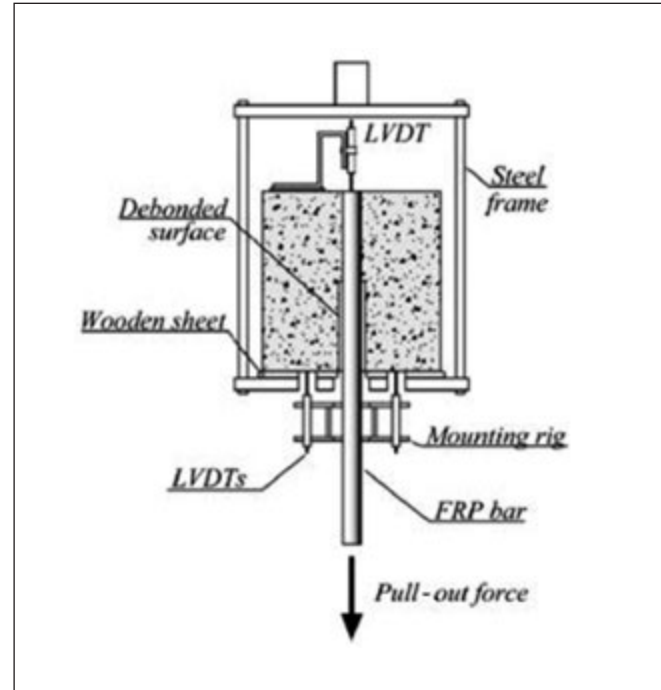


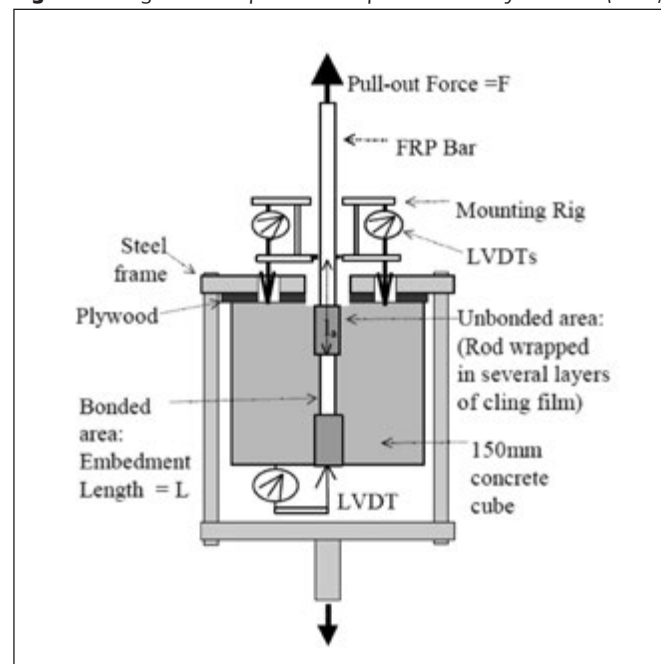
Fig. 4: Loading frame and pull-out test specimen (Guadagnini et al., 2005)

important issue is that the stress conditions during pull-out tests differ from that occurring in the tension zone of flexural members. In pull-out test the concrete surrounding the rebar is under longitudinal compression having generally favourable influence on the bond mechanism.

The pull-out test can be classified as a function of the location of bonded part of FRP rebar inside of the concrete specimen. A scheme of a direct pull-out test is shown in Fig.4. In this case the bonded part is in the outside part of the concrete specimen. It is considered to be the best solution, however special attention is needed when placing the LVDT (Linear Variable Displacement Transducer) at the free and of the FRP rebar, since the embedment length of the rebar is at the very end of the specimen. In this case, any deformation at the end of the concrete due to the pull-out load would be recorded as rebar slip although it is not actually slip (Achillides, Pilakoutas, 2004).

A scheme of another type of direct pull-out test is shown

Fig. 5: Loading frame and pull-out test specimen used by Achillides (1998)



in Fig.5. In this case the bonded part is in the middle segment of the concrete specimen. The above mentioned phenomena (concrete movement could be considered slip) is avoided in this test arrangement, however the wedging effect appears. This is due to the fact that the bonded part of the rebar is slipping out of the concrete specimen during pull-out meanwhile the unbonded part enters into the embedment length zone and it adds additional resistance to the pull-out load (Achillides, Pilakoutas, 2004).

The above phenomenon is irrelevant for steel rebars as the bond failure takes place in the surrounding concrete. Consequently, the unbonded part of the rebar which enters the embedment length zone does not contribute significantly to the bond resistance of the rebar since the bond failure interface is approximately at the height of the tips of rebar deformations (Achillides, Pilakoutas, 2004).

Achillides, Pilakoutas (2004) investigated the difference between the two above mentioned pull-out tests in order to quantify the variation of the bond strength. Analysis of the results showed that the residual bond stress was much lower in that case when the embedment length was located at the end of the specimen (see Fig. 4) (Achillides, 1998). Achillides, Pilakoutas (2004) reported in the study, that the position of the embedment length in the concrete cube does not influence the maximum bond stress developed or the initial bond stiffness of round FRP rebars. The explanation for this is, that the unloaded end slip values recorded up to the maximum pull-out load were less than 1 mm in all the specimens and the wedging effect could not be significantly activated in such a short distance.

Efforts have been taken by different researchers in designing alternative tests in order to minimize the presented disadvantages. The issue of the frictional stresses at bearings could be addressed by the use of low friction materials between support and specimen.

A specially designed test was considered in a study done by Tastani, Pantazopoulou (2006). The authors of the study used a test, for investigation of the bond behaviour, called Direct Tension Pull-out (DTP) test, where the anchorage was forced to occur in the presence of a uniform tensile stress field. A schematic representation of DTP test is shown in Fig. 6. The test specimens had prismatic shapes, with a length of 250 mm. A total number of thirty specimens were tested. The main variables of the study were: the rebar roughness and diameter, the size effect (expressed by the constant cover to rebar diameter ratio) and the external confining pressure (exerted over the anchorage length by transverse externally bonded FRP sheets). The bond length was kept constant of $5d_b$ (d_b - rebar diameter). Experimental results confirmed the unaccountable favourable influence of compression field in conventional pull-out tests, as local bond strength of GFRP rebars anchored in DTP test was in the order of 6-10 MPa, which is lower than the values reported in the international literature that were obtained with conventional pull-out tests.

Another attempt to minimize the disadvantages presented

Fig. 6: Schematic representation of Direct Tension Pull-out test (Tastani, Pantazopoulou, 2006)

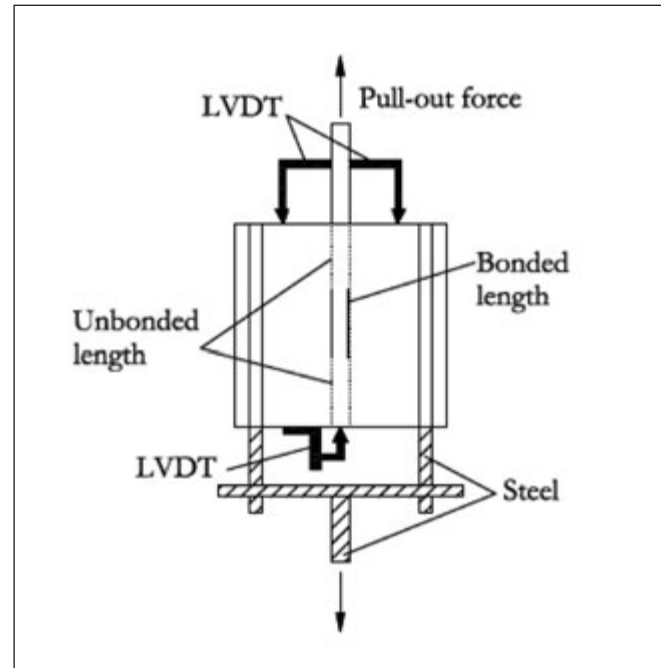
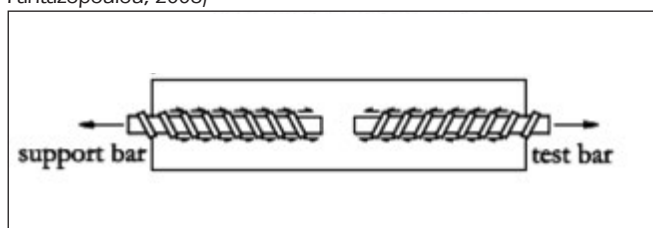


Fig. 7: Scheme of the modified pull-out test (Aiello, Leone, Pecce, 2007)

in case of the traditional pull-out test is presented by Aiello, Leone, Pecce (2007). In this study a modified pull-out test is reported. It was designed so that compression stresses on the concrete were avoided. A schematic representation of the test is shown in Fig. 7. Different FRP rebars (AFRP, CFRP and GFRP) with various surface characteristics (sanded, spiral wound and ribbed) were considered in the study. Bond length of 5 and 7 rebar diameter was studied. Four different concrete grades were used ranging from 30 to 52 MPa. In case of the steel and ribbed FRP rebars, the compression action on concrete, introduced in traditional pull-out test was beneficial, because the possibility of concrete cracking was reduced by the compressive action. Nevertheless, the compression stresses in the concrete gave a negative effect on the bond when sanded and spiral wound FRP rebars were used. The stress increase at the interface promoted the damage of the ribs, considering that in this case surface deformations were less effective in terms of mechanical interlocking with respect to the previous case.

4.2 Beam test

It is generally believed that beam tests can realistically simulate the stress conditions of reinforced concrete elements subjected to bending (Tighiouart, Benmokrane, Gao, 1998). Test beam consists of two rectangular blocks of reinforced concrete joined at the top by a steel hinge joint and at the bottom by the reinforcement to be tested for bonding with the concrete. The dimensions of the beam are indicated in Fig. 8. Only a part of the reinforcement is anchored in each block, while the remaining part is isolated from the concrete. The test beam is loaded when it is resting on two roller bearings by two equal forces applied symmetrically on both sides of the hinge joint using a hydraulic testing system. The slips at each free end of the rebar can be measured by LVDT. The value of the tensile force T in the rebar can be directly calculated by the following relationship:

$$T = P d / (2 h)$$

where:

d distance from the location of the vertical half load to the axis of the beam support

h distance between the center of the steel hinge and the axis of the rebar.

The average bond strength τ_b over the embedment length could be calculated as:

$$\tau_b = T / (\pi d_b \ell_b)$$

where:

d_b nominal rebar diameter

ℓ_b embedment length.

An attempt to further develop the beam test was achieved by Pecce et al. (2001). The modified beam test present a great reduction of the compression stresses in the concrete core is. The test setup allowed two bond tests on the two concrete elements to be conducted simultaneously. The specimen scheme and the dimensions as well as a schematic representation of the test setup are shown in Fig. 9 and Fig. 10, respectively.

5. CONCLUSIONS

The deterioration of concrete structures due to corrosion has turned the attention of structural engineers to the possible use of non-metallic (therefore non-corrosive), FRP (Fibre Reinforced Polymer) rebars in concrete structures.

Fibre material can be glass, aramid, carbon or basalt fibres.

Fig. 8: Scheme of beam test (Tighiouart, Benmokrane, Gao, 1998)

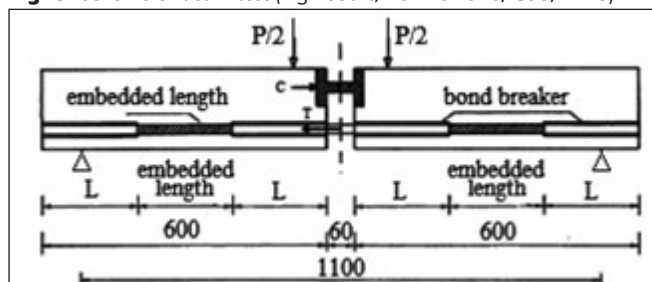


Fig. 9: Specimen configuration (Pecce et al., 2001)

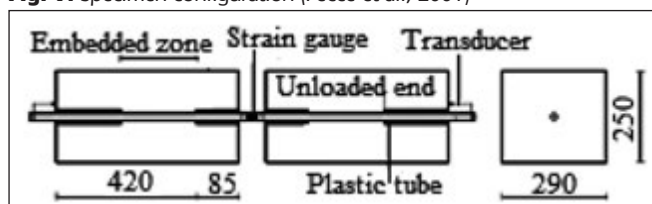
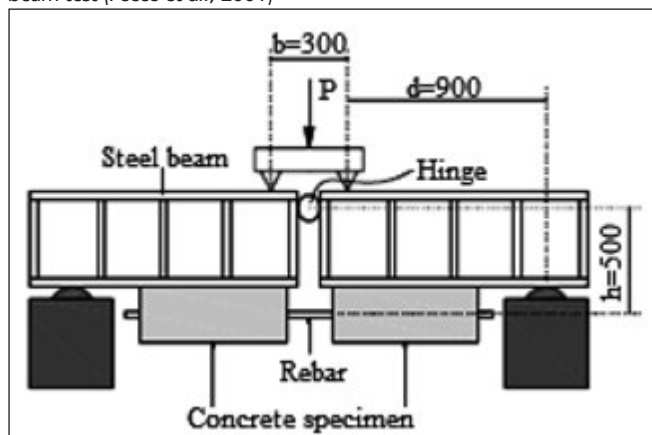


Fig. 10: Schematic representation of the arrangement of modified beam test (Pecce et al., 2001)



The matrix is usually epoxy. FRP rebars have mechanical properties and surface characteristics which are considerably different from that of the conventional steel reinforcements and provide excellent resistance to environmental factors such as freeze-thaw cycles, chemical attack etc. Young's moduli of FRPs can be higher or lower than that of steel. FRPs are linearly elastic and brittle materials. Therefore, the risk of brittle failure has to be taken into account during design. However, a major advantage of FRP rebars is, that they can be engineered to have the desired mechanical and physical properties.

Due to various constituent materials, manufacturing processes and surface treatments of non-metallic reinforcement, both bond performance and failure of bond can take place in different ways than in the case of conventional reinforcement.

There are two basic types of test methods for investigating of bond behaviour of FRP rebars in concrete: *pull-out tests* and *beam tests*.

Pull-out tests are the most widely used, since they offer the simplest approach to determine the bond strength of rebars in concrete. However, it has to be mentioned that, the stresses developed in the concrete during pull-out tests rarely occur in practice and the bond values developed under these tests differ substantially from those developed in reinforced concrete elements under practical conditions.

It is generally believed that beam tests can realistically simulate the stress conditions of reinforced concrete elements subjected to bending, nevertheless it is not as cost and time effective than the pull-out test method.

FRP reinforcement, most likely, will never totally replace the steel reinforcement. However, owing to the several advantageous properties (e.g.: excellent resistance to environmental factors, high strength to weight ratio) the use of FRP materials leads to more durable structural solutions in many cases.

6. ACKNOWLEDGEMENTS

The authors gratefully acknowledge the financial support of European Network for Durable Reinforcement and Rehabilitation Solutions (**endure**), Networks for Initial Training (ITN), Seventh Framework Programme of the European Union (Grant: PITN-GA-2013-607851) and COST Action TU1207 „Next Generation Design Guidelines for Composites in Construction”.

7. REFERENCES

- Achillides, Z., Pilakoutas, K. (2004): “Bond behavior of fiber reinforced polymer bars under direct pullout conditions”, *Journal of Composites for Construction*, 8 (2), pp. 173-181 [http://dx.doi.org/10.1061/\(ASCE\)1090-0268\(2004\)8:2\(173\)](http://dx.doi.org/10.1061/(ASCE)1090-0268(2004)8:2(173))
- ACI Committee 408 (2003): “Bond and development of straight reinforcing bars in tension (ACI408-03)”, *American Concrete Institute*, Farmington Hills, MI, 49 pp.
- ACI Committee 440 (2004): “Guide Test Methods for Fiber-Reinforced Polymers (FRPs) for Reinforcing or Strengthening Concrete Structures (ACI 440.3R-04)”, *American Concrete Institute*, Farmington Hills, MI, 40 pp.
- Aiello, M. A., Leone, M., Pecce, M. (2007): “Bond performances of FRP rebars reinforced concrete”, *Journal of Materials in Civil Engineering*, 19(3), pp. 205-213
- Baena Muñoz, M. (2010): “Study of bond behaviour between FRP reinforcement and concrete”, *PhD Thesis*, University of Girona
- Balázs, G. L., Borosnyói, A. (2000): “Non-metallic (FRP) reinforcement for bridge construction”, *Vasbetonépítés*, Vol. 2, 2000/2, pp. 45-52 (in Hungarian)
- Benmokrane, B., Maceachern, M., That T. T., Zhang B. (1999): “Evaluation

- of bond characteristics of GFRP rebars embedded in polymer and normal cement concrete”, *Technical report no. 7*, University of Sherbrooke
- Borosnyói, A., Balázs, G. L. (2001): “Application of non-metallic (FRP) reinforcement in concrete bridges”, *Concrete Structures*, Vol. 2, pp. 21-28
- Borosnyói, A., Balázs, G. L. (2002): “Bond of non-metallic (FRP) reinforcements”, *Vasbetonépítés*, Vol. 4, 2002/4, pp. 114-122 (in Hungarian)
- Borosnyói, A. (2015): “Influence of service temperature and strain rate on the bond performance of CFRP reinforcement in concrete”, *Composite Structures*, doi: <http://dx.doi.org/10.1016/j.compstruct.2015.02.076>
- CEB (1982): “Bond action and bond behaviour of reinforcement”, State-of-the-Art Report, *Committee Euro-international du Béton*, CEB Bulletin 151
- fib (2000): “Bond of Reinforcement in Concrete”, State-of-art Report, *Bulletin 10*, fib - International Federation for Structural Concrete, Lausanne
- fib (2007): “FRP reinforcement in RC structures”, Technical report, *Bulletin 40*, fib - International Federation for Structural Concrete, Lausanne
- Guadagnini, M., Pilakoutas, K., Waldron, P., Achillides, Z. (2005): “Tests for the evaluation of bond properties of FRP bars in concrete”, *2nd International Conference on FRP Composites in Civil Engineering* (CICE 2004), pp. 343-350
- Lublóy, É., Balázs, G. L., Borosnyói, A., Nehme, S. G. (2005): “Bond of CFRP wires under elevated temperature”, *Proceedings “Bond Behaviour of FRP in Structures”* (Eds. Teng and Chen) 7-9. Dec. 2005 Hong Kong, China, ISBN 962-367-506-2, pp. 163-167. http://www.iifc-hq.org/proceedings/BBFS_2005/Basic%20Bond%20Mechanisms/Bond%20of%20CFRP%20Wires%20Under%20Evaluated%20Temperature.pdf
- Pecce, M., Manfredi, G., Realfonzo, R., Cosenza, E. (2001): “Experimental and analytical evaluation of bond properties of GFRP bars”, *Journal of Materials in Civil Engineering*, July/August 2001, pp. 282-290
- Sólyom, S., Balázs, G. L. (2015a): “Fibre Reinforced Polymer (FRP) rebars – I. Material Characteristics”, *Vasbetonépítés*, Vol.17, 2015/1, pp. 13-16. (in Hungarian)
- Sólyom, S., Balázs, G. L. (2015b): “Bond strength of FRP rebars”, *Concrete Structures*, Vol. 16. pp. 62-68
- Soong, W. H., Raghavan, J., Rizkalla, S. H. (2011): “Fundamental mechanisms of bonding of glass fiber reinforced polymer reinforcement to concrete”, *Construction and Building Materials*, 25, pp. 2813–2821
- Szabó, Zs. K. (2013): “Bond characteristics of NSM reinforcements based on advanced test method”, *PhD Thesis*, Budapest University of Technology and Economics
- Szabó, Zs. K., Balázs, G. L. (2007): “Near surface mounted FRP reinforcement for strengthening of concrete structures”, *Periodica Polytechnica*, 51/1, pp. 33-38, doi: 10.3311/pp.ci.2007-1.05
- Tastani, S.P., Pantazopoulou, S.J. (2006): “Bond of GFRP bars in concrete: Experimental study and analytical interpretation”, *Journal of Composites for Construction*, 10(5), pp. 381-391
- Tighiouart, B., Benmokrane, B., Gao, D. (1998): “Investigation of bond in concrete member with fibre reinforced polymer (FRP) bars”, *Construction and Building Materials*, 12, pp. 453-462
- Sándor Sólyom** (1984) Civil Engineer, Early Stage Researcher at Budapest University of Technology and Economics (BME). Main fields of interest: application possibilities of Fibre Reinforced Polymer (FRP) rebars in reinforced concrete structures, bond in concrete, strengthening with advanced composites. Member of the fib T5.1 “FRP (Fibre Reinforced Polymer) reinforcement for concrete structures” and the Hungarian Group of fib. Research fellow in endure (European Network for Durable Reinforcement and Rehabilitation Solutions).
- Prof. György L. Balázs** (1958) Civil Engineer, PhD, Dr.-habil., professor of structural engineering, head of Department of Construction Materials and Technologies and Deputy Dean of the Civil Engineering Faculty of Budapest University of Technology and Economics (BME). His main fields of activities are experimental investigation and modelling of RC, PC, FRC structures, HSC, fire resistance of concrete. He is chairman of several commissions and task groups of fib. He is president of Hungarian Group of fib, Editor-in-chief of the Journal “Concrete Structures” and the honorary President of fib.
- Assoc. Prof. Adorján Borosnyói** (1974) Civil Engineer (MSc), PhD, associate professor at the Department of Construction Materials and Technologies, Budapest University of Technology and Economics (BME). Main fields of interest: application of non-metallic (FRP) reinforcements for concrete structures, bond in concrete, non-destructive testing of concrete. Member of the fib T2.1 „Serviceability Models”, fib T5.1 “FRP (Fibre Reinforced Polymer) reinforcement for concrete structures” and the Hungarian Group of fib. Corresponding member of RILEM Technical Committee ISC “Non destructive in situ strength assessment of concrete”.

REINFORCEMENT CORROSION IN ASPECT OF CRACK WIDTH OF CONCRETE



Réka Anna Nagy

In this paper literature review is given on experiments and case studies investigating the effect of crack width on reinforcement corrosion in concrete. Results are compared and attention is drawn to their inconsistency. Crack width variation within concrete cover is presented as a reason. The influencing factors of corrosion are collected with special regard to crack geometry.

Keywords: concrete, reinforcement corrosion, crack width, tortuosity

1. INTRODUCTION

The corrosion mechanism of steel in reinforced concrete is introduced in the technical literature in details (Bertolini et al 2004; Richardson 2002; Malhotra, Carino 2004). Steel reinforcement corrodes when oxygen and water is supplied and the protection of steel is ceased due to either carbonation of concrete or the presence of chloride ions (fib, 2010). Corrosion can be described as a diffusion process where the corrosive agents (oxygen, water, carbon-dioxide and chloride ions) migrate inside the concrete to balance the outside concentration gradient (Duracrete, 2000). Permeability of concrete is one of the governing factors of corrosion and can be quantified by diffusion coefficients.

Cracks develop under loading in reinforced concrete structures. The permeability of concrete increases in the presence of cracks. Studies (Djetbi 2008; Jung 2011) confirm that the diffusion coefficient of cracked concrete increases with larger surface crack width. Therefore, corrosive agents migrate faster towards the reinforcement and it can be assumed that corrosion initiates sooner and propagates at a higher rate in case of larger surface crack width. This is a reason why surface crack width is limited by design codes in order to delay corrosion.

In the technical literature both confirming and contradicting results can be found on the relationship between crack width and corrosion. The aim of this paper is to review the relevant literature, draw attention to the inconsistencies and find possible reasons.

2. CRACK WIDTH AND CORROSION – LITERATURE REVIEW

2.1 Rehm, Nürnberger and Neubert (1988)

The authors examined the corrosion condition of the reinforcement within the 30 years old concrete piers of Helgoland, Germany. Fifty core samples were taken and chloride content, crack width and steel corrosion were surveyed. The

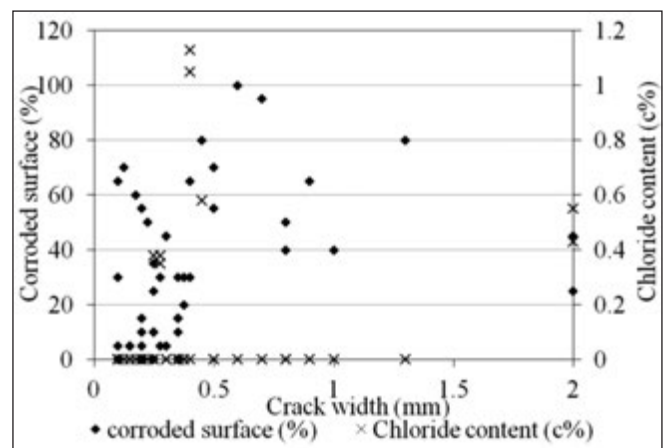


Figure 1: Corroded steel surface, chloride content (percentage of cement mass) and crack width (based on Rehm et al, 1988)

corrosion was measured as the ratio of corroded reinforcement surface, additionally to corrosion grades that were defined by the authors based on the thickness and area of rust.

In Fig. 1 the percentage of corroded steel surface and chloride content (relative to mass of cement) are presented together with the corresponding crack width. The degree of corrosion shows an increasing tendency with larger crack width, although the data are scattered. Based on the observations the chloride content does not depend on the crack width and corrosion occurs in case of negligible chloride content as well.

2.2 Berke, Dellaire, Hicks, and Hoopes (1993)

Mechanically cracked reinforced concrete beams were ponded with 3% NaCl solution in the study of the authors. Two weeks wet and two weeks dry cycles were applied for 16 months then chloride concentration and corroded reinforcement area were measured near the crack. Fig. 2 shows that chloride content can be found within the same range for all specimens, however, the corroded area varies. The low number of specimens is due to the fact that the authors investigated the effect of calcium nitrate on corrosion and these were the reference specimens. The present paper does not have the aim of discussing the influence of calcium nitrate on the corrosion of embedded steel.

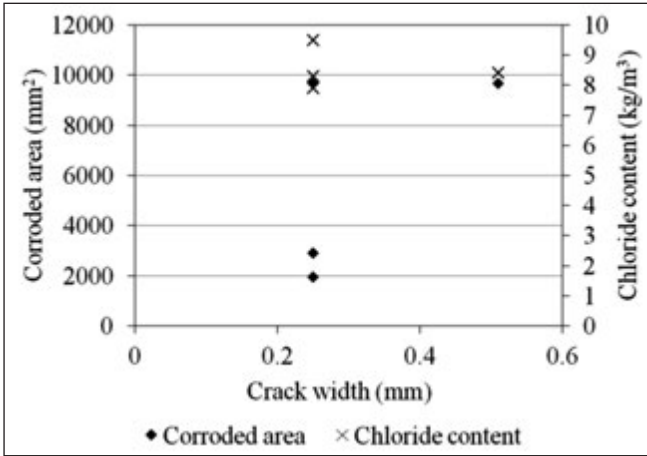


Figure 2: Corroded steel surface, chloride content and crack width (based on Berke et al, 1993)

An explanation to the observations of the authors can be that chloride reaches the reinforcement even through cracks of smaller widths and accelerates corrosion nevertheless the necessary oxygen supply is less effective in this case.

2.3 Sagüés, Kranc et al (1994)

A thorough study was carried out on several coastal reinforced concrete bridges in Florida, USA. The source of chloride ions was sea water and mist. Core drilling sample pairs

Figure 3: Ratio of chloride content in cracked and sound concrete and crack width of different bridges, in 25-38 mm depth (based on Sagües, Kranc et al, 1994) *Note: bridge identification according to the original paper

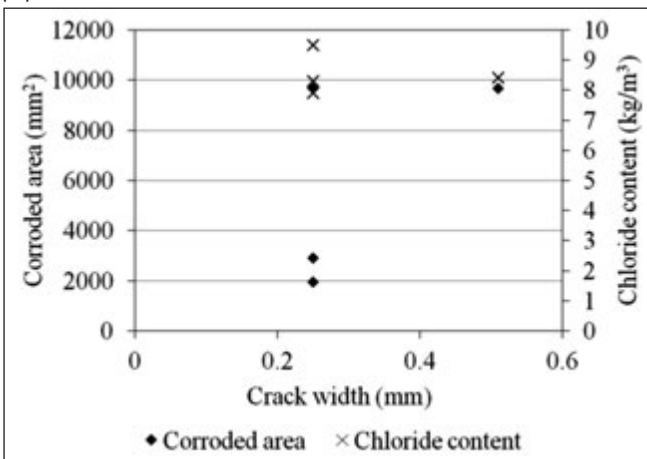
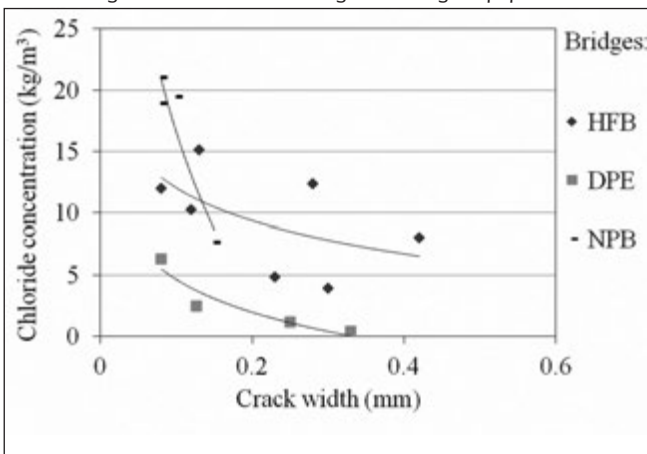


Figure 4: Crack width and absolute chloride concentration in 3 bridges, in 21-37 mm depth (based on Sagües, Kranc et al, 1994) *Note: bridge identification according to the original paper



were taken from cracked and sound concrete of the same location and their chloride content was determined. In Fig. 3 the ratio of the chloride content of cracked and corresponding sound samples is presented as the function of crack width based on the data published by the authors. It does not show any trend, therefore, it cannot be concluded that the increasing crack width results increasing chloride concentration.

Further conclusions can be drawn by the analysis of those bridges where sufficient number of measurements was taken. In Fig. 4 the absolute chloride concentration is given as the function of crack width. It shows that chloride concentration decreases with increasing crack width on the contrary to that would be expected.

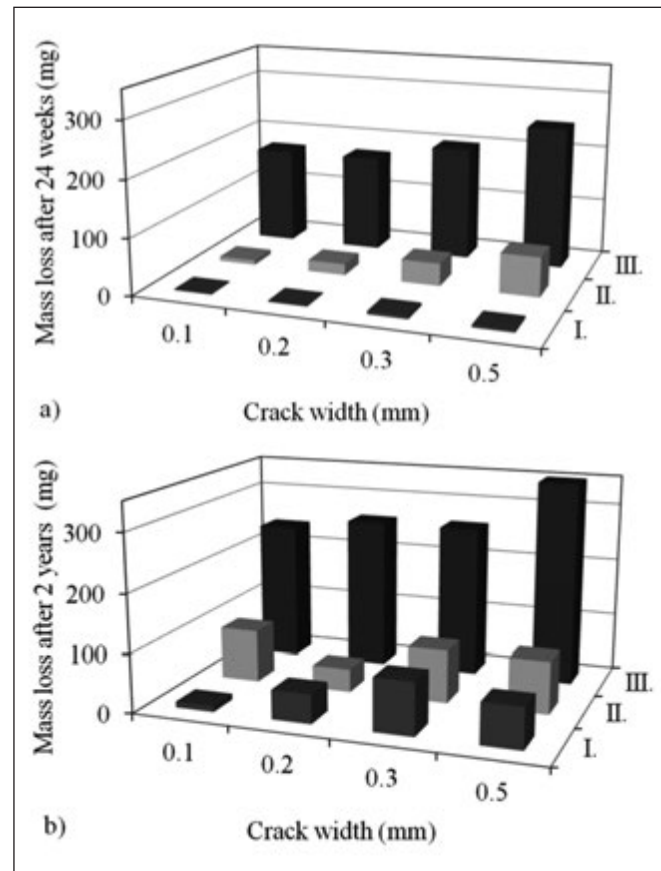
Concrete binds part of the chloride ions and chloride content measurement includes ions both in chemically bonded and in free form. Higher crack width results in thicker carbonated depth and carbonated concrete has lower ability to bind chlorides; therefore, the total chloride content is smaller.

2.4 Schießl and Raupach (1997)

The authors studied mechanically cracked reinforced concrete beams subjected to 1% chloride solution modelling the splash zone of motorways during winter. Twelve wetting cycles were performed which were repeated again after one year. The effect of crack width, crack spacing, concrete cover (c) and water-to-cement ratio (w/c) was investigated. Corrosion was defined as mass loss of the reinforcement and it was measured after 24 weeks and 2 years. Fig. 5 a and b represent the experimental results.

It was concluded that the quality and the thickness of concrete cover are more dominant influencing factors of corrosion than crack width. The effect of crack width decreased with time. The authors carried out calculations and found that

Figure 5: Mass loss of reinforcement with crack width, I. c=35 mm, w/c=0.5; II. c=35 mm, w/c=0.6; III. c=15 mm, w/c=0.6 a) after 24 weeks b) after 2 years (Schießl and Raupach, 1997)



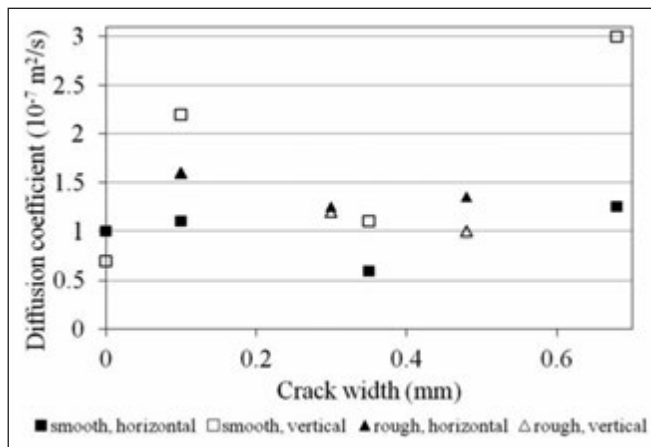


Figure 6: Chloride diffusion coefficient and crack width in case of smooth and rough surfaced cracks, chloride penetration measured in horizontal and vertical direction (Rodríguez and Hooton, 2003)

smaller reinforcement diameter – which is a common practice for limiting crack width – results in higher loss of cross section.

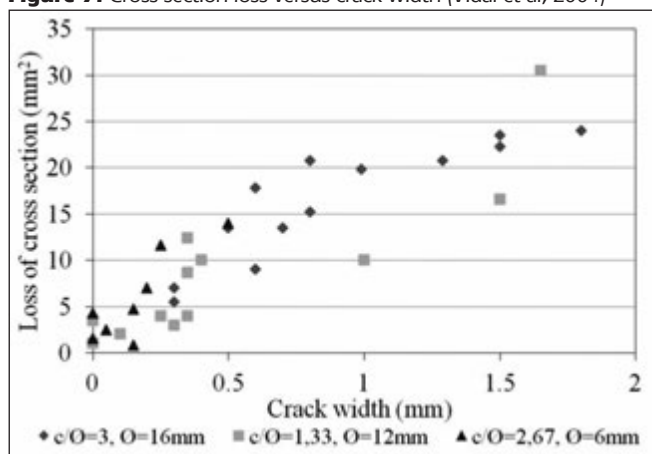
2.5 Rodríguez and Hooton (2003)

Parallel cracks were produced in concrete cylinder specimens by splitting and sawing, resulting rough and smooth surfaced cracks. Crack widths were in the range of 0.08–0.68 mm. Chloride migration tests were performed in a 40 day period and the diffusion coefficient was calculated from the depth of chloride penetration both in vertical and horizontal direction (parallel and perpendicular to the flow respectively) as a measure of corrosion resistance. *Fig. 6* shows the diffusion coefficients for different crack widths. The experiment did not indicate a correlation between diffusion coefficient and crack width or crack surface roughness.

2.6 Vidal, Castel and François (2004)

Reinforced concrete beams were kept under long term loading in salt fog (3.5% NaCl to model the effect of sea water) for 17 years, applying wet-dry cycles. Widths of corrosion cracks were read at the end of the experimental period and the steel bars were cleaned from corrosion products. Loss of cross section was calculated from mass loss per unit length. *Fig. 7* presents the calculated loss of cross section versus crack width with different cover to reinforcement diameter ratios. Significant trend can be observed between crack width and cross section loss, although it has to be emphasised that the cracks were induced by corrosion and not bending moment, therefore, the correlation can be considered evident. It

Figure 7: Cross section loss versus crack width (Vidal et al., 2004)



has been also concluded that the appearance of cracks was mostly influenced by the cover to diameter ratio.

2.7 Otieno, Alexander & Beushausen (2009)

The authors investigated reinforced concrete specimens with no crack, as well as with cracks of 0.4 and 0.7 mm widths. The specimens were subjected to a 16 weeks wet-dry cycle (3 days 5% NaCl solution, 4 days drying). It was concluded that the presence of cracks accelerates the corrosion process. Larger crack width resulted in more severe corrosion when the same cement type and water-to-cement ratio was applied. The cement type, the addition of supplementary cementing materials and the water-to-cement ratio did not influence the corrosion rate as much as the presence of cracks. Therefore, the permeability of concrete is the governing parameter of corrosion only as long as it is uncracked.

2.8 Andrade, Muñoz, Torres-Acosta (2010)

The relation between crack width and corrosion was studied on 16 years old reinforced concrete beams and columns. CaCl₂ accelerating admixture was added to the concrete mix but the corrosion process took place in natural environment. Corrosion penetration in the steel reinforcement was measured. *Fig. 8* shows its value normalised with the ratio of concrete cover to reinforcement diameter versus crack width and a definite trend can be seen: corrosion penetration increases with larger crack width.

2.9 Summary of literature review

The experiments introduced here were carried out under different circumstances, specimens had different sizes and composition and the observed parameters varied as well (cross section loss, chloride penetration, diffusion coefficient, electrical resistance, etc.). *Table 1* summarises if any correlation was found between crack width and corrosion and additional information on concrete cover, water-to-cement ratio, range of measured crack widths, reinforcement diameter, presence of chloride ions and the period of experiments or observations. Based on the data presented no confirmation or disconfirmation of the presumed correlation can be taken.

Figure 8: Corrosion penetration depth (corrected with concrete cover and reinforcement diameter) versus crack width (Andrade et al., 2010)

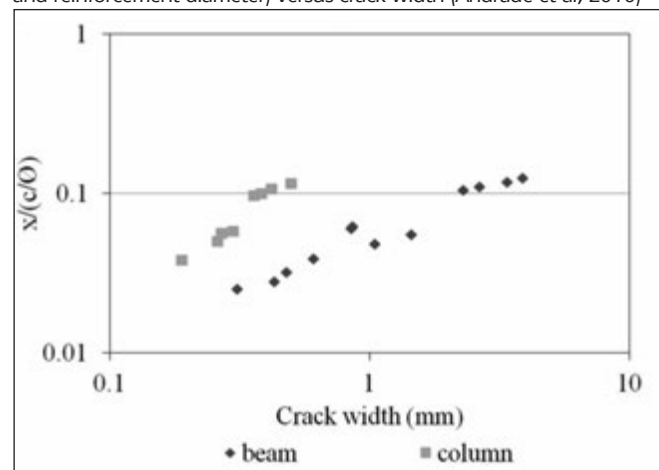


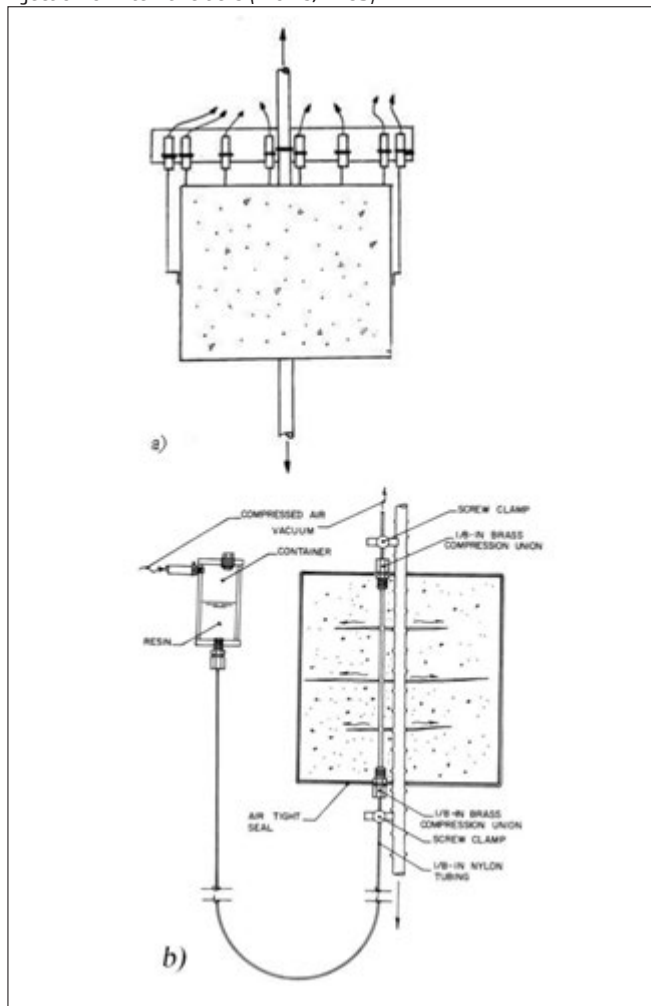
Table 1 Summary of literature on crack width and corrosion

Study	Period	parameter	correlation	Cl	W_{min} (mm)	W_{max} (mm)	c (mm)	w/b	Ø(mm)
2.1.	30 years	corroded surface area	yes	sea water	0.1	2	35+	0.5	20 (16)
2.2.	16 months	corroded surface area	no	NaCl	0.25	0.51	43	0.5	13
2.3.	3-9 years	chloride concentration	no	sea water	0.08	0.42	varies	varies	varies
2.4.	2 years	mass loss	not clear	NaCl	0.1	0.5	15 or 35	0.5 or 0.6	14
2.5.	40 days	diffusion coefficient	no	NaCl	0.1	0.68	-	0.4	-
2.6.	17 years	cross section loss	evident	NaCl fog	0.05	1.8	10 or 40	0.5	12 or 16
2.7.	16 weeks	corrosion rate	yes	NaCl	0.08	0.68	40	0.4 or 0.55	10
2.8.	14 years	corrosion penetration	yes	CaCl ₂	0.19	3.9	30	0.7	12

3. CRACK WIDTH VARIATION WITHIN CONCRETE COVER

Crack width is usually measured on the outer surface of concrete. Design codes limit crack widths also on concrete surface in order to reduce reinforcement corrosion. However, crack width varies within the concrete cover and has different values at the reinforcement surface where corrosion happens. This chapter introduces studies on crack width variation within concrete cover which can add to the understanding of above contradictions.

Figure 9: a) displacement measurement along the cross section b) injection of internal cracks (Broms, 1965)

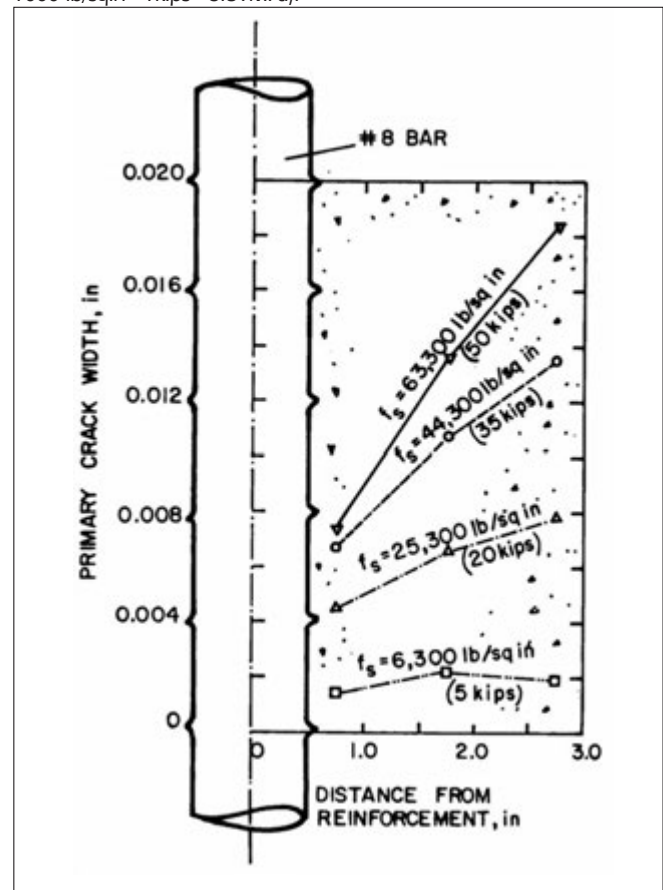


3.1 Broms (1965)

The author conducted tensile tests on reinforced concrete tie elements. The displacements at several locations along the end cross section were measured to obtain crack width within the concrete (Fig. 9). The length of the test specimens was selected so that only one crack could develop. The measured displacements would include the internal secondary cracks. Resin injection was applied in order to avoid compromising the results and the width of internal cracks was subtracted from the displacements and the crack width variation was provided.

It was found that crack width varies within concrete cover; it shows lower values next to the reinforcement surface than at the outer concrete surface. Fig. 10 presents the crack

Figure 10: Crack width versus distance from reinforcement at different stress (Broms, 1965) (#8 bar=25.4mm diameter bar; 1in=25.4 mm; 1000 lb/sqin= 1 kips=6.89MPa).



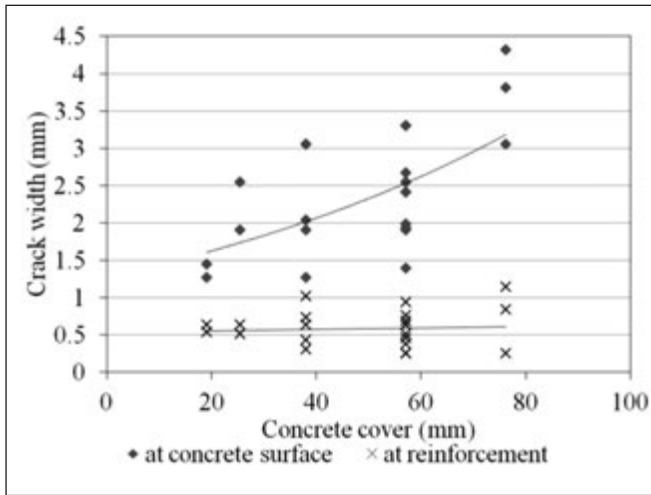


Figure 11: Crack width at outer concrete surface and at reinforcement versus concrete cover (Husain, Ferguson, 1968)

widths at different distances from reinforcement and increasing stress level. Applying higher stresses the crack width increased at the concrete surface to a greater extent than at the level of the reinforcement. In other words crack width variation is more significant at higher stress levels.

3.2 Husain, Ferguson (1968)

The authors performed flexural tests on reinforced concrete beams. Cracks were injected with resin then cut parallel to the axis of reinforcement. Crack widths were read at steel and

concrete surfaces as well. Fig. 11 presents crack widths measured both at outer concrete surface and at reinforcement for beams with different concrete covers. It was concluded that crack width is nearly constant at reinforcement surface and it is independent from the concrete cover. Crack width measured at concrete surface increased with increasing concrete cover; however, the relationship is not linear.

3.3 Borosnyói, Snóbli (2010)

The authors performed tensile tests on reinforced concrete ties. Cracks were fixed by resin injection and the elements were cut to read crack width inside. Hand microscope was used to read crack widths at every 2 mm inside the concrete cover. Crack widths were presented as function of distance from reinforcement (Fig. 12). Results confirmed that crack width can significantly differ at reinforcement and at concrete surface and the thickness of concrete cover can be one of the governing factors.

It can be assumed that if there is correlation between crack width at reinforcement and at outer concrete surface it is non-linear. Measuring crack width at concrete surface can be one of the reasons for the lack of definite relationship between crack width and corrosion.

4. DISCUSSION

Based on literature it can be concluded that corrosion is a complex process with a number of influencing factors (Fig. 13). One of the factors is evidently the environment: the out-

Figure 12: Crack width variation within concrete cover - 20, 40, 60 and 80 mm cover (Borosnyói, Snóbli, 2010)

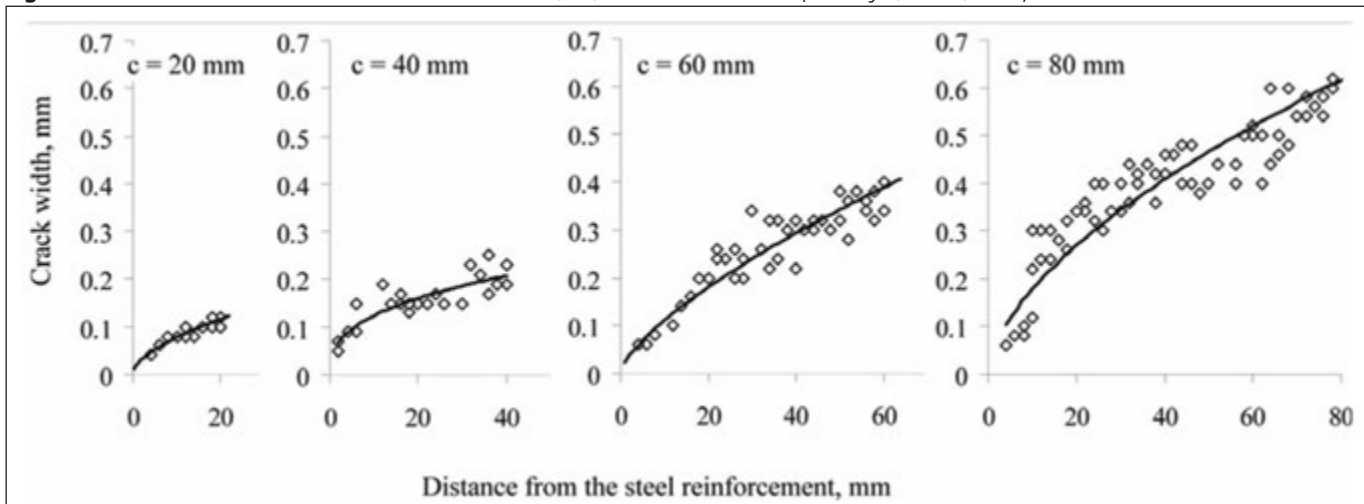
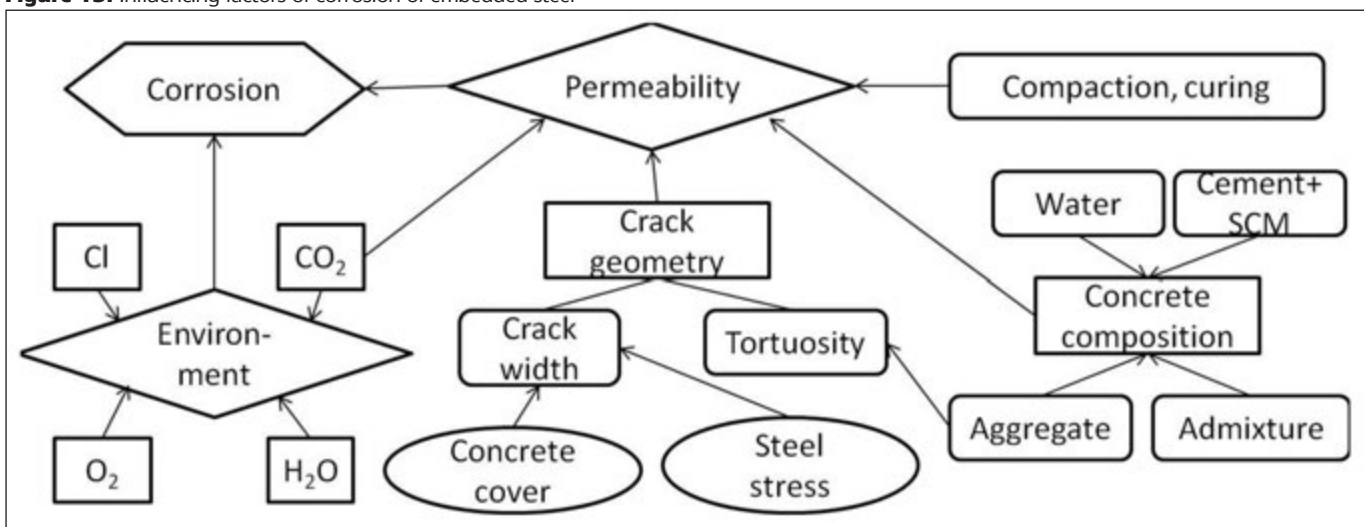


Figure 13: Influencing factors of corrosion of embedded steel



side concentration of corrosive agents starts migration inside the concrete to reach equilibrium. Other factor is the material itself: permeability of concrete has a key role delaying the diffusion of corrosive agents towards reinforcement. Permeability depends on concrete composition, compaction, curing, age and the presence and geometry of cracks.

There have been limited studies on crack geometry and its influence on permeability or corrosion. Akhavan et al (2012) investigated the water permeability of cracked mortars considering crack width, tortuosity and crack roughness. The authors concluded that all of these parameters are necessary to describe the permeability of hardened mortar. It can be assumed that studying crack geometry rather than crack width at concrete surface can bring us closer to understand corrosion processes.

4.1 Tortuosity

Tortuosity is a property of a curve that expresses the relation of the length of the curve (L) and the straight line (X) connecting the start and end point of the curve (Fig. 14). There is no agreement in an exact formula for the definition of tortuosity, therefore, it is usually chosen arbitrarily to fit the investigated property. Akhavan et al (2012) used the square of the arc-chord ratio (that is the ratio of the length of the curve, L to the distance between the ends of it, X; see Eq. 1.) and they found that it matches the experimental data on water permeability.

$$\tau = \left(\frac{L}{X}\right)^2 \quad (1)$$

Tortuosity of concrete may differ from that of mortar. Maximum aggregate size (MSA) is larger which can result more tortuous shape of the cracks. Fig. 15 presents a scanned image of a cracked concrete tie element (details of the experiment can be found in: Nagy, 2013) demonstrating the effect of aggregate size on crack geometry.

Tortuosity is not a scale invariant quantity: it depends on the sampling length that was chosen to determine the length of the curve as the sum of straight segments. In Fig. 16 tortuosity of crack in a reinforced concrete tie element is presented calculated with Eq. 1. as the function of sampling length. It is shown that the value of tortuosity decreases with increasing sampling length.

Future work is needed in this field. It is aimed to study crack geometry and clarify its influence on corrosion. Further analysis is needed to find the optimum sampling length for calculating tortuosity. Future experiments are planned to investigate the effect of maximum size of aggregate (MSA).

Figure 14: Schematic image of crack tortuosity

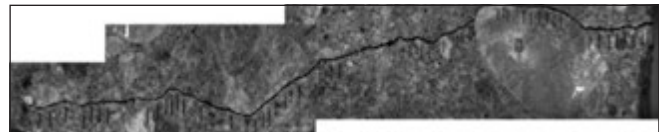
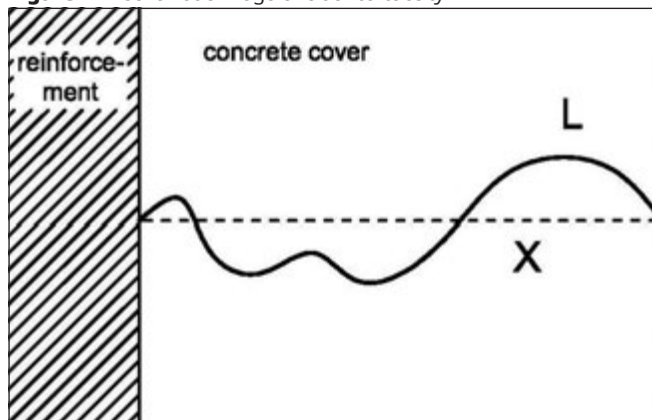


Figure 15: Scanned image of a crack within concrete

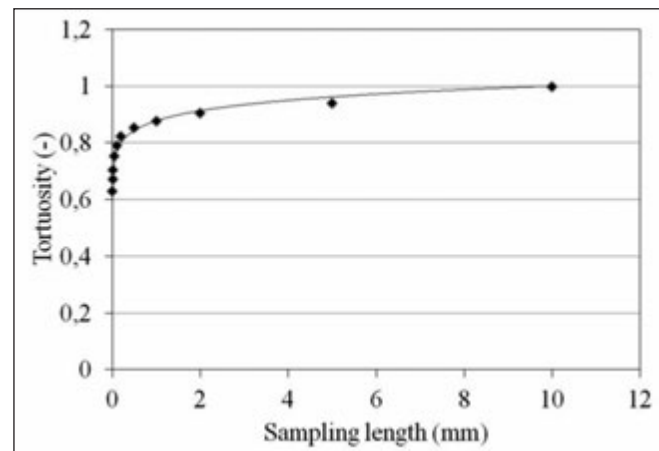


Figure 16: Effect of sampling length on tortuosity

5. CONCLUSIONS

Based on literature data the following conclusions can be drawn:

- there is no definite correlation between reinforcement corrosion and crack width measured at concrete surface;
- chloride concentration does not always increase with surface crack width;
- crack width measured at outer concrete surface differs from that at the level of the reinforcement; their relationship is nonlinear;
- further parameters are needed to be introduced to describe the effect of crack width on corrosion,
- future research is suggested to be directed toward the detailed study of tortuosity of cracks in concrete, its influencing parameters and the relationship with permeability.

6. REFERENCES

- Djerbi, A., Bonnet, S., Khelidj, A., Baroghel-bouny, V., (2008) Influence of traversing crack on chloride diffusion into concrete, *Cement and Concrete Research* 38, pp. 877–883.
- Alireza Akhavan, Seyed-Mohammad-Hadi Shafaatian, Farshad Rajabipour (2012) Quantifying the effects of crack width, tortuosity, and roughness on water permeability of cracked mortars, *Cement and Concrete Research* 42, pp. 313-320.
- Andrade, C., Muñoz, A., Torres-Acosta, A. (2010) Relation between crack width and corrosion degree in corroding elements exposed to the natural atmosphere, *Korea Concrete Institute*, 2010
- Berke, N.S., Dellaire, M.P., Hicks, M.C., Hoopes, R.J. (1993) Corrosion of Steel in Cracked Concrete. *Corrosion*, Vol. 49, No. 11, 1993, pp. 934-943.
- Bertolini, L., Elsener, B., Pedferri, P., Polder, R. (2004) Corrosion of Steel in Concrete: Prevention, Diagnosis, Repair, *WILEY-VCH*, 392 p.
- Borosnyói, A., Snóbli, I. (2010) Crack width variation within the concrete cover of reinforced concrete members, *Építőanyag-JSBCM*, Vol. 62, No. 3., pp. 70-74.
- Broms, B. (1965) Crack width and crack spacing in reinforced concrete members, *ACI Journal*, Vol. 62, No. 10, 1965, pp. 1237-1256.
- DuraCrete (2000) Final Technical Report: General Guidelines for Durability Design and Redesign, *The European Union – Brite EuRam III, DuraCrete*, Probabilistic Performance based Durability Design of Concrete Structures, Document BE95-1347/R17, May 2000, 144 p.
- fib (2010) Bulletin 53, Structural Concrete Textbook on behaviour, design and performance, Second edition, Volume 3, *Fédération Internationale du Béton*, 391 p.
- Husain, S. I. and Ferguson, P. M. (1968) Flexural Crack Widths at the Bars in Reinforced Concrete Beams. *Center for Highway Research*, The University of Texas at Austin, Research Report No. 102,1F, 1968.

- Malhotra, V.M., Carino, N.J. (2004) Handbook on non-destructive testing of concrete, *CRC Press LLC*, 384 p.
- Nagy, R. (2013) Structural cracking of reinforced concrete members, *Second Conference of Junior Researchers in Civil Engineering*, 17-18 June 2013, Budapest, Hungary, pp. 136-141.
- Otieno, M.B., Alexander, M.G., Beushausen H.D. (2009) Corrosion propagation in cracked and uncracked concrete, 2nd International Conference on Concrete Repair, Rehabilitation and Retrofitting, *Taylor & Francis Group*, London, 2009
- Rehm, G., Nuernberger, U., Neubert, B. (1988) Chloridkorrosion von Stahl in gerissenem Beton – Untersuchungen an der 30 Jahre alten Westmole in Helgoland, *Schriftenreihe des Deutschen Ausschusses für Stahlbeton*, Beuth, Berlin, 390, pp. 43-144.
- Richardson, M. G. (2002) Fundamentals of Durable Reinforced Concrete, *Spon Press*, London, 272 p.
- Rodriguez, O.G., Hooton, R.D. (2003) Influence of Cracks on Chloride Ingress into Concrete, *ACI Materials Journal*, Vol. 100, No. 2., 2003, pp. 120-126.
- Sagüés, A.A., Kranc, S.C., Presuel-Moreno, F., Rey, D., Torres-Acosta, A., Yao, L. (2001) Corrosion Forecasting for 75-Year Durability Design of Reinforced Concrete, *Final Report* No. BA502 submitted to Florida Department of Transportation by University of South Florida, December 31, 2001.
- Schiebl, P., Raupach, M. (1997) Laboratory studies and calculations on the influence of crack width on chloride-induced corrosion in concrete, *ACI Materials Journal*, Vol. 94, No. 1, 1997, pp. 56-61.
- Seung Yup Jang, Bo Sung Kim, Byung Hwan Oh: Effect of crack width on chloride diffusion coefficients of concrete by steady-state migration tests, *Cement and Concrete Research* 41 (2011) pp. 9-19.
- Vidal, T., Castel, A., François, R. (2004) Analyzing crack width to predict corrosion in reinforced concrete. *Cement and Concrete Research*, Vol. 34, 2004, pp. 165-174.
- Réka Anna Nagy** (1988) civil engineer (MSc), PhD candidate at the Department of Construction Materials and Technologies, Budapest University of Technology and Economics (BME). Main fields of interest: cracking of concrete, durability of structural materials, use of FRP reinforcements for concrete structures.

STATIC HARDNESS TESTING AND DEM MODELLING OF HARDENED CONCRETE



Zoltán Gyurkó – Adorján Borosnyói

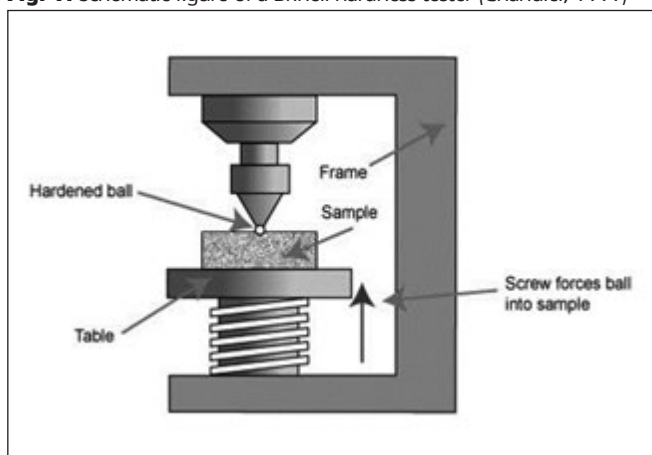
In the present study Brinell macro hardness tests and Depth Sensing Indentation tests were performed on hardened concrete specimens and the results were compared with a discrete element model, created by the authors of this paper. The results of the investigations have demonstrated the satisfactory use of discrete element modelling with a good correlation with own results, as well as a confirmation of earlier results which can be found in the literature.

Keywords: Brinell hardness, depth-sensing indentation test, strength, porous solids, concrete, discrete element method.

1. INTRODUCTION

Hardness testing was a frequently studied area in the past in case of different solid materials, like metals, but only a few studies dealt with the hardness testing of porous building materials, like concrete. These studies applied mostly Brinell method or Depth Sensing Indentation test (DSI; aka. Instrumented Indentation Test, IIT), but only using a low number of load levels (mostly one or two) to understand the phenomenon of hardness and to find a well correlated relationship between hardness and compressive strength. In the present study a wider range of load levels were applied to analyse the characteristics of hardness based on static loading. During our previous research a special characteristic of hardness was observed on hardened concrete (Szilágyi et al, 2010). It was found that the Brinell hardness in case of concrete has a peak value in the function of the testing load. It represents well the elastic-plastic behaviour of the material and it shows that under the indenter in the material a local densification behaviour can be postulated. In Fig. 2 the results of the earlier experiments are shown, which indicates the maximum values of the Brinell hardness in function of the testing load. This increasing-decreasing behaviour of the hardness can be shown also in function of the indentation diameter.

Fig. 1: Schematic figure of a Brinell hardness tester (Chandler, 1999)



The aim of the present study was to investigate the behaviour of the above mentioned earlier observations of the authors by using Discrete Element Modelling, to be able to confirm or disprove the validity of earlier findings for concrete. The main purpose of the numerical model experiment was that hardness tests are more reliable in case on solid materials and in case of porous materials a large number of experiments should be carried out to avoid the effect of the measurement outlier values.

2. DESCRIPTION OF STATIC HARDNESS TESTING

Hardened concrete (strength class: C35/45), an elastic-plastic porous building material was selected for the investigations, since it was aimed to study a material that is widely used in the civil engineering practice. The particle size distribution of the aggregate of the concrete is given in Table 1. During the numerical modelling the real particle size distribution was followed to create an accurate model of the material.

During our experimental studies a Brinell hardness tester machine was used. In case of the testing process a polished, hardened steel sphere penetrates into the surface of the material with a given testing load, which can be differ based on the selected material. In this study the same material was used and a wide range of load levels was applied. Maximum loads by the Brinell tests were taken in the range of 1.5 kN to 17.5 kN. These loads are applied on the specimens for a specific time; mostly 10-15 seconds in case of metals and around 30 seconds in case of porous materials. During this period of time plastic deformations occur in the material. For the present experimental test 30 seconds were selected to keep the peak load. In our future research, we are planning to examine the effect of the loading time.

The Brinell test was carried out by using a $D = 10$ mm diameter hard steel indenter. The material tests were conducted at the Budapest University of Technology and Economics, Faculty of Civil Engineering, Department of Construction Materials and Technology. Fig. 3 shows one of the tested specimens after hardness testing (standard cube of 150 mm dimension).

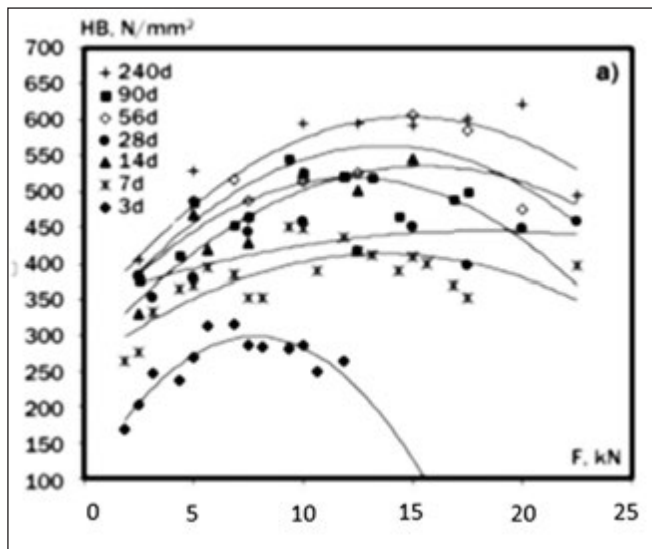


Fig. 2: The relationship between the Brinell hardness and the load (Szilágyi et al, 2010)

3. GENERAL OVERVIEW OF THE DISCRETE ELEMENT METHOD

Discrete Element Method (DEM) is a special numerical method, which uses a large number of small particles to compute the motion and effect of these elements. DEM is a rather new method, but it is already used in a wide range of applications in the engineering practice. It can be used to model granular materials, in which the particles are not connected to each other at the material level, or to model structures, which are built of granular materials or bricks.

DEM is used extensively to study particles of no cohesion (Cundall, Strack, 1979), soils with cohesion (Liu et al, 2003; Yao, Anandarajah, 2003), rock (Moon et al, 2007; Potyondy, Cundall, 2004), asphalt (You, Buttlar, 2004; You et al, 2008; Liu, You, 2009), geotechnical and geological studies (Campbell et al, 1995; Hardy, Finch, 2006; Hazzard, Young, 2004), for the interaction of granular media (soil and rock) (Kanou et al, 2003). In the last two decades the DEM has been successfully applied in various areas of mining, powder metallurgy,

Fig. 3: One of the concrete specimens used for the investigations

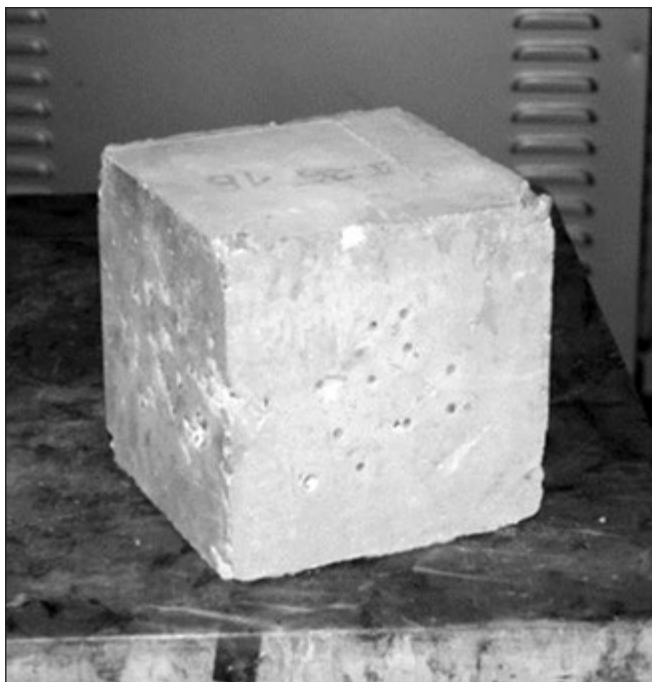


Table 1: Particle size distribution of the aggregate (Szilágyi et al, 2010)

Particle size	Proportion
0-4 mm	40 %
4-8 mm	22 %
8-16 mm	38 %

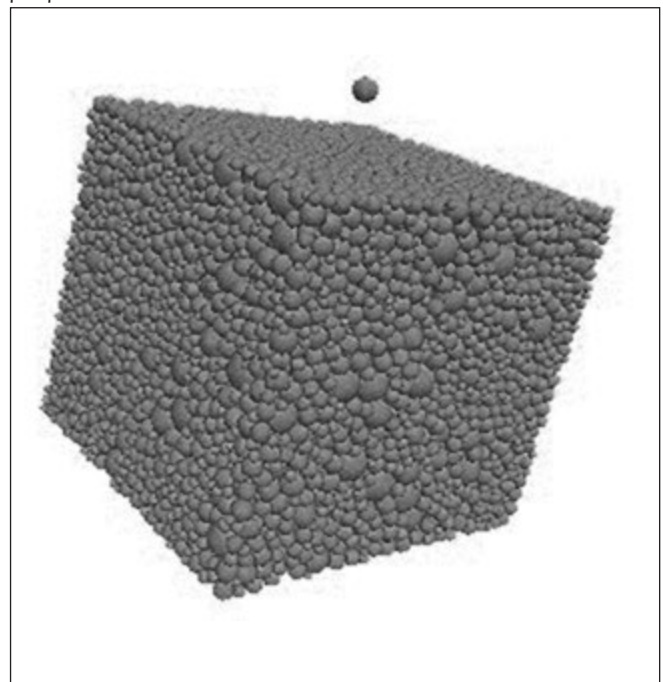
civil engineering and in the oil industry. Recently, DEM is also used for the modelling of the behaviour of fresh concrete (Shyshko, Mechtcherine, 2013; Hoornahad, Koenders, 2014; Remond, Pizette, 2014) and hardened concrete (Szilágyi et al, 2009, Tran et al, 2011; Iturrioz et al, 2013; Zivaljic et al, 2014; Riera et al, 2014).

A numerical modelling technique can be called to a discrete element method if it satisfies some conditions, like the elements can have large displacements and these elements can come into contact with each other and with the boundaries of the model. A discrete element model has to consist of separate, finite-sized elements (called discrete elements), which can move independently (Bagi, 2012).

A special version of DEM was proposed by Cundall, called the distinct element method (Cundall, 1971). The modified version of this method is used by the most software, which are used in the engineering practice. Here the particles are considered as rigid elements and their behaviour can be expressed by the equation of motion. Among the elements springs are considered, which can create contact with the neighbouring elements, and this spring can represent the arising force between two particles. The equations are solved with numerical integration along the time. The most softwares use central difference method for the time integration.

During the last decades the computer technology improved greatly, which made it possible to simulate numerically a large number of particles by using only a single processor (Cundall, 1988). In the new millennium, an appropriate level of computational technology was reached, when the DEM became an effective method to use in the daily engineering practice, too. However the methods are still considered to be computationally expensive (compared to finite element method), but it has advantages in case of modelling porous

Fig. 4: The model with the steel sphere in the initial phase in perspective view



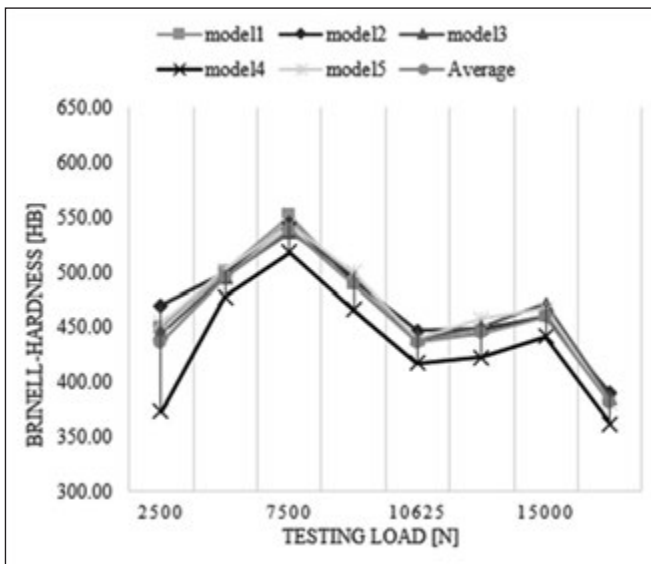


Fig. 5: Testing load vs. average indentation diameter relationships of the 5 numerical models

materials and powders or simulate local effects. The discrete element models are composed of two types of components, the finite-sized particles (the discrete elements) and the contacts among these elements. The elements can have a different meaning in the model, but in case of porous material modelling it is corresponding to the aggregate particles of the modelled material. The element can have various shapes, but most software packages are applying spherical elements, because they are the best to be tackled (Bagi, 2012). Mostly it is allowed to define the parameters of the elements and even create deformable elements with a complex geometry, but it can greatly increase the computational time. The aggregate particles of the most granular materials are in a much higher stiffness range than the composed material, thus the particles are considered to be rigid, which is an acceptable approximation.

Between two elements a contact is formed when the distance between the elements becomes zero. During the material generation process it happens also sometimes, that the distance between the elements become even less than zero (numerical singularity), and the elements are intersecting each other.

Table 2: The mean indentation diameter and the average Brinell hardness values corresponding to the numerical models

Loading force [N]	Average Model	
	d_{rm} [mm]	HB [HB]
2500	2.676	436.40
5000	3.529	494.74
7500	4.117	538.41
10000	4.934	488.96
10625	5.348	436.33
12500	5.707	444.96
15000	6.0997	460.04
17500	7.067	380.90

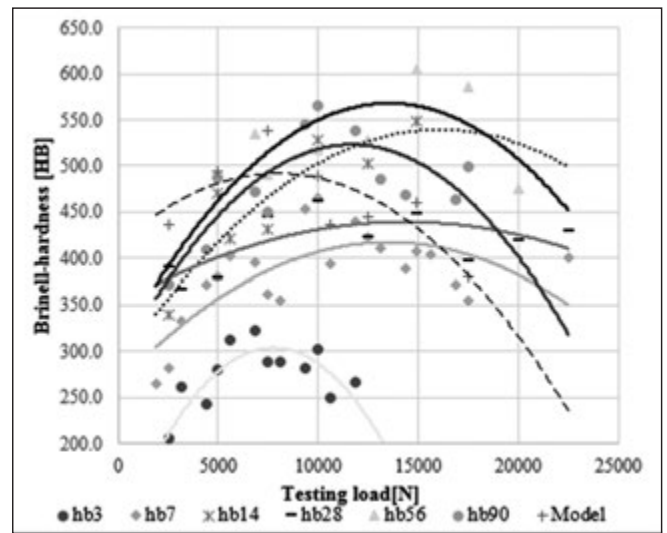


Fig. 6: Comparison of the experimental and the numerical model: Testing load vs. Brinell hardness relationship

4. MODELLING OF HARDNESS TESTING WITH DEM

To model the Brinell hardness test procedure, a concrete cube was generated by using the DEM software *PFC3D*. This type of numerical method was chosen, due to the particles may have large displacements in case of static indentation testing and this method is more suitable to model porous materials, like concrete. The model was set to follow the particle size distribution and other properties (density, stiffness, porosity) of the real material (See *Table 1*). The smallest particle size distribution was chosen to 0.1 mm, because in the real material less than 5% of under this diameter was found. The built in functions of the software support the users to generate the material, after a sufficient parameter set up. A steel sphere was generated above the sample and it was pushed with a given force into the surface of the material to simulate Brinell hardness test. Here one has to apply some calculation cycles to move the steel ball sufficiently close to the surface of the material.

In case of Brinell hardness testing we are able to apply load in different magnitudes as it was already mentioned in Chapter 2. During our investigation the following testing loads were applied on the model:

- 2.5 kN
- 5 kN
- 7.5 kN
- 10 kN
- 10.625 kN
- 12.5 kN
- 15 kN
- 17.5 kN

To apply the force we have to run a given number of calculation cycles, during the steel sphere is penetrating into the concrete. During this process one can plot and save different attributes, like the position or the contact forces of the steel ball.

When the loading phase of the test is finished, one has to apply a load, perpendicularly to the surface again, but now in the opposite direction, to model the unloading phase. Thus the steel ball is removed from the model. Here one has to apply some calculation cycles again not only for removing the ball, but to leave some time for the particles to finish ordering, during which the bond strength of the particles are reducing. Based on that reason it can be useful here to give

some more cycles that would be necessary to the removal of the sphere.

During the test one has to apply the calculation cycles three times, first to move the ball close to the surface, then to push it into the surface and lastly to remove it. In this case it requires about 6000 cycles, which can be considered a small number in discrete element modelling terms, where much larger numbers are usual. That shows if one has the model sample, to model the test itself does not require large computational effort and the test can be carried out relatively fast. Since the material model has to be structured only once, a large amount of testing can be done within a short period of time, even faster than the real laboratory tests. When the steel ball is removed and the other particles are in a steady state, the test is finished.

After the hardness testing procedure was finished (the steel ball moved sufficiently away from the specimen), with the help of the measuring tool provided by the software, the distance between the edges of the residual ball print can be measured in two diagonals, which are perpendicular to each other (the diagonals along axis X and Y; this is the standard procedure in case of measuring indentation diameter). These measurements are performed on every load level (8 different loading levels were modelled, see above) and on each specimen.

The diameter of the indentation imprint was measured between the elements on the upper edge of the imprint. The closest point of these elements to each other was chosen for the measurements, because these points approximate best the edges of the print in reality. In reality the aggregates are not always on the surface of the print and they are covered with cement paste, which serves as a damping material. However the particles in the model represent the aggregates surrounded with cement paste, thus the inner distance of these elements is the realistic value.

Five models were created to give a statistical nature to the investigation and these models have the same properties, thus the results of the five different models can be averaged too. The Brinell hardness was not averaged from the previous data, but it was calculated from the average diameters. If the previous data would be averaged, the results would be very similar to the data given in *Table 2*, so it has no substantive significance which method is chosen.

After the model averaging the highest Brinell hardness value appears in case of the 7.5 kN loading, and the smallest in case of the highest load. It can be also observed that in the diameter values between the first and the second as well as between the last two values a quite large difference appears. Those differences are much higher than the other differences between other two values and cause a bigger difference in the Brinell hardness values as well. The reason is that between those two load levels the particles in the model have larger movements, than in other cases. The numerical reason of the observation could be that at those two load levels more parallel bond connections break, which allows more movement to the particles, as it was mentioned earlier.

The earlier mentioned phenomena of the peak value of hardness in function of loading force can be observed in the numerical model results too. In *Fig. 5* the testing load is plotted in the function of the Brinell hardness for each model with the average values. *Fig. 5* shows the differences among the models. It can be observed in the diagram that the figure has a peak point at 7.5 kN, and a small peak at 15 kN too. The smallest values belong to the extreme testing load values in every case.

As it was already mentioned, the Brinell hardness depends on the loading force and it was observed earlier that the Brinell hardness has a maximum point in function of the loading force.

In *Fig. 6* the experimental (measured in different ages) and the average model testing load – Brinell hardness relationships can be seen (the dashed trend line belongs to the model results). It can be stated that in both cases the model has a peak value, but this location in case of the model appears at the 7.5 kN load level, while in case of the laboratory test it is around 12.5 kN. It is also worth to mention that in both figures the extreme testing load values belong to a smaller hardness value than the maximum hardness value. It can be concluded that the assumption, that the Brinell hardness has a maximum value in function of the loading force, can be observed in the numerical model as well. Possible reason of this behaviour is the porosity of the examined material, because in case of solid materials (like steel) this behaviour cannot be observed.

5. CONCLUSIONS

The aim of our laboratory experiments was to analyse the previous observations on concretes. The investigations have shown that the earlier findings for the Brinell hardness of concrete can be considered as correct. Based on the data evaluation of numerical model results it can be stated that the DEM model was able to sufficiently describe a hardness testing method. With the help of these models the laboratory test procedures can be simulated in a large number, without using real specimens. In that way one can create statistically correct results without a large number of material tests and laboratory resources can be saved. The numerical model was capable to create a residual indentation ball print on the surface of the material and follow the particle size distribution of the real material. The present Brinell model is able to follow hardness testing in case of medium loading forces. In case of extreme (very large and very small) forces, the model has small differences from the experimental data.

As a final conclusion it can be stated that the Discrete Element Method is a useful method for the simulation of Brinell hardness testing of hardened concrete.

6. REFERENCES

- Bagi, K. (2012) Fundamentals of the discrete element method, *Lecture notes*, 2012
- Campbell, C. S., Cleary, P. W., Hopkins, M. A. (1995) Large-scale landslide simulations: Global deformations, velocities, and basal friction. *Journal of Geophysical Research*, Vol. 100, No. B5, pp. 8267–8283.
- Chandler, H. (1999) Hardness testing. *ASM International*, 192 p.
- Cundall, P. A. (1971) A computer model for simulating progressive large scale movements in blocky rock systems. *Procs. Symposium of the International Society of Rock Mechanics*, Nancy, France, Vol. 1., Paper II-8, 1971
- Cundall, P. A. (1988) Formulation of a three-dimensional distinct element model – Part I: A scheme to detect and represent contacts in a system composed of many polyhedral blocks. *Int. J. Rock Mech. Min. Sci. & Geomech. Abst.*, Vol. 25, pp. 107–116, 1988
- Cundall, P. A., Strack, O. D. L. (1979) A discrete numerical model for granular assemblies. *Geotechnique*, Vol. 29, No. 1, pp. 47–65.
- Hardy, S., Finch, E. (2006) Discrete element modelling of the influence of cover strength on basement-involved fault-propagation folding. *Tectonophysics*, Vol. 415, No. 1–4, pp. 225–238.
- Hazzard, J. F., Young, R. P. (2004) Dynamic modelling of induced seismicity. *International Journal of Rock Mechanics and Mining Sciences*, Vol. 41, No. 8, pp. 1365–1376.
- Hoomahad, H., Koenders E. A. B. (2014) Simulating macroscopic behavior of self-compacting mixtures with DEM. *Cement & Concrete Composites*, Vol. 54, pp. 80–88.

- Iturrioz, I., Lacidogna, G., Carpinteri, A. (2013) Experimental analysis and truss-like discrete element model simulation of concrete specimens under uniaxial compression. *Engineering Fracture Mechanics*, Vol. 110, pp. 81-98.
- Kanou, S., Amano, M., Terasaka, Y., Matsumoto, N., Wada, T. (2003) Terra-mechanical simulation using distinct element method. *Komatsu Technical Report*, Vol. 49, No. 151, pp. 13-19.
- Liu, S. H., Sun, D. A., Wang, Y. (2003) Numerical study of soil collapse behavior by discrete element modelling. *Computers and Geotechnics*, Vol. 30, No. 5, pp. 399-408.
- Liu, Y., You, Z. (2009) Visualization and simulation of asphalt concrete with randomly generated three-dimensional models. *ASCE Journal of Computing in Civil Engineering*, Vol. 23, No. 6, pp. 340-347.
- Moon, T. H., Nakagawa, M., Berger, J. R. (2007) Measurement of fracture toughness using the distinct element method. *International Journal of Rock Mechanics and Mining Sciences*, Vol. 44, No. 3, pp. 449-456.
- Potyondy, D. O., Cundall, P. A. (2004) A bonded-particle model for rock. *International Journal of Rock Mechanics and Mining Sciences*, Vol. 41, No. 8, pp. 1329-1364.
- Remond, S., Pizette, P. (2014) A DEM hard-core soft-shell model for the simulation of concrete flow. *Cement and Concrete Research*, Vol. 58, pp. 169-178.
- Riera, J. D., Miguel, L. F. F., Iturrioz, I. (2014) Assessment of Brazilian tensile test by means of the truss-like Discrete Element Method (DEM) with imperfect mesh. *Engineering Structures*, Vol. 81, pp. 10-21.
- Shyshko, S., Mechtcherine, V. (2013) Developing a Discrete Element Model for simulating fresh concrete: Experimental investigation and modelling of interactions between discrete aggregate particles with fine mortar between them. *Construction and Building Materials*, Vol. 47, pp. 601-615.
- Szilágyi, K. (2009) DEM modelling of the Brinell-testing of concrete, Micro-mechanics of granular media – Manuscript, BME Faculty of Civil Engineering, Budapest, 2009
- Szilágyi, K. – Borosnyói, A. – Dobó, K. (2011) Static indentation hardness testing of concrete: A long established method revived. *Építőanyag*, Volume 63, Issue 1-2, 2011, pp. 2-8.
- Tran, V. T., Donzé, F.-V., Marin, P. (2011) A discrete element model of concrete under high triaxial loading. *Cement & Concrete Composites*, Vol. 33, No. 9, pp. 936-948.
- Yao, M., Anandarajah, A. (2003) Three-dimensional discrete element method of analysis of clays. *Journal of Engineering Mechanics*, Vol. 129, No. 6, pp. 585-596.
- You, Z., Adhikari, S., Dai, Q. (2008) Three-dimensional discrete element models for asphalt mixtures. *Journal of Engineering Mechanics*, Vol. 134, No. 12, pp. 1053-1063.
- You, Z., Buttlar, W. G. (2004) Discrete element modeling to predict the modulus of asphalt concrete mixtures. *ASCE Journal of Materials in Civil Engineering*, Vol. 16, No. 2, pp. 140-146.
- Zivaljic, N., Nikolic, Z., Smoljanovic, H. (2014) Computational aspects of the combined finite-discrete element method in modelling of plane reinforced concrete structures. *Engineering Fracture Mechanics*, Vol. 131, pp. 669-686.

Zoltán Gyurkó (1989) civil engineer (MSc), PhD candidate at the Department of Construction Materials and Technologies, Budapest University of Technology and Economics. *Main fields of interest:* non-destructive testing of concrete and porous building materials, Discrete Element Modelling.

Adorján Borosnyói (1974) civil engineer (MSc), PhD, associate professor at the Department of Construction Materials and Technologies, Budapest University of Technology and Economics. *Main fields of interest:* non-destructive testing of concrete, supplementary cementing materials for concrete, non-metallic (FRP) reinforcements for concrete, bond in concrete, fibre reinforced concrete. Member of the Hungarian Group of *fib* and of *fib* TG 4.1 „Serviceability Models”. Member of RILEM Technical Committee ISC “Non destructive in situ strength assessment of concrete”.

FREEZE-THAW SALT SCALING RESISTANCE OF HPC WITH COMBINED METAKAOLIN AND SILICA FUME SLURRY USAGE



Emese Gál – Adorján Borosnyói

The aim of the study was to investigate the freeze-thaw resistance of high performance concrete with different laboratory tests, particularly salt scaling test. The performance of HPC was improved with different types of supplementary cementing materials (SCMs): metakaolin and silica fume slurry. The effect of combined usage of metakaolin and silica fume slurry was investigated as well. The results demonstrated that the separate application of metakaolin or silica fume slurry can significantly enhance the performance of HPC. The combined application of metakaolin and silica fume slurry however less effectively improved the freeze-thaw resistance of concrete.

Keywords: salt scaling, freeze-thaw resistance, high performance concrete (HPC), metakaolin, silica fume slurry, supplementary cementing materials (SCMs)

1. INTRODUCTION

The durability of concrete is an important factor that defines the areas of efficient application of a specific mixture. Structures, which are from durable materials help to preserve environmental resources, to reduce the amount of waste materials, and to increase the resistance against physical, chemical and mechanical effects (*Mindess, Young, 1981*). Both durability and strength of stone like materials can be improved with the increase of apparent density of the material. There are three factors that can influence durability and strength: 1) the strength of cement matrix, 2) the adhesion between the cement matrix and the aggregates, 3) the strength, ratio and particle size distribution of aggregates. The strength of cement matrix is influenced by the characteristic strength of cement and the porosity of the matrix. The porosity depends on the water-to-cement ratio, the rate of compaction, the rate of hydration and can be influenced by the usage of supplementary cementing materials and their amount in the concrete (*Balázs, 1999*).

Different types of supplementary cementing materials (SCMs) were utilised and studied during this research; metakaolin (MK) and silica fume slurry (SF) was used. Metakaolin is usually produced by the calcination of kaolinite clay mineral (*Hassan et al, 2012*). Metakaolin is a pozzolanic material; as such it can react with cement and lime (*Eichler, 1991*). Silica fume slurry is an amorphous polymorph of silicon dioxide; it is also a pozzolanic material (*Kausay, 2009*). The durability can be investigated with various direct and indirect laboratory tests such as strength, watertightness, abrasion resistance, porosity, freeze-thaw and salt scaling resistance tests. (*Petersson, Luping, 2004; Rösli, Harnik, 1980; Stark, 2004; Valenza, Scherer, 2007*)

The aim of the present study was to understand the effects of metakaolin and silica fume slurry on the freeze-

thaw resistance of concrete in the presence of de-icing salt. Supplementary cementing materials were used separately as well as in combination in the studied mixtures.

2. CONCRETE MIXTURES

Thirteen concrete mixtures were selected and tested with various laboratory methods. The following parameters were kept unchanged in each concrete mixture:

- the particle size distribution (MSA = 16 mm),
- the type of cement (CEM I 42.5 N),
- the water-to-binder ratio, w/b = 0.4,
- the consistency of fresh concrete,
- the total mass of cement and supplementary cementing material was altogether 325 kg/m³ in each mixture.

The varied parameters were:

- the mass of cement,
- the mass of metakaolin and silica fume slurry,
- the water-to-cement ratio,
- the mass of aggregate.

The reference mixture did not contain any supplementary cementing material. In twelve mixtures the supplementary cementing materials were applied in different amounts.

The silica fume slurry content was 3 m%, 5 m%, 10 m% and 15 m% relative to the mass of cement, the metakaolin content was 10 m%, 17 m%, 25 m%, 33 m% also relative to the mass of cement. In case of combined use of supplementary cementing materials the mixtures contained 7 m% metakaolin and 3 m% silica fume slurry, 12 m% metakaolin and 5 m% silica fume slurry, 17 m% metakaolin and 8 m% silica fume slurry, 25 m% metakaolin and 8 m% silica fume slurry.

The amount of metakaolin and silica fume slurry in these investigated mixtures was occasionally higher than the amounts applied generally in the concrete industry. The aim of the study was to examine the effect of higher dosages of

supplementary cementing materials in concrete. Experimental study of metakaolin and silica fume supplementary cementing materials in high dosage or in combined usage is a deficiency in the technical literature.

3. SALT SCALING RESISTANCE TEST

A short summary is given here on the freeze-thaw test in the presence of de-icing salt, referred to as the salt scaling resistance test. A Technical Specification of CEN gives instructions about the details of the test method (CEN/TS 12390-9). Two specimens were prepared for the test from each mixture with the dimensions of 100×100×50 mm. Polyethylene plates of 5 mm thickness were fixed on five sides of the specimens, extending at least 20 mm above the examined surface of the samples. The contact edge of concrete and the surface of the polyethylene layer were sealed with silicone mastic. The surface of the specimens was treated with 50 ml of distilled water for 72 ± 2 hours under laboratory temperature, after that the water was changed to 3% NaCl aqueous solution and the specimens were placed in the freeze-thaw testing machine. There was solution on the surface of the samples both during the freeze and the thaw periods of the temperature cycles. One freeze-thaw cycle lasted 24 hours. The tests were started at the age of 180 days of the specimens. After specific cycles (7, 14, 21, 28, 42, 56, 70, 85, 97, 109, 119, 129, 136, 143, 150, 158, 165, 175 cycles) the scaled concrete was collected, dried in a ventilated oven and the loss in mass was determined.

4. RESULTS

The applied 175 freeze-thaw cycles is considered to be much longer than usual testing periods in practice for salt scaling performance test (that is 56 freeze-thaw cycles). The results were evaluated after 56 freeze-thaw cycles and at the end of the test as well. The results are introduced in the present paper by diagrams with respect to the number of freeze-thaw cycles and the amount of supplementary cementing materials.

4.1. Salt scaling resistance after 56 freeze-thaw cycles

4.1.1. Reference mixture

The average amount of scaled concrete considering the reference mixture was 1301 g/m², which is 2.6 times higher than the limit given for exposure class XF2 in the Hungarian National Annex of EN 206 European Standard (i.e. 500 g/m²). Despite the low water-to-cement ratio (w/c = 0.4) the reference mixture could not provide salt scaling resistance after 56 freeze-thaw cycles (Fig. 1).

4.1.2. Effect of silica fume slurry content

The use of silica fume slurry significantly decreased the average amount of scaled concrete compared to the reference mixture. As the amount of silica fume slurry content was increased until 10 m% the average amount of scaled concrete decreased. However in case of 15 m% of silica fume slurry content the average amount of scaled concrete increased compared to the lower dosages of silica fume slurry. Apparently the higher amount of silica fume slurry reduced the salt scaling resistance of concrete. The results are presented in Table 1. and in Fig. 2.

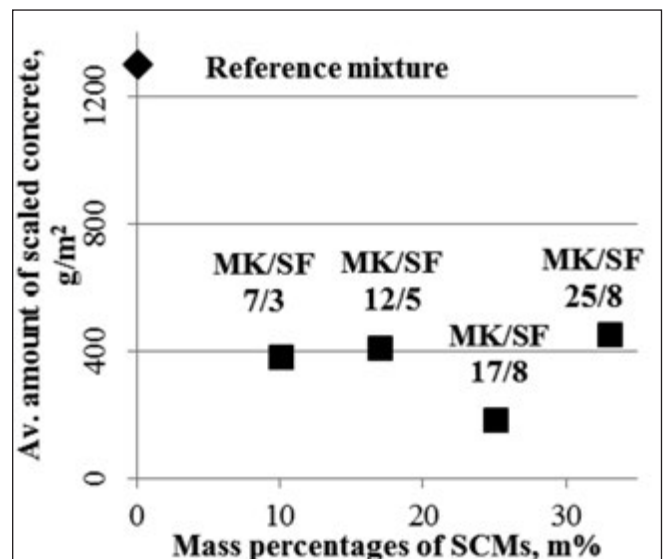


Fig. 1: Average amount of scaled concrete after 56 freeze-thaw cycles in case of the reference mixture and mixtures with combined usage of metakaolin and silica fume slurry

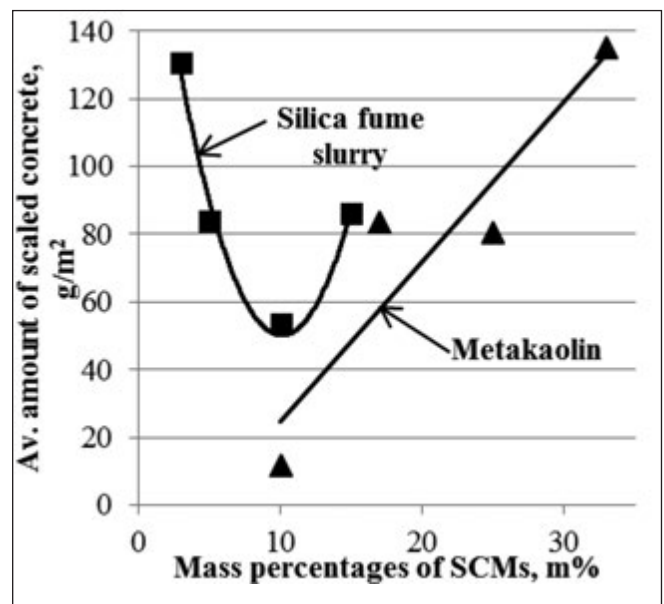


Fig. 2: Average amount of scaled concrete after 56 freeze-thaw cycles in case of mixtures containing metakaolin or silica fume slurry

Table 1: Amount of scaled concrete after 56 freeze-thaw cycles in case of mixtures containing silica fume slurry

Mass percentages of silica fume slurry content	Amount of scaled concrete	Percent of scaled concrete compared to the ref. mix.
3 m%	130 g/m ²	10 %
5 m%	84 g/m ²	6 %
10 m%	54 g/m ²	4 %
15 m%	86 g/m ²	7 %

4.1.3. Effect of metakaolin content

The use of metakaolin also significantly decreased the average amount of scaled concrete. As the mass percent of metakaolin was increased the average amount of scaled concrete also increased. The results are presented in Table 2 and in Fig. 2.

The salt scaling resistance of mixtures containing metakaolin was rather good, although the higher amount of metakaolin content decreased the performance of concrete (Fig. 2).

Table 2: Amount of scaled concrete after 56 freeze-thaw cycles in case of mixtures containing metakaolin

Mass percentages of metakaolin content	Amount of scaled concrete	Percent of scaled concrete compared to the ref. mix.
10 m%	12 g/m ²	1 %
17 m%	83 g/m ²	6 %
25 m%	81 g/m ²	6 %
33 m%	135 g/m ²	10 %

The amount of scaled concrete for mixtures containing either silica fume slurry or metakaolin did not exceed the limit given for exposure class XF4 in the Hungarian National Annex of EN 206 European Standard (i.e. 250 g/m²) after 56 freeze-thaw cycles; furthermore, the highest amount of scaled concrete was only 135 g/m² (33 m% metakaolin content).

4.1.4. Effect of metakaolin and silica fume slurry content

In case of mixtures with combined use of metakaolin and silica fume slurry the amount of scaled concrete was higher than in case of mixtures containing either metakaolin or silica fume slurry separately. The combined use of the two supplementary cementing materials resulted minor performance compared to the scaling resistance observed for the separate use of SCMs. The concrete mixture containing 17 m% metakaolin and 8 m% silica fume slurry did not exceed the limit given for exposure class XF4 in the Hungarian National Annex of EN 206 European Standard (i.e. 250 g/m²). The results are presented in Table 3 and in Fig. 1.

4.2 Salt scaling resistance after 175 freeze-thaw cycles

The long term effect of metakaolin and silica fume slurry content was investigated so the freeze-thaw test was continued until 175 cycles. The salt scaling resistance was evaluated at the end of the test too.

4.2.1. Reference mixture

The amount of scaled concrete of the reference mixture was 11 097 g/m² after 143 freeze-thaw cycles, when the condition of specimens indicated that the test could not be continued. The amount of scaled concrete increased more intensively after about 70 freeze-thaw cycles as may be observed in the change of the gradient of the graph. The results are presented in Fig. 3.

4.2.2. Effect of silica fume slurry content

The amount of scaled concrete in case of the mixture containing 3 m% of silica fume slurry increased significantly after about 85 freeze-thaw cycles. The amount of scaled concrete increased almost linearly as the number of freeze-thaw cycles increased in case of 5 m%, 10 m% and 15 m% of silica fume slurry content. The salt scaling resistance of concrete was observed to increase up to the use of 10 m% of silica fume slurry, but in case of 15 m% of silica fume slurry content the performance became less favourable after 175 freeze-thaw cycles. The silica fume slurry content was the most effective at an optimum dosage of around 10 m%.

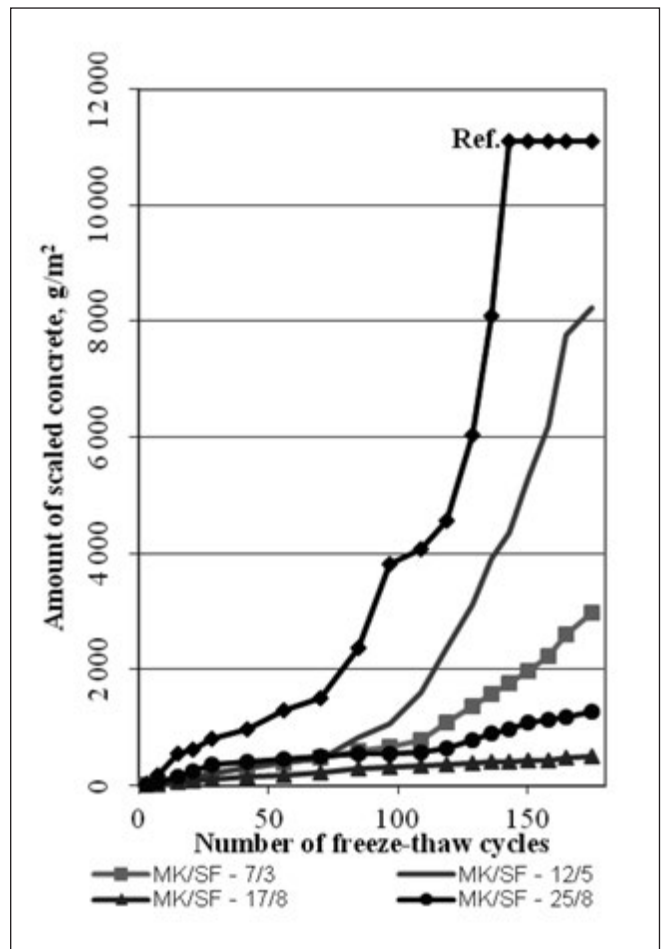


Fig. 3: The amount of scaled concrete with respect to the number of freeze-thaw cycles in case of the reference mixture and mixtures with combined usage of metakaolin and silica fume slurry

These results were all under the limit given for exposure class XF4 in the Hungarian National Annex of EN 206 European Standard (i.e. 250 g/m²). It can be concluded that the silica fume slurry content of concrete significantly increased the freeze-thaw resistance in the presence of de-icing salt. The results can be studied in Table 4 and in Fig. 4.

4.2.3. Effect of metakaolin content

The increasing amount of metakaolin decreased the salt scaling resistance of concretes, investigated after 175 freeze-thaw cycles, but the amount of scaled concrete for all mixtures was under the limit given for exposure class XF4 in the Hungarian National Annex of EN 206 European Standard (i.e. 250 g/m²). The most resistant mixture contained 10 m% of metakaolin: in this case the amount of scaled concrete was only 19 g/m² after 175 freeze-thaw cycles.

The salt scaling resistance of mixtures containing 17 m% and 25 m% of metakaolin was the same until about 100 freeze-thaw cycles, then the amount of scaled concrete increased more intensively in case of 25 m% of MK content, where a change in the gradient of the graph can be observed. It can be concluded that the metakaolin content significantly increased the salt scaling resistance of concrete. The results are presented in Table 5 and in Fig. 4.

Comparing the mixtures containing 10 m% of silica fume slurry or 10 m% of metakaolin separately, one can realise that these mixtures were the most resistant against freeze-thaw cycles in the presence of de-icing salt. The amount of scaled concrete was 124 g/m² with the use of silica fume slurry and 19 g/m² with the use of metakaolin.

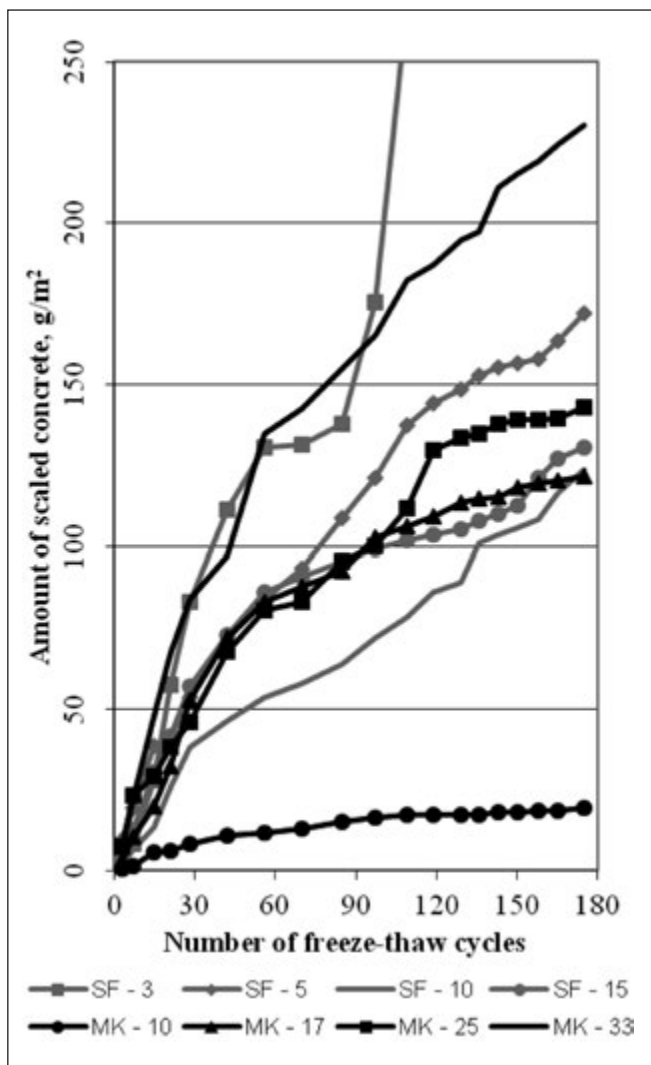


Fig. 4: The amount of scaled concrete with respect to the number of freeze-thaw cycles in case of mixtures containing metakaolin or silica fume slurry

4.2.4 Effect of metakaolin and silica fume slurry content

In case of mixtures contained 17 m% of metakaolin and 8 m% of silica fume slurry the gradient of the graph increased almost linearly, the amount of scaled concrete was 517 g/m² after 175 freeze-thaw cycles, which just exceeded the limit given for exposure class XF2 in the Hungarian National Annex of EN 206 European Standard (i.e. 500 g/m²). Until about 70 freeze-thaw cycles the amount of scaled concrete was the same in case of mixtures containing 7 m% of MK and 3 % of SF, 12 m% of MK and 5 m% of SF. After about 70 freeze-thaw cycles in case of the mixture containing 12 m% of MK and 5 m% of SF a more intensive change of the gradient of the graph can be observed. The results are presented in *Table 6* and in *Fig. 3*.

The combined use of the two supplementary cementing materials resulted minor performance compared to the scaling resistance observed for the separate usage of SCMs.

5. CONCLUSIONS

The freeze-thaw resistance of concrete in the presence of de-icing salt could be significantly enhanced with silica fume slurry or metakaolin. The concrete mixture with 10 m% of metakaolin provided the highest resistance, only 19 g/m² scaling occurred after 175 freeze-thaw cycles. This amount is far less than the limit given for exposure class XF4 in the

Table 3: Amount of scaled concrete after 56 freeze-thaw cycles in case of mixtures with combined usage of metakaolin and silica fume slurry

Mass percentages of metakaolin and silica fume slurry content	Amount of scaled concrete	Percent of scaled concrete compared to the ref. mix.
7/3 m%	385 g/m ²	30 %
12/5 m%	413 g/m ²	32 %
17/8 m%	186 g/m ²	14 %
25/8 m%	456 g/m ²	35 %

Table 4: Amount of scaled concrete after 175 freeze-thaw cycles in case of mixtures containing silica fume slurry

Mass percentages of silica fume slurry content	Amount of scaled concrete
3 m%	754 g/m ²
5 m%	172 g/m ²
10 m%	124 g/m ²
15 m%	131 g/m ²

Table 5: Amount of scaled concrete after 175 freeze-thaw cycles in case of mixtures containing metakaolin

Mass percentages of metakaolin content	Amount of scaled concrete
10 m%	19 g/m ²
17 m%	122 g/m ²
25 m%	143 g/m ²
33 m%	230 g/m ²

Table 6: Amount of scaled concrete after 175 freeze-thaw cycles in case of mixtures with combined usage of metakaolin and silica fume slurry

Mass percentages of metakaolin and silica fume slurry content	Amount of scaled concrete
7/3 m%	2984 g/m ²
12/5 m%	8238 g/m ²
17/8 m%	517 g/m ²
25/8 m%	1280 g/m ²

Hungarian National Annex of EN 206 European Standard (i.e. 250 g/m²). In case of mixtures containing both silica fume slurry and metakaolin, the freeze-thaw resistance could also be improved, but less effectively compared to mixtures containing silica fume slurry or metakaolin separately. The results of this research could contribute to the design of freeze-thaw resistant concretes without the need of air entraining agents.

6. ACKNOWLEDGEMENTS

This research was supported by OTKA, Hungarian Scientific Research Fund (National Office for Research, Development and Innovation), Project No. OTKA K 109233.

7. REFERENCES

- Balázs Gy. (editor) (1999) Protection, repair and strengthening of concrete and reinforced concrete structures. Vol. 1, *BME Publishing*, Budapest, 407 p. (in Hungarian)
- CEN/TS 12390-9 Testing hardened concrete – Freeze-thaw resistance – Scaling

- Eichler, W-R. (1991) *Microsilica in der Anwendung aus der sicht eines Baustoffchemikers*. Microsilica in der modernen Betontechnologie, Conference proceedings, Konstanz, 1991, *Elkem GmbH*, Allensbach. pp. 71 – 78.
- EN 206 Concrete - Specification, performance, production and conformity, European Standard
- Hassan, A.A.A., Lachemi, M., Hossain, K.M.A. (2012) Effect of metakaolin and silica fume on the durability of self-consolidating concrete, *Cement & Concrete Composites* 34, 2012, pp. 801-807.
- Kausay, T. (2009) Silica fume, microsilica slurry, *Concrete*, 2009. May, pp. 18-20. (in Hungarian)
- Petersson, P-E., Luping, T. (2004) Internal frost damage of HPC subjected to the slab test, Durability of high-performance concrete, Conference proceedings, *AEDIFICATIO Publishers*, 79104 Freiburg, 2004, pp. 207-217.
- Rösli, A., Harnik, A.B. (1980) Improving the durability of concrete to freezing and de-icing salts, in P.J. Sereida, G.G. Litvan (Eds.), *Durability Build. Mater. and Components*, *ASTM Special Technical Publication STP-691*, ASTM, Philadelphia, 1980, pp. 464-473.
- Valenza, J.J. Scherer, G. W., (2007) A review of salt scaling: II. Mechanisms, *Cement and Concrete Research* 37, 2007, pp. 1022-1034.
- Mindess, S., Young, J. F. (1981) *Concrete*, *Prentice Hall International*, London, 671 p.
- Stark, J. (2004) Investigation into the frost de-icing salt resistance of HPC, Durability of high-performance concrete, Conference proceedings, *AEDIFICATIO Publishers*, 79104 Freiburg, 2004, pp. 219-230.
- Emese Gál** (1989) civil engineer (MSc), research assistant at the Department of Construction Materials and Technologies, Budapest University of Technology and Economics. *Main fields of interest*: concrete technology, supplementary cementing materials for concrete.
- Adorján Borosnyói** (1974) civil engineer (MSc), PhD, associate professor at the Department of Construction Materials and Technologies, Budapest University of Technology and Economics. *Main fields of interest*: non-destructive testing of concrete, supplementary cementing materials for concrete, non-metallic (FRP) reinforcements for concrete, bond in concrete, fibre reinforced concrete. Member of the Hungarian Group of *fib* and of *fib* TG 4.1 „Serviceability Models”. Member of RILEM Technical Committee ISC “Non destructive in situ strength assessment of concrete”.

BOND STRENGTH OF FRP REBARS



Sándor Sólyom – György L. Balázs

The system of bond stresses for force transfer between reinforcement and surrounding concrete is the basis of the existence of reinforced concrete. Without a proper transfer of stresses between concrete and reinforcement, reinforced concrete structures would not be feasible without end anchorages. In order to construct more durable reinforced concrete structures, in the most severe environmental conditions, corrosion of steel rebars should be prevented. One possible way is to replace the traditional steel reinforcement with Fibre Reinforced Polymers (FRP). Despite of the high amount of research carried out in the field, the adoption of FRP as embedded reinforcement in new structures is relatively slow. The most important reason is the lack of design guidance. Therefore, to develop design rules for the use of FRP as internal reinforcement, the understanding of bond mechanism and the effect of different parameters on the bond behaviour is essential. This paper provides a comprehensive overview of the present state of knowledge of bond characteristics of FRP rebars in concrete and also reports in detail the influence of various parameters that affect bond strength and development, such as: embedment length, type, surface characteristics and diameter of the rebar as well as concrete strength.

Keywords: FRP (Fibre Reinforced Polymer), bond strength, force transfer, sand coating, loading rate

1. INTRODUCTION

Steel rebars have been used over the last century with success as reinforcement in reinforced concrete structures. Although steel reinforcement has a high number of advantages (similar coefficient of thermal expansion to that of the concrete, ductile behaviour, high tensile strength, bendability etc.) it presents some drawbacks too. Most significant disadvantage is that the steel reinforcement is susceptible to corrosion, when the concrete structure is exposed to chloride ions, for instance in case of structures close to seawater or subjected to frequent use of de-icing salts.

Corrosion of steel reinforcement is considered to be the most important factor in limiting the life expectancy of reinforced concrete structures. Over the last few decades, different measures have been taken to overcome the durability issue of structures. The most significant methods to resolve the corrosion of the rebars are: increased concrete cover, introduction of additives to make the concrete less permeable, use of stainless steel reinforcement or epoxy coated steel rebars. Nevertheless, none of these attempts resulted in desired outcome completely.

Non-metallic (FRP) reinforcements provide a promising alternative to steel reinforcement excluding electrolytic corrosion in concrete structures because of the lack of ferrous material (Borosnyói, Balázs, 2001).

Fibre reinforced polymers are manufactured from different fibres (glass, carbon, aramid or basalt) bound together with various resins (polyester, vinyl ester or epoxy). They have mechanical properties and surface characteristics which are considerably different from that of the conventional steel reinforcements and provide excellent resistance to environmental effects such as freeze-thaw cycles, chemical attack etc. (Borosnyói, 2013; Sólyom, Balázs, 2015).

Tensile strengths and Young's moduli of FRP reinforcements depend mainly on type of fibre and resin, volumetric ratio of fibres (usually 60-70 V%), angle between the fibres and the longitudinal axis of reinforcement, shape and size of the cross section of the reinforcement. Tensile strengths of FRP rebars are in the range of 450 to 3 500 N/mm², Young's moduli are in the range of 35 000 and 580 000 N/mm² and failure strains are in the range of 0.5 to 4.4% (Balázs, Borosnyói, 2000; *fib*, 2007; Borosnyói, 2013). The most significant differences between FRP and steel reinforcements are their linear elastic behaviour up to failure without any plasticity and considerable release of elastic energy at failure. A major advantage of FRP rebars is that they can be engineered to have the desired mechanical and physical properties.

During the last decades, polymer composite materials have been used in civil engineering applications in various forms including rebars for concrete structures, sheets for flexural and shear strengthening and sheets to wrap concrete columns and bridge piers to increase confinement. FRP rebars are excellent alternatives to steel rebars, especially where corrosion can occur. While design codes are well established for steel reinforced concrete, they are slowly evolving for FRP rebars. Development of these codes requires understanding of bond between FRP rebars and concrete and the relationship between the bond strength and various material parameters and test conditions. Despite the large amount of research done in order to understand the bond behaviour of FRP rebars, owing to the high number of parameters which are affecting the bond properties, there is still debate among researchers about the effect of particular parameters. Due to various constituent materials, manufacturing processes and surface treatments of non-metallic reinforcement, both bond performance and failure of bond can occur in different ways than in the case of conventional steel reinforcement (Sólyom, Balázs, Borosnyói, 2015).

In this article the authors intend to summarize the parameters which have an effect on bond of FRP rebars, highlight the ones where further research is needed due to disagreement among existing results, or due to lack of experimental data.

2. INFLUENCING FACTORS OF BOND OF FRP REBAR IN CONCRETE

There are several factors that affect the bond between FRP rebars and concrete. The effect of some of these is well understood due to exhaustive research, however the effect of a few parameters is not obvious from the available experimental results. These parameters should be studied in more details in order to understand the bond behaviour of FRP rebars to concrete.

According to *fib* Bulletin 10 (*fib*, 2000) the bond behaviour of FRP rebars in concrete depends mostly on the following parameters: shape of the rebar cross section, rebar deformations, elastic modulus in axial direction, elastic modulus in transverse direction, transverse pressure, Poisson effect, position of the rebar in the cross section, wedging effect, bends in anchored rebars, concrete cover, distances between parallel rebars, coefficient of thermal expansion, environmental influences, rebar diameter, concrete strength, transverse reinforcement.

Further parameters are: embedment length of FRP rebar, loading rate, cyclic loading, fibre/resin type, concrete density (e.g. lightweight concrete), service temperature, elevated temperature, type of rebar surface etc.

2.1 Type of rebar surface

According to Guadagnini et al. (2005), Baena et al. (2009), Wang, Belarbi (2010) and many other researchers the bond strength developed by the rebars appears to be considerably influenced by the type of surface treatment on the rebars. However, as it can be seen in Eq. (1) developed from the database collected by Wambeke, Shield (2006), the bond strength seems to not depend on the surface treatment, but only on concrete compressive strength, concrete cover (and the distance between two adjacent rebars), rebar diameter and embedment length. For SI units, it has the following form:

$$\frac{\tau_{b,max}}{0.083\sqrt{f_c}} = 4.0 + 0.3 \frac{c}{\phi_b} + 100 \frac{\phi_b}{l_b} \quad (1)$$

CSA S806-02 (2002) specifies modification factors for taking into account the different surface characteristics of the FRP rebars. A modification factor of 1.0 is assigned to sand-coated or braided surfaces; 1.05 is assigned to spiral pattern or ribbed surfaces; 1.80 is assigned to indented surfaces. It can be observed, that according to CSA S806-02 (2002), indented surfaces present the weakest bond strength, followed by spiral pattern and ribbed surfaces and sand-coated and braided surfaces provide the highest bond strength.

According to *fib* Bulletin 10 (*fib*, 2000) the surface characteristics of the FRP (braided, strand, sand-coated, ribbed) influence considerably the bond strength and slip behaviour. If shearing off of the lugs takes place, the height of the lugs has no significant influence on the bond strength. Flat

or square cross-section rebars may have higher bond strength than that of round rebars, but may lead to increased splitting forces in the surrounding concrete.

From the above discussion, it can be concluded that no definite trend has been established so far for the effect of rebar surface on bond strength. As a consequence, there is need for more experimental data and a general equation for bond stress should be developed with the help of this data which can take into account the effect of surface characteristics.

The effect of rebar surface on bond strength is a complex phenomenon, because the rebar can have various surface configurations. Unlike steel reinforcement, no standard surface configuration has been set for FRP rebars. Different surface configurations lead to differences in bond behaviour. The bond stress of the FRP rebar with sand coating drops rapidly after reaching the maximum bond stress, whereas FRP rebars with helical wrapping and sand coating exhibit a more gradual reduction of the bond stress. The bond failure for steel rebars always occurs by concrete failure, irrespective of the concrete compressive strength, while bond strength and failure mode of FRP rebars depend on the relative shear strengths of concrete-resin and resin-fibre interfaces as well. Failure happens at concrete-resin interface when normal strength concrete is used, in contrary, resin-fibre interface failure occurs when high strength concrete is used.

Baena et al. (2009) carried out pull-out experiments on 88 concrete cube specimens and concluded that failure does not occur at the concrete matrix and rebar surface treatment has significant influence on the bond strength. They used six different FRP rebars with various surface configurations and fibre types. In the case of CFRP (Carbon FRP) rebars (R1 – sand-coated and R3 – textured surface), higher bond strengths were obtained with the sand-coated rebars (R1). This observation was valid for both concrete grades used in their experiments (C1: 28.63 N/mm², C2: 52.19 N/mm²; mean values of concrete compressive strengths). Both sand-coated and textured surfaces can be considered as non-deformed, with the bond strength strongly dependent on the friction resistance provided by the surface treatment. In the case of GFRP (Glass FRP) rebars (R2 – sand-coated, R4 – helical wrapping and sand-coated, R5 – grooved surface, R6 – helical wrapping) all the rebars had deformed surfaces, except rebar R2. In order to be able to compare the effect of different surface geometries, the researchers used two separate geometric ratios: CLR and a_r . The concrete lug ratio (CLR) is only applicable for indented rebars and it is defined as the ratio between the concrete lug width and the sum of the FRP rebar lug width and the concrete lug width. The projected rib area to rib spacing ratio (a_r) is applicable for both indented and deformed rebars. It is defined as the ratio of the projected rib area normal to the axis to the centre-to-centre rib spacing. The highest bond strength was obtained with R6 rebars. Rebar R6 also had the highest a_r ratio.

Hao et al. (2009) performed pull-out tests on 90 specimens to study the behaviour of GFRP rebars with ribbed surfaces with varying rib geometries in 28.7 N/mm² mean compressive strength concrete. The aim of the study was to provide better understanding of the role of rib spacing and rib height on the bond-slip characteristics of ribbed GFRP rebars with specially designed rib geometries. The conclusion of the research was that the optimal rib geometry for the materials used is: rib spacing equal to the rebar diameter and rib height equivalent is 6% of the diameter, resulting relative rib area of the rebar to be 0.06 (*Fig. 1*).

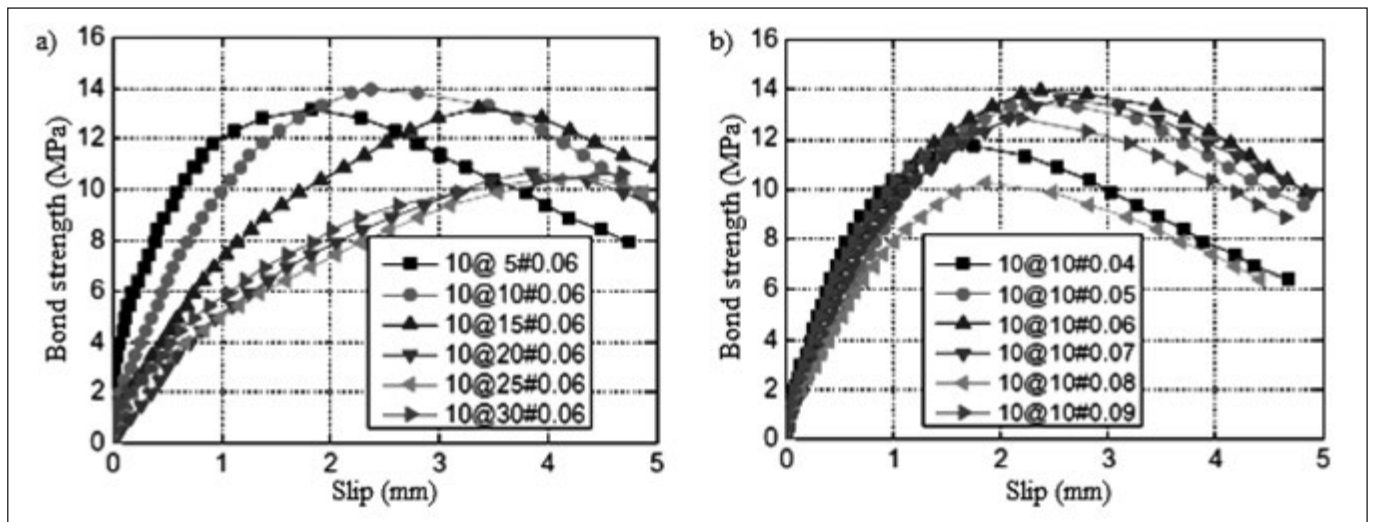


Fig. 1: Bond-slip curves of ribbed GFRP rebars with different rib geometries; rebar diameter: $d_b = 10$ mm (Hao et al., 2009); Legend: rebar diameter@rib spacing#rib height
 a) distance between indentations: $0.5d_b - 3d_b$ (5-30 mm); depth of indentations: $0.06d_b$
 b) depth of indentations: $0.04d_b - 0.09d_b$; distance between indentations: $1.0d_b$

2.2 Type of fibres

According to Eq. (1) which can be found in ACI 440.1R-06 (2006), the bond strength of FRP rebars does not depend on the fibre type, but only on concrete compressive strength, concrete cover (and the distance between two adjacent rebars), rebar diameter and embedment length. This equation is a result of a comprehensive analysis of the database collected by Wambeke, Shield (2006). The database contains beam bond tests carried out before year 2002.

The claim that the bond strength of FRP rebars is not affected by rebar type (in case of glass and carbon fibres) was confirmed also by Achillides, Pilakoutas (2004), who found that GFRP and CFRP rebars developed 72% of the bond strength of steel rebars.

Eq. (1) is only appropriate for embedment lengths which are less than $100d_b$ (where d_b is the rebar diameter), since the dataset used to develop it did not include bond failure with embedment lengths greater than $100d_b$. Embedment lengths shorter than $20d_b$ are not recommended.

According to ACI 440.1R-06 (2006) bond stress of CFRP rebars, despite the fact that no data exists in the database for CFRP rebars, can be taken as the bond stress of GFRP rebars, since it is anticipated that the much larger stiffness of CFRP rebars will likely increase bond stress. Limited data available for AFRP (Aramid FRP) rebars, but based on these few tests the bond stress of AFRP rebars appears to be similar to that of GFRP rebars.

Other design codes such as CSA S6-06 (2006) and JSCE (1997) do not distinguish between different types of fibres in the determination of bond strength, whereas the CSA S806-02 (2002) design code does make this distinction. According to CSA S806-02 (2002), CFRP and GFRP give the same bond strength, but AFRP shows lower bond strength in comparison to CFRP and GFRP. Modification factor with a value of 1.0 is assigned to CFRP and GFRP rebars, whereas a modification factor of 1.25 is assigned to AFRP rebars in the determination of the average bond strength (modification factor is inversely proportional to the bond strength).

According to *fib* Bulletin 10 (*fib*, 2000) the resin type, rather than the fibre type, controls the bond strength in case of normal and high strength concrete.

Similar results were found from a research conducted by

Nanni et al. (1995). It can be observed that bond strength of FRP is controlled by resin type, rather than fibre type, since the average bond stresses for glass-vinyl ester and carbon-vinyl ester (fibre/resin configuration of FRP rebar) are similar, whereas carbon-epoxy rebars developed much higher bond strength.

Owing to the lack of experimental data in case of AFRP and CFRP rebars, further experiments are needed in order to understand the effect of rebar type on bond strength of FRPs.

2.3 Concrete compressive strength

According to a research carried out at University of Girona (Baena et al., 2009) the compressive strength of concrete affects not just the bond strength, but also the failure mode of bond of the FRP rebars during pull-out. For concrete with compressive strength greater than 30 N/mm^2 , the bond failure occurs at the surface of the FRP rebars. As a result, the bond strength of FRP rebars does not depend greatly on the value of concrete strength, but rather on the surface characteristics of rebars. Failure mode changes for lower concrete grades (about 15 N/mm^2) and bond failure takes place at the concrete matrix interface. The same conclusion was drawn by researchers from The University of Sheffield (Achillides, Pilakoutas, 2004) and others (*fib*, 2000; Pecce et al., 2001; Lee et al., 2008).

The effect of concrete strength on the bond behaviour was also studied by Makitani et al. (1993), Benmokrane, Tighiouart, Chaallal (1996) and Tighiouart, Benmokrane, Gao (1998). It was concluded that the increase of bond strength was proportional to the square root of the compressive strength of concrete.

In the research published by Baena et al. (2009) 88 pull-out experiments were performed studying the effect of different parameters on the bond behaviour of FRP rebars. They used two different concrete types, C1 concrete with mean value of the compressive strength equal to 28.63 N/mm^2 and C2 equal to 52.19 N/mm^2 . The results compared for different FRP rebars are shown in Fig. 2. Seven different rebars were used in this study, six of them were FRP (carbon and glass) and for the sake of comparison steel rebars were also used. Materials gained from different manufacturers with different surface characteristics. For a better understanding of Fig. 2,

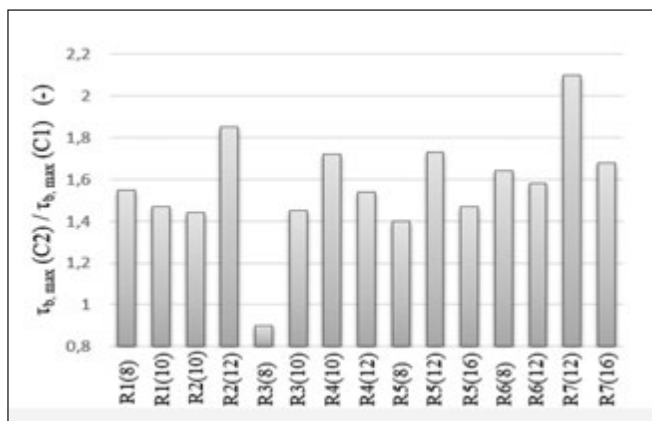


Fig. 2: Ratio of the bond strengths ($\tau_{b,max}$) of different concrete grades (C1: 28.63 N/mm², C2: 52.19 N/mm²). Rebars are named R1 to R7 followed by diameter (8, 10, 12 and 16 in mm, based on: Baena et al., 2009)

the following explanation is given: FRP rebars are named with codes from R1 to R7 followed by diameter (for example: 8, 10, 12 and 16 in mm). Table 1 contains the most important information about rebar surface characteristics.

Table 1: Rebar surface characteristics (Baena et al., 2009)

	Fibre	Resin	Surface treatment
R1	Carbon	Vinyl ester	Sand coating
R2	Glass	Vinyl ester	Sand coating
R3	Carbon	Epoxy	Surface texture
R4	Glass	Vinyl ester	Helical wrapping and sand coating
R5	Glass	Urethane vinyl ester	Grooves
R6	Glass	Polyester	Helical wrapping
R7	Steel	-	-

It is clearly visible that the higher the concrete strength, the higher the bond strength, except in case of R3(8) where the ratio is lower than 1. However, the increase in strength also depends on the type of rebar: values of the ratio vary between 0.9 and 2.1, indicating the effect of the concrete strength on bond strength.

2.4 Concrete cover

The larger the concrete cover, the higher the confinement provided by the concrete, which will increase the bond strength of the rebars.

ACI 440.1R-06 (2006) specifies that bond failure occurs by splitting of the concrete when the member does not have adequate concrete cover. On the other hand, when sufficient concrete cover is provided, splitting failure can be prevented or delayed, resulting in a pull-out failure. As a consequence, concrete cover affects not only the bond strength, but also the failure mode of the reinforced concrete member.

In a research carried out by Ehsani, Saadatmanesh, Tao (1996), 48 beam specimens with GFRP rebars were tested. It was concluded that splitting failure occurred when the specimen had concrete cover of one rebar diameter, whereas pull-out failure or rebar fracture occurred when the concrete cover was two times the rebar diameter or more. On the other hand, Aly, Benmokrane, Ebead (2006) concluded that the side concrete cover is more effective in increasing the bond

strength than the bottom concrete cover. Bottom concrete cover should not be larger than the side concrete cover. Six full-scale beams were investigated by Aly, Benmokrane, Ebead (2006) to study the effect of concrete cover on the bond strength of tensile lap splicing of GFRP rebars. The concrete cover was varied between one and four rebar diameters ($d_b < c < 4d_b$) and it was observed that the bond strength increased by 27% as the concrete cover increased from one to four rebar diameters. It was also noted that the effect of concrete cover on bond strength was nonlinear.

The bond strength increases with an increase in the concrete cover due to the increased confining effect and that the bond strength for pull-out mode of failure is higher than that for splitting mode of failure for same c/d_b .

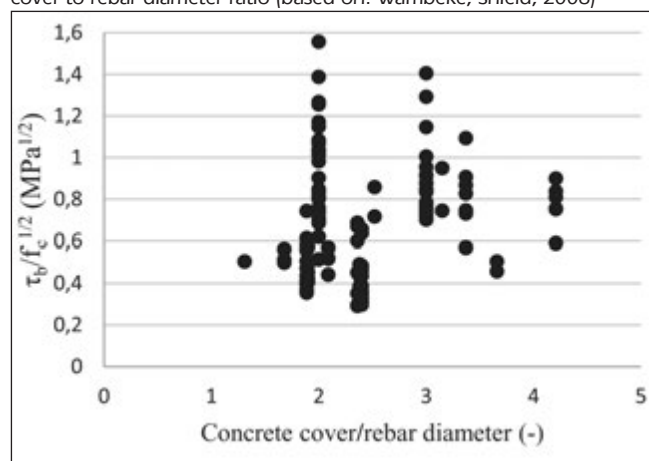
It was observed that the normalized slip (s_m/l_b) decreased with an increase in the concrete cover. This was attributed to the confining action of the concrete cover which resulted in the peak bond stress to occur at a relatively smaller slip.

Variation of normalized average bond stress ($\tau_b/f_c^{1/2}$) with concrete cover to rebar diameter (c/d_b) ratio is indicated in Fig. 3 (Wambeke, Shield, 2006).

2.5 Rebar diameter

The relationship between rebar diameter and bond strength of FRP rebars has been investigated by Achillides, Pilakoutas (2004), Guadagnini et al. (2005), Baena Muñoz (2010) and many others. The outcome of their experimental research shows similarity with the result obtained for steel rebars: the bond strength increased with the decrease in the rebar diameter. According to the above mentioned researchers the reasons of this is fourfold. Firstly, due to the increase in the diameter more water can be trapped underneath the rebar which in turn creates more voids than would form under a smaller rebar. The presence of voids decreases the contact area between the rebar and the surrounding concrete and hence the bond strength is reduced. Secondly, the Poisson effect may also have an influence on this phenomenon. When FRP rebar is pulled, the diameter is reduced and as a consequence, stresses from mechanical interlock and friction between FRP rebar and concrete will be reduced. The reduction is more pronounced for larger diameters. Furthermore, larger diameter rebars result in longer embedment lengths, since for the experiments it is a common practice that the embedment length is a function of the diameter. The peak bond stress moves gradually from the loaded end towards the unloaded end of the rebar during pull-out test, as a consequence, in case of longer embedment lengths the average bond stress is

Fig. 3: Variation of normalized average bond stress with concrete cover to rebar diameter ratio (based on: Wambeke, Shield, 2006)



lower. Finally, the “shear lag” effect could be also responsible for this phenomenon. When FRP rebar is pulled, differential movements can be formed at the surface of the rebar and in the core of the rebar, since shear stiffness of FRP rebar is lower than that of steel rebar. It results a non-uniform distribution of normal stresses through the cross section of the rebar, thus the stress at the surface is higher than the calculated average stress. The difference is greater in large diameter rebars which is expected to reduce the average bond stress.

The dependence of bond strength on rebar diameter can be observed in Fig. 4. This figure was prepared from the experimental data of a research done by Baena et al. (2009).

2.6 Embedment length

According to Benmokrane, Tighiouart, Chaallal (1996), Ehsani, Saadatmanesh, Tao (1996), Achillides (1998), Pecce et al. (2001), Belarbi, Wang (2004) and many others, the maximum average bond stress decreases with an increase of the embedment length, which is similar to the behaviour of steel rebars. It is thought to be a result of the non-linear distribution of bond stresses over the rebar. The embedment length has also significant influence on the initial bond stiffness of FRP rebars as well as on the failure mode of bond.

From the research done by Achillides and Pilakoutas (2004) it was found, that the rate of bond stress increase was greater for smaller embedment lengths than for larger embedment lengths. This is also attributed to the non-uniform distribution of the bond stresses over the rebar.

The dependence of bond strength on the embedment

Fig. 4: Influence of rebar diameter on bond strength (normalized with the concrete strength, based on: Baena et al, 2009)

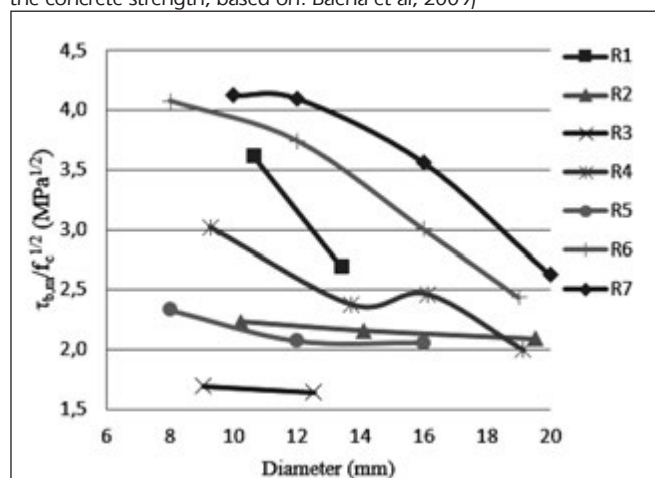
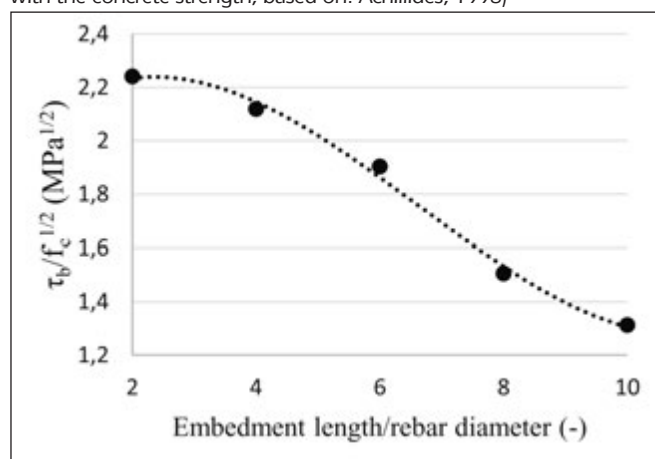


Fig. 5: Influence of embedment length on bond strength (normalized with the concrete strength, based on: Achillides, 1998)



length is indicated in Fig. 5. The figure was prepared from the experimental data of a research done by Achillides (1998). On the abscissa values are given as a ratio between the embedment lengths and rebar diameter, on the ordinate mean values of bond strengths are normalized with the square root of concrete compressive strength.

2.7 Loading rate

There are some experimental data in the literature that shows the effect of loading rate on bond strength. The loading rate of applied force can affect the results, consequently it is needed to control the loading rate while evaluating the interfacial bond strength using the pull-out test. It is also necessary to take into account the loading rate of applied force when comparing experimental results for different researchers.

Borosnyói (2015) published a study in which the effect of loading rate on bond strength of FRP rebars was investigated. In his experimental work, three different concrete grades were studied. Quasi-static pull-out loading, $\dot{\epsilon} = 1.16 \times 10^{-4} \text{ s}^{-1}$ and impact pull-out loading, $\dot{\epsilon} = 4.63 \times 10^{-2} \text{ s}^{-1}$, were considered at room temperature. The results showed a clear tendency: higher strain rate results increase of bond stiffness, bond strength and residual bond strength for all the three concrete grades tested.

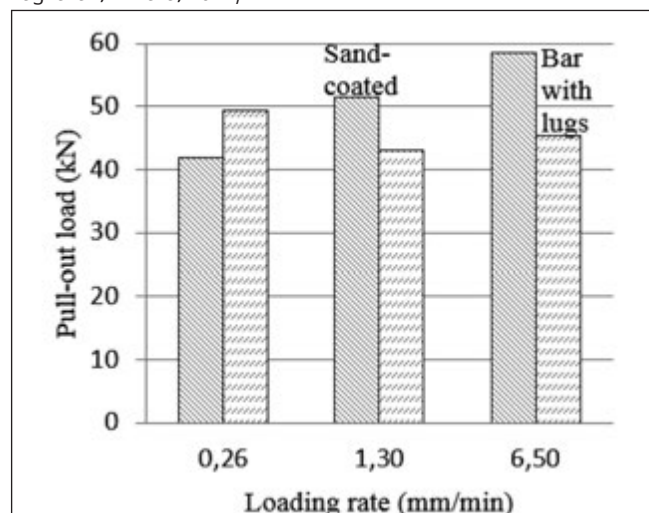
The effect of loading rate of applied force was also studied by Soong, Raghavan, Rizkalla (2011). The pull-out load for sand-coated specimens increased with increase of loading rate as shown in Fig. 6. However, in case of rebars with lugs this trend could not be observed. A reason for this might be that there is higher contribution from frictional resistance in sand-coated specimens than in case of specimens with deformed rebars. Nevertheless, further investigation is required to clearly understand the relationship between the loading rate and the frictional resistance and the bearing resistance.

2.8 Service temperature

The surfaces of the FRP rebars are rich in matrix. The glass transition temperature (T_g) of matrices are between +60°C and +180°C. When the temperature reaches the glass transition temperature, the modulus of elasticity and strength of matrices reduces rapidly. As a consequence the FRP rebars are more affected of the service temperature than the steel rebars (Lublóy et al., 2005).

According to a study realized by Borosnyói (2015), the bond strength of FRP rebars depends not only on the

Fig. 6: Influence of loading rate on pull-out load (based on: Soong, Raghavan, Rizkalla, 2011)



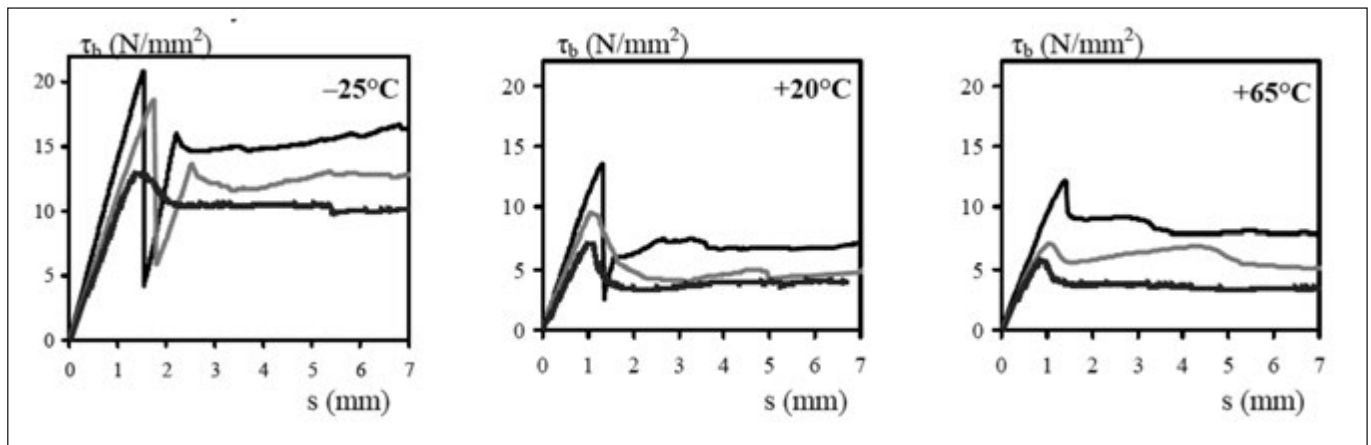


Fig. 7: Testing temperature and typical bond stress (τ_b) vs. slip (s) diagrams during static pull-out testing for sand-coated CFRP wires (Borosnyói, 2015)

compressive strength of concrete (which itself is also temperature dependent), but on the temperature dependent behaviour of the resin matrix as well. In his experiment Borosnyói (2015) used sand-coated CFRP wires, with 5 mm diameter. Higher stiffness of surface layers of the resin results higher bond strength at low temperature and the softening of the surface layers of the resin results lower bond strength at elevated temperature.

In Fig. 7 the effect of service temperature on bond stress–slip law during static pull-out testing is presented. Three different concrete grades are indicated. The reduction of bond strength as the temperature increases is clearly visible.

In a research carried out by Galati et al. (2006), 36 cube specimens were investigated by pull-out test. The effect of service temperature on bond between FRP rebars and concrete was studied. The authors considered different embedment lengths and concrete covers. Three different types of specimens were prepared based on the position of the rebar, namely: centrally placed and two or three times the diameter from the outer faces. 9.5 mm diameter GFRP rebars were used for the experiments placed in 152 mm (6 inch) side concrete cubes. The heat treated specimens (half of the specimens were not heat treated, they were used for comparison) were placed into an environmental chamber for 200 h at a temperature of 70°C and at a humidity of 80%, corresponding to 70% of the glass transition temperature (T_g) of the GFRP rebars used. The pull-out testing of the specimens was carried out at room temperature.

On the basis of the experimental investigations, important conclusions can be drawn. In most cases the thermal treatment induced a slight degradation in the bond performance. Furthermore, the effect of the thermal treatment was more pronounced for the bond stress–slip curves in terms of slip values owing to the degradation of the resin. The highest effect of the service temperature was observed when small concrete cover was used. Such behaviour can be explained with the microcracking of the concrete due to the stresses induced during thermal treatment.

3. CONCLUSIONS

Fibre Reinforced Polymer (FRP) rebars offer an effective solution to the challenges of steel durability in aggressive environments and where the magnetic or electrical properties of steel are undesirable. By applying FRP reinforcement there is no ferrous material to corrode in the reinforced concrete. The mechanical properties and surface characteristics can be considerably different from those of steel reinforcement

which leads to numerous open questions, among these is the bond behaviour of FRP rebars in concrete.

Both bond action and failure mode of bond can be affected by the type of rebar. Owing to the different material characteristics, manufacturing processes and surface treatments, bond of FRP rebars differ from that of steel reinforcement (Borosnyói, 2006).

Bond action of smooth FRP rebars is attributed to only two components: the adhesion at zero slip and the friction as slip is developed. However, depending on the sand coating characteristics, magnitude of bond strength of smooth FRP rebars can be similar to that of deformed steel reinforcement.

In case of deformed FRP rebars the mechanical interlock (also known as bearing) plays the most important role among the components of bond action. Deformed FRP rebars can develop higher bond strength than smooth FRP rebars. Bond strength of deformed FRP rebars is usually reached at higher slips due to higher deformation capacity of the surface layers and lower modulus of elasticity of the rebars than that of steel rebars.

In normal strength concrete, bond failure of deformed FRP reinforcement is influenced by both the concrete strength and the properties of the reinforcement, not only by the concrete strength as in case of steel reinforcement.

During pull-out failure, the surface layers can be peeled off, ribs of the reinforcement can fail in shear or ribs can be torn off and in case of relatively low concrete strength, concrete lugs between FRP ribs can be sheared off. If the concrete cover is not large enough, splitting of concrete can also happen.

FRP rebars, most likely, cannot completely replace steel reinforcements. Nonetheless, it is expected to find increasing use in niche applications where the particular chemical, physical and mechanical properties of FRPs may lead to more practical or economic solutions. Regardless of the advancement made in the use of FRP rebars as internal reinforcement for reinforced concrete structures, many aspects of their structural behaviour still require further examination, before their full potential can be exploited.

4. ACKNOWLEDGEMENTS

The authors gratefully acknowledge the financial support of European Network for Durable Reinforcement and Rehabilitation Solutions (**endure**), Networks for Initial Training (ITN), Seventh Framework Programme of the European Union (Grant: PITN-GA-2013-607851) and COST Action TU1207 „Next Generation Design Guidelines for Composites in Construction”.

5. REFERENCES

- Achillides, Z. (1998): "Bond behaviour of FRP bars in concrete", *PhD Thesis*, The University of Sheffield
- Achillides, Z., Pilakoutas, K. (2004): "Bond behavior of fiber reinforced polymer bars under direct pullout conditions", *Journal of Composites for Construction*, 8 (2), pp. 173-181 [http://dx.doi.org/10.1061/\(ASCE\)1090-0268\(2004\)8:2\(173\)](http://dx.doi.org/10.1061/(ASCE)1090-0268(2004)8:2(173))
- ACI Committee 440 (2006): "Guide for the Design and Construction of Structural Concrete Reinforced with FRP Bars (ACI 440.1R-06)", *American Concrete Institute*, Farmington Hills, MI, 44 pp.
- Aly, R., Benmokrane, B., Ebead, U. (2006): "Tensile lap splicing of bundled CFRP reinforcing bars in concrete", *Journal of Composites for Construction*, V. 10, No. 4, pp. 287-294
- Baena, M., Torres, L., Turon, A., Barris, C. (2009): "Experimental study of bond behaviour between concrete and FRP bars using a pull-out test", *Composites: Part B - Engineering*, 40 (2009), pp. 784-797
- Baena Muñoz, M. (2010): "Study of bond behaviour between FRP reinforcement and concrete", *PhD Thesis*, University of Girona.
- Balázs, G. L., Borosnyói, A. (2000): "Non-metallic (FRP) reinforcement for bridge construction", *Vasbetonépítés*, Vol. 2, 2000/2, pp. 45-52 (in Hungarian)
- Belarbi, A., Wang, H. (2004): "Bond-Slip response of FRP reinforcing bars in Fiber Reinforced Concrete (FRC) under direct pullout", In: *International Conference on Fiber Composites, High Performance Concretes and Smart Materials*, pp. 409-419
- Benmokrane, B., Tighiouart, B., Chaallal, O. (1996): "Bond strength and load distribution of composite GFRP reinforcing bars in concrete", *ACI Materials Journal*, Vol. 3, pp. 246-253
- Borosnyói, A., Balázs, G. L. (2001): "New structural materials for concrete bridges", *Vasbetonépítés*, Vol.3, 2001/4, pp. 100-106 (in Hungarian)
- Borosnyói, A. (2006): "FRP reinforced concrete - brittle or ductile behaviour?", *Vasbetonépítés*, Vol. 8, No.3, 2006/3, pp. 71-80 (in Hungarian)
- Borosnyói, A. (2013): "Corrosion resistant concrete structures with innovative Fibre Reinforced Polymer (FRP) materials", *Építőanyag*, Vol. 65/1, pp. 26-31. <http://dx.doi.org/10.14382/epitoanyag-jsbcm.2013.6> (in Hungarian)
- Borosnyói, A. (2014): "Use of corrosion resistant Fibre Reinforced Polymer (FRP) reinforcements for the substitution of steel bars in concrete", *Korróziós figyelő*, Vol. 54, No.1, pp. 3-15 (in Hungarian)
- Borosnyói, A. (2015): "Influence of service temperature and strain rate on the bond performance of CFRP reinforcement in concrete", *Composite Structures*, doi: <http://dx.doi.org/10.1016/j.compstruct.2015.02.076>
- CAN/CSA S6-06 (2006): "Canadian highway bridge design code", *Canadian Standards Association*, Rexdale, Ontario, Canada, 788 pp.
- CAN/CSA S806-02 (2002). "Design and construction of building components with fibre reinforced polymers", *Canadian Standards Association*, Rexdale, Ontario, Canada, 177 pp.
- Ehsani, M. R., Saadatmanesh, H., Tao, S. (1996): "Design recommendations for bond of GFRP rebars to concrete", *Journal of Structural Engineering*, pp. 247-254
- fib (2000): "Bond of Reinforcement in Concrete", State-of-art Report, Bulletin 10, fib – International Federation for Structural Concrete, Lausanne
- fib (2007): "FRP reinforcement in RC structures", Technical report, Bulletin 40, fib - International Federation for Structural Concrete, Lausanne
- Galati, N., Nanni, A., Dharani, L. R., Focacci, F., Aiello, M. A. (2006): "Thermal effects on bond between FRP rebars and concrete", *Composites Part A: Applied Science and Manufacturing*, 37, pp. 1223-1230
- Guadagnini, M., Pilakoutas, K., Waldron, P., Achillides, Z. (2005): "Tests for the evaluation of bond properties of FRP bars in concrete", *2nd International Conference on FRP Composites in Civil Engineering (CICE 2004)*, pp. 343-350
- Hao, Q., Wang, Y., He, Z., Ou, J. (2009): "Bond strength of glass fiber reinforced polymer ribbed rebars in normal strength concrete", *Construction and Building Materials*, 23, pp. 865-871
- Japanese Society of Civil Engineers (JSCE) (1997): "Recommendations for design and construction for concrete structures using continuous fibre reinforcing materials", *Concrete Engineering Series*, No. 23, Tokyo.
- Lee, J. Y., Kim, T. Y., Kim, T. J., Yi, C. K., Park, J. S., You, Y. C., Park, Y. H. (2008): "Interfacial bond strength of glass fiber reinforced polymer bars in high-strength concrete", *Composites: Part B Engineering*, 39, pp. 258-270
- Lublóy, É., Balázs, G. L., Borosnyói, A., Nehme, S. G. (2005): «Bond of CFRP wires under elevated temperature», Proceedings "Bond Behaviour of FRP in Structures" (Eds. Teng and Chen) 7-9. Dec. 2005 Hong Kong, China, ISBN 962-367-506-2, pp. 163-167. http://www.iifc-hq.org/proceedings/BBFS_2005/Basic%20Bond%20Mechanisms/Bond%20of%20CFRP%20Wires%20Under%20Evaluated%20Temperature.pdf
- Makitani, E., Irisawa, I., Nishiura, N. (1993): "Investigation of bond in concrete member with fibre reinforced plastic bars." *Fibre-Reinforced-Plastic Reinforcement for Concrete Structures-Int. Symp.*, ACI SP138-20, pp. 315-331
- Nanni, A., Al-Zahrani, M. M., Al-Dulajjan, S. U., Bakis, C. E., Boothby, T. E. (1995): "Bond of FRP reinforcement to concrete - Experimental results", In: L. Taerwe, editor. *Second International Symposium on Non-Metallic (FRP) Reinforcement for Concrete Structures*, pp. 135-145
- Pecce, M., Manfredi, G., Realfonzo, R., Cosenza, E. (2001): "Experimental and analytical evaluation of bond properties of GFRP bars", *Journal of Materials in Civil Engineering*, July/August 2001, pp. 282-290
- Sólyom S., Balázs G. L. (2015): "Fibre Reinforced Polymer (FRP) rebars – 1. Material Characteristics", *Vasbetonépítés*, Vol.17, 2015/1, pp. 13-16 (in Hungarian)
- Sólyom, S., Balázs, G. L., Borosnyói, A. (2015): "Material characteristics and bond tests for FRP rebars", *Concrete Structures*, Vol. 16. pp. 38-45
- Soong, W. H., Raghavan, J., Rizkalla, S. H. (2011): "Fundamental mechanisms of bonding of glass fiber reinforced polymer reinforcement to concrete", *Construction and Building Materials*, 25, pp. 2813-2821
- Tighiouart, B., Benmokrane, B., Gao, D. (1998): "Investigation of bond in concrete member with fibre reinforced polymer (FRP) bars", *Construction and Building Materials*, 12, pp. 453-462
- Wang, H., Belarbi, A. (2010): "Static and Fatigue Bond Characteristics of FRP Rebars Embedded in Fiber-reinforced concrete", *Journal of Composite Materials*, pp. 1605-1622
- Wambeke, B. W., Shield, C. K. (2006): "Development length of glass fibre-reinforced polymer bars in concrete", *ACI Structural Journal*, V. 103, No. 1, pp. 11-17

Sándor Sólyom (1984) Civil Engineer, Early Stage Researcher at Budapest University of Technology and Economics (BME). Main fields of interest: application possibilities of Fibre Reinforced Polymer (FRP) rebars in reinforced concrete structures, bond in concrete, strengthening with advanced composites. Member of the *fib* T5.1 "FRP (Fibre Reinforced Polymer) reinforcement for concrete structures" and the Hungarian Group of *fib*. Research fellow in endure (European Network for Durable Reinforcement and Rehabilitation Solutions).

Prof. György L. Balázs (1958) Civil Engineer, PhD, Dr.-habil., professor of structural engineering, head of Department of Construction Materials and Technologies and Deputy Dean of the Civil Engineering Faculty of Budapest University of Technology and Economics (BME). His main fields of activities are experimental investigation and modelling of RC, PC, FRC structures, HSC, fire resistance of concrete. He is chairman of several commissions and task groups of *fib*. He is president of Hungarian Group of *fib*, Editor-in-chief of the Journal "Concrete Structures" and the honorary President of *fib*.

CREATING THE **FUTURE**



A-HÍD

A-HÍD ZRt.
H-1138 BUDAPEST
KARIKÁS FRIGYES U. 20.

www.ahid.hu



By using the services of the team of ÉMI-TÜV SÜD Ltd.

your work will be crowned with success in the fields of quality systems and safety techniques.

We offer testing, quality control, certification, assessment of conformity and expertise in the following fields:

- basic evaluation, monitoring and certification of in-process control of construction products (pre-cast concrete, reinforced concrete, pre-stressed concrete, lightweight concrete, masonry blocks and related products)
- load-bearing structures and non-load-bearing building structures
- elevators, escalators, stage technical equipment
- hoisting machines, cranes and conveyor equipments
- pressure vessels, boilers and gas-containers
- welding technologies, welders, welding plants
- design approval
- consumer goods, technical products, light industry products, chemical products and food products
- assessment of conformity and C€ marking
- inspection and certification of management systems based on national and international accreditation, quality management- and environment-orientated management systems, Hungarian Health Care Provision Standard (MEES), Occupational Health and Safety Management System (MEBIR), Food Safety Management System (ÉBIR / HACCP / BRC / QS / GLOBALGAP), Automotive Industry Quality Management Systems (VDA 6.1 / TS 16949), Information Security Management System (IBIR), EMAS verification and verification of reports about green house gas emissions
- training of experts in the field of quality management and safety engineering



ÉMI-TÜV

**Choose certainty.
Add value.**

